저작자표시-비영리-변경금지 2.0 대한민국

이용자는 아래의 조건을 따르는 경우에 한하여 자유롭게

- 이 저작물을 복제, 배포, 전송, 전시, 공연 및 방송할 수 있습니다.

다음과 같은 조건을 따라야 합니다:

저작자표시. 귀하는 원저작자를 표시하여야 합니다.

비영리. 귀하는 이 저작물을 영리 목적으로 이용할 수 없습니다.

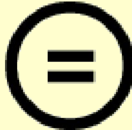

변경금지. 귀하는 이 저작물을 개작, 변형 또는 가공할 수 없습니다.

- 귀하는, 이 저작물의 재이용이나 배포의 경우, 이 저작물에 적용된 이용허락조건을 명확하게 나타내어야 합니다.
- 저작권자로부터 별도의 허가를 받으면 이러한 조건들은 적용되지 않습니다.

저작권법에 따른 이용자의 권리는 위의 내용에 의하여 영향을 받지 않습니다.

이것은 이용허락규약(Legal Code)을 이해하기 쉽게 요약한 것입니다.

Disclaimer

dCollection

[UCI]I804:21028-200000105246

공학박사 학위논문

Study on the Terahertz Nondestructive Testing Method for Multi-chip Package Inspection using a Resonant Slit-type Probe with Rounded Matching Structure

라운드 매칭 구조를 가지는 공진형 슬릿 프로브를 이용한 다중 칩 패키지 검사를 위한 테라헤르츠파 비파괴 검사 방법에 관한 연구

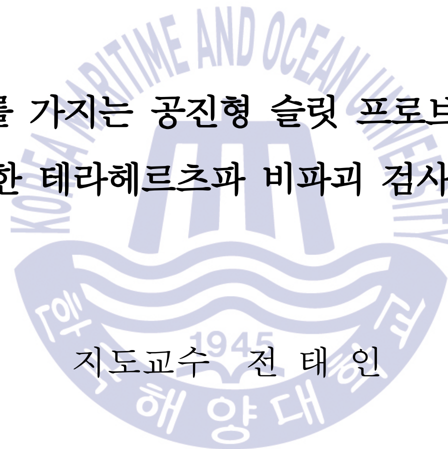

지도교수 전 태 인

2018년 7월

한국해양대학교 대학원

전기전자공학과

김 근 주

Collection @ kmou

공학박사 학위논문

Study on the Terahertz Nondestructive Testing Method for Multi-chip Package Inspection using a Resonant Slit-type Probe with Rounded Matching Structure

라운드 매칭 구조를 가지는 공진형 슬릿 프로브를 이용한 다중 칩 패키지 검사를 위한 테라헤르츠파 비파괴 검사 방법에 관한 연구

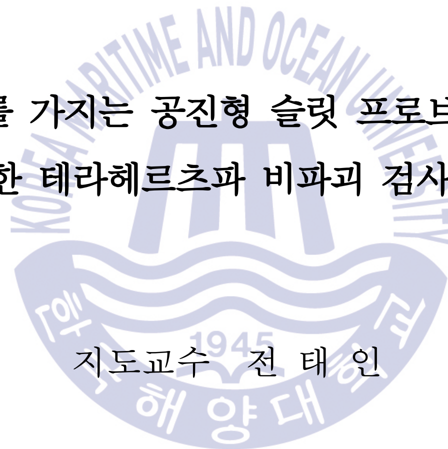

지도교수 전 태 인

2018년 7월

한국해양대학교 대학원

전기전자공학과

김 근 주

dCollection @ kmou

dCollection @ kmou

본 논문을 김근주의 공학박사 학위논문으로 인준함.

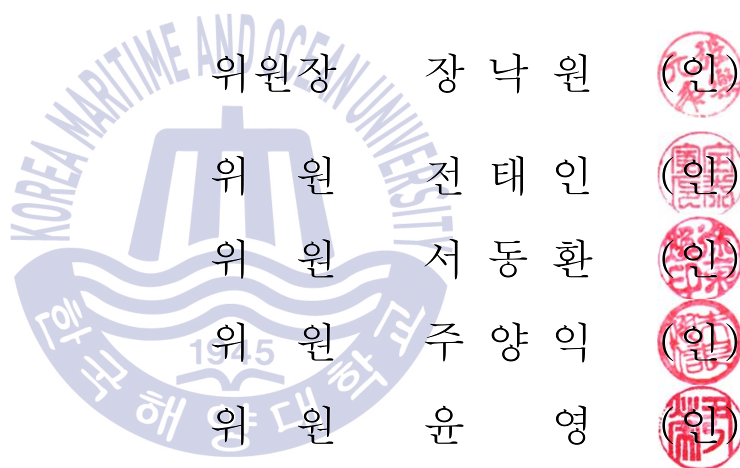

위원장	장 낙 원	(인)
위 원	전 태 인	(인)
위 원	서 동 환	(인)
위 원	주 양 익	(인)
위 원	윤 영	(인)

2018년 7월 10일

한국해양대학교 대학원

dCollection @ kmou

Collection @ kmou

Table of contents

Table of contents i

List of figures v

List of tables x

Abstract xi

1. Introduction 1

1.1 Motivation 1

1.2 Outline 3

2. Background 5

2.1 Multi-chip package inspection technology and their Limit 5

2.1.1 Multi-chip package inspection using ultrasound.................................... 5

2.1.2 Multi-chip package inspection using infra-Red (IR) 6

2.1.3 Multi-chip package inspection using X-ray 8

2.2 THz inspection technology 9

2.2.1 Advantages of THz inspection technology 9

2.2.2 Issues in the THz inspection technology 12

2.2.3 THz technology for multi-chip package inspection 16

3. Resonant slit-type probe 19

3.1 Design of a resonant slit-type probe 19

3.1.1 Advantages of resonant slit-type probe 19

3.1.2 Theory of resonant slit-type probe 20

Collection @ kmou

3.1.3 Resonant slit-type probe for THz wave 23
3.1.4 Matching structure of resonant slit-type probe 27
3.2 Resonant slit-type probe with rounded matching structure............................ 27
3.2.1 Resonant slit-type probe with rounded matching structure 27
3.2.2 Fabrication of slit-type probe with rounded matching structure........... 34
3.2.3 Measurement of slit-type probe with rounded matching structure 37

4. Experimental setup 39
4.1 Components for CW THz imaging system 40
4.1.1 CW THz source 40
4.1.2 CW THz detector 41
4.1.3 FPGA based on fast lock-in amplifier.. 41
4.1.4 Fabrication of standard sample 48
4.2 CW THz Transceiver module for multi-chip package inspection 51
4.2.1 Design of THz transceiver module 51
4.2.2 Magic-tee based THz transceiver 56
4.2.3 Directional coupler based THz transceiver 56

5. Measurements and results 59
5.1 Verification of performance of THz imaging system 59
5.1.1 Measurement of spatial resolution of resonant slit-type probe with rounded matching structure 59
5.1.2 High-speed signal processing and image acquisition............................ 60
5.2 Semiconductor chip inspection using pulsed THz wave 65
5.2.1 Inspection system using pulsed THz wave 65
5.2.2 Semiconductor chip inspection using pulsed THz wave 67
5.2.3 Transmission characteristics according to the polarization 72
5.3 Semiconductor chip inspection using CW THz wave 73
5.3.1 Semiconductor chip inspection using CW THz system based on directional Coupler 77

Collection @ kmou

5.3.2 Semiconductor chip inspection using CW THz system based on magic-tee 80
5.3.3 Semiconductor chip inspection using CW THz wave 83
5.4 Multi-chip package inspection using CW THz wave 83
5.4.1 THz propagation in voids of multi-chip package in lateral inspection 83
5.4.2 Multi-chip package inspection using lateral inspection methode............ 85
5.4.3 Improvement of void image using image processing technique 89
5.4.4 Another application using slit-type probe (Food inspection) 93

6. Conclusion 99

Reference 103

Collection @ kmou

Collection @ kmou

List of figures

Figure

2-1 230 MHz acoustic image of an underfilled memory die (Upper) & the DSP die (Bottom) 7

2-2 IR image of bonded wafer pair showing particle generated voids ... 7

2-3 Failed QFN (quad-flat no-lead) joint connections due to lack of solder paste 9

2-4 Applications of THz wave 10

2-5 Falling weight impact testing system and sample(Left) THz reflection image and ultrasonic C-scan image 11

2-6 Comparison of available THz sources of high power 13

2-7 An aperture with bull's eye structure 15

2-8 A needle probe with a metal wire waveguide 15

2-9 Schematic diagram of the split conical waveguide 16

3-1 Photograph of flash memory chip 20

3-2 Equivalent circuit according to iris structure in waveguide 22

3-3 Rectangular slit antenna with dimensions a and b 22

3-4 Dual antennas - (left) the slit antenna, (right) the dipole antenna ... 24

3-5 Slit antenna attached rectangular waveguide 24

3-6 Schematic of the resonant slit-type probe with right angle structure The inset shows the cross-sectional view at the slit 26

3-7 Return loss according to the slit thickness for the resonant slit-type probe with right angle structure when a = 150 μm and b = 740 μm 28

3-8 Schematic diagram of tapered Resonant slit waveguide (Left) and Stepped Resonant slit waveguide (Right) 29

3-9 Schematic of a resonant slit probe with a rounded matching structure The inset shows the cross-sectional view at the slit 31

Collection @ kmou

3-10	Shift of the resonant frequency according to slit thickness for a resonant slit-type probe (a) with right angle structure (b) with rounded matching structure of 100 μm and (c) 200 μm. The height , and width of the slit were fixed at 150 μm and 740 μm. The insets show the expanded resonant frequency	32
3-11	A reflection signal according to a scanning position when a metal foreign objects is detected using a resonant slit-type probe with right angle structure slit of a = 740 μm, b = 150 μm and t=90 μm and a resonant slit-type probe with rounded matching structure of a = 740 μm, b = 150 μm, t= 290 μm, and r = 100 μm	33
3-12	Electroforming process sequence (upper) and fabrication of resonant slit structure (bottom)	35
3-13	A resonant slit probe with a rounded matching structure manufactured by electroforming process	36
3-14	(a) Fabricated resonant probe with a rounded matching structure slit and experimental setup to measure return loss using the VNA (b) Comparison of the VNA measurement values of and CST MWS simulation results of the designed and fabricated a resonant slit-type probe with rounded matching structure	39
4-1	Schematic diagram of multi-chip package structure	40
4-2	THz source module configured for high-speed & high-power operation	42
4-3	WR5.1ZBD detector (VDI) and frequency-dependent responsivity ...	42
4-4	Detector response according to TTL frequency (a) TTL Frequency = 10kHz, (b) TTL Frequency = 125kHz	44
4-5	Phase measurement in lock-in amplifier	46
4-6	Schematic diagram of CW THz System with FPGA-Based Lock-in Amplifier	46
4-7	Comparison of FPGA-based lock-in amplifier and AMETEK 7256 lock-in amplifier	47
4-8	Signal response of AMETEK 7256 according to Time Constant	49

Collection @ kmou

4-9 Comparison of detection signals of FPGA-based lock-in amplifier according to time constant (a)TC=10us (b)TC=1ms (c)None FPGA 50
4-10 The optical properties of silicon in the THz region 52
4-11 The optical properties of polymers in the THz region 52
4-12 Manufactured standard sample 53
4-13 Comparison of THz paths in Off-axis and On-axis measurement 55
4-14 Schematic Diagram of Reflective THz transceiver module 55
4-15 THz Transceiver module based on magic tee 58
4-16 THz Transceiver module based on directional coupler 58
5-1 Reflective THz imaging system based on (left) a waveguide matched hybrid-tee. (Right) Photograph of the standard sample 61
5-2 (a) Amplitude THz image (b) Phase image of the standard sample (c) (Bottom) Profile of the amplitude and (top) phase signals represented by the dashed line. 62
5-3 Signal measurement synchronized with motor speed 63
5-4 Sample with 350 ㎛ line width 64
5-5 Image comparison according to sample moving speed (upper) 10 mm/s (bottom) 1000 mm/s 64
5-6 Transmission-type THz wave system based on 4-parabolic mirrors . 66
5-7 THz transmission characteristics according to pin-hole and adhesive tape 66
5-8 Experimental setup for semiconductor chip inspection using pulsed THz wave 68
5-9 (a) Measured THz pulse and spectra for a flash memory with 1 mm diameter voids (b) Photograph of sample (c) Reconstructed THz image at 4 ps and 0.55 THz, respectively 69
5-10 (a) Measured pulse and spectra for a flash memory with 1 mm diameter voids. (b) Photograph of sample (c) Reconstructed image at 5.2 ps and 0.65 THz, respectively 70

Collection @ kmou

5-11 (a) Measured pulse and spectra for a DRAM with 1 mm diameter voids (b) Photograph of sample (c) Reconstructed image at 4 ps and 0.65 THz, respectively 71
5-12 THz image according to polarization direction for a flash memory with 1 mm diameter voids 74
5-13 THz image according to polarization direction for a flash memory with 2 mm diameter voids 75
5-14 THz image according to polarization direction for a DRAM with 1 mm diameter voids 76
5-15 Continuous THz source module based on directional coupler 78
5-16 Experimental Setup for measuring standard samples 78
5-17 The amplitude and phase signals measured on the ITO coated surface using a DC-based THz transceiver module 79
5-18 THz image obtained from ITO coated surface using DC-based THz transceiver module 79
5-19 THz image for standard sample using DC-based THz transceiver module (left) Coated surface (right) Void surface 79
5-20 Continuous THz Source module based on magic tee 81
5-21 Experiment setup and signal detection configuration 81
5-22 The amplitude and phase signals measured on the ITO coated surface using a magic-tee based THz Transceiver module 82
5-23 THz image obtained from ITO coated surface using magic-tee based THz transceiver module 82
5-24 THz image for standard sample using magic-tee based THz transceiver module (left) Coated surface (left) Coated surface (right) Void surface 82
5-25 Semiconductor chip inspection using CW THz wave 84
5-26 THz image measured by reflection method 84

Collection @ kmou

5-27	Simulation modeling to verify the propagation characteristics of THz waves in the multi-chip package by lateral inspection	86
5-28	Simulation results for THz propagation characteristics with or without voids and void sizes in a multi-chip package	87
5-29	THz power distribution measured on the line in figure 5-27	88
5-30	THz experiment setup for multi-chip package inspection using the lateral inspection method	90
5-31	THz a image obtained using the lateral inspection method for two voids in a multi-chip package	91
5-32	The amplitude and phase signals measured when a THz wave passes through a layer with a diameter of 1 mm	92
5-33	Contrast stretching transformation	94
5-34	THz image for amplitude and phase versus input power for a sample with a 1 mm void in the multi-chip package	94
5-35	THz image obtained by applying the contrast stretching transformation function to the amplitude image of Figure 5-31	95
5-36	The optical photo of the flour containing the foreign object. The inset is the top view of foreign objects before filling with the flour	97
5-37	The THz image according to flour thickness *t* and flour-to-probe distance *d*. (a) *t* =1.5 mm, *d* =0.5 mm (b) *t* =1 mm, *d* =0.5 mm (c) *t* =0.5 mm, *d* =0.5 mm (d) *t* =1.5 mm, *d* =1 mm (e) *t* =1 mm, *d* =1 mm (f) *t* =0.5 mm, *d* =1 mm	98

Collection @ kmou

List of figures

Table

4-1 Optical properties of coating material in standard sample 53

Collection @ kmou

Study on the Terahertz Nondestructive Testing Method for Multi-chip Package Inspection using a Resonant Slit-type Probe with Rounded Matching Structure

Kim Geun Ju

Division of electrical and electronics engineering
Graduate School, Korea Maritime and Ocean University

Abstract

This paper presents a terahertz (THz) non-destructive testing (NDT) method for multi-chip package (MCP) inspection. A resonant slit-type probe was used to obtain high resolution while using a source in the low Th frequency region for the Th inspection. However, the conventional resonant slit structure is difficult to manufacture due to the thin thickness of the slit, as well as the problem of increasing the change of the resonance frequency and the loss of reflection due to the thickness error of the slit.

A resonant slit-type probe with a rounded matching structure was proposed to improve the coupling efficiency while improving the slit thickness problem in the Th region. The proposed probe can reduce the resonance frequency change according to the thickness error while maintaining the high coupling efficiency despite the increase of the slit thickness. It is possible to reduce the FWHM by more than 40% by using the proposed structure than the conventional resonant slit structure in the foreign object detection simulation using the slit probe. A

Collection @ kmou

probe with a resonant frequency of 205 GHz using the proposed structure was fabricated by electroforming and compared with VNA measurement results and CST MWS simulation results. From the measurement results, it was confirmed that the proposed probe has a simple structure and high coupling efficiency.

Using the pulsed THz system, the transmission characteristics of the semiconductor chip according to the polarization direction were verified, and it was confirmed that the semiconductor inspection using the THz wave was possible. A continuous (CW) THz inspection system that can be applied to process inspection has been established. A THz transceiver module based on directional coupler and a THz transceiver module based on Magic-tee have been constructed. In addition, FPGA-based high-speed lock amplifiers have been built to improve detection rates for process inspections. Standard samples were used to verify the performance of the measurement system and probes. It was confirmed that the magic-based THz transceiver module is more suitable for defect detection. The probe structure fabricated using the proposed structure was able to detect defects of 100 μm, and the high - speed signal detection module was able to detect defects stably even at a sample moving speed of 1000 mm/s.

In the semiconductor chip inspection, a lateral inspection method has been proposed because the conductivity of the semiconductor surface is high. The CST Microwave Studio simulation confirmed that side inspection enabled void detection. A lateral inspection system was constructed and a void of 500 ㎛ in diameter in the multi-chip package was detected. In addition, a simple contrast-transformed image filter is applied to the detected image so that defects in the laminated structure can be easily discriminated. As a result, it is confirmed that THz wave system using the proposed probe is a new inspection tool for detecting voids of multi-chip package

KEY WORDS: Terahertz, Nondestructive Inspection, Resonant Slit-type Probe, Rounded Matching Structure, Multi-chip Package

Collection @ kmou

라운드 매칭 구조를 가지는 공진형 슬릿 프로브를 이용한 테라헤르츠파 비파괴 검사 응용에 관한 연구

김 근 주

한국해양대학교 전기전자공학부
공과대학원

요약문

본 논문에서는 다중 칩 패키지 검사를 위한 테라헤르츠 비파괴 검사 방법을 제시하였다. 테라헤르츠파 검사를 위해 저주파 영역의 테라헤르츠 광원을 사용하면서도 고해상도의 분해능을 얻기 위한 방법으로 공진형 슬릿 프로브를 적용하였다. 그러나 종래의 공진형 슬릿 구조는 슬릿 두께가 얇아 제작이 어려울 뿐만 아니라 슬릿 두께 오차에 따른 공진주파수 변화 및 반사손실(Return loss)이 증가하는 문제가 발생한다. 테라헤르츠파 영역에서의 슬릿 두께 문제를 개선하면서도 결합 효율을 높이기 위한 방법으로 둥근 정합 구조를 가진 공진형 슬릿 프로브를 제안하였다. 제안 된 프로브는 슬릿 두께의 증가에도 불구하고 높은 결합 효율을 유지함과 동시에 두께 오차에 따른 공진주파수 변화를 감소시킬 수 있다. 또한, 슬릿 프로브를 이용한 이물 검출 시뮬레이션에서 기존의 공진형 슬릿 구조보다 제안된 구조를 이용함으로써 반치폭 (FWHM)을 40% 이상 감소시킬 수 있었다. 제안된 구조를 적용한 공진 주파수가 205 GHz인 프로브를 전기도금 방식으로 제작하였으며, VNA 측정 결과와 CST MWS 시뮬레이션 결과와 비교하였다. 측정 결과로부터 제안된 프로브가 구조적으로 간단하면서도 높은 결합 효율을 가짐을 확인하였다.

Collection @ kmou

펄스형 테라헤르츠파 시스템을 구성, 반도체 칩의 편광 방향에 따른 투과 특성을 검증하여 테라헤르츠파를 이용한 반도체 검사가 가능함을 확인하였다. 공정 검사 적용이 가능한 연속형 테라헤르츠파 검사 시스템을 구축하였다. 방향성 커플러 (Directional coupler) 기반의 테라헤르츠파 송수신기 모듈과 매직 티 (Magic-tee) 기반의 테라헤르츠파 송수신기 모듈을 구성하였다. 또한, 공정 검사를 위한 검출 속도를 개선하기 위해 FPGA 기반의 고속 락인앰프 (lock-in amplifier)가 제작되었으며 반도체 표면의 도전성을 고려한 표준 샘플을 제작하여 측정 시스템과 프로브의 성능 검증을 위해 사용되었습니다. 매직 티 기반의 테라헤르츠파 트랜시버 모듈이 결함 검출에 더 적합함을 확인하였으며, 시스템을 이용한 프로브의 공간 분해능 검증 결과 100 μm의 공간 해상도을 가졌다. 또한, 고속 신호 처리 모듈을 이용하여 1000mm/s의 고속 이동 중에도 안정적으로 영상 검출이 가능함을 확인하였다.

반도체 칩을 이용한 검사에서는 반도체 표면의 높은 도전성으로 반사형 테라헤르츠파 시스템으로는 Void 검출이 어려워 측 방향(lateral) 검사 방식을 제안하였다. CST Microwave Studio 시뮬레이션을 통하여 측 방향 검사로 보이드 (Void) 검출이 가능함을 확인하였다. 측 방향 검사 시스템을 구성하였으며 적층 반도체 내의 직경 500 ㎛의 보이드를 검출하였다. 또한, 검출 영상에 간단한 콘트라스트 스트레칭 변환 영상 필터를 적용하여 프로브 구조에 따른 검출 신호를 개선함으로써 적층 구조 내의 결함을 쉽게 판별이 가능하도록 하였다. 결과적으로 제안된 프로브를 적용한 테라헤르츠파 시스템이 적층 반도체 내의 Void 검출을 위한 새로운 검사 방법임을 확인하였다.

키워드 : 테라헤르츠, 비파괸 검사, 공진형 슬릿 프로브, 라운드 매칭 구조, 다중 칩 패키지

Collection @ kmou

1. Introduction

1.1 Motivation

In recent semiconductor technology, a multi-chip package in which a plurality of semiconductor chips are stacked is commonly used to integrate chips in a small area in accordance with miniaturization and high density [1]. A die attach film (DAF) is most widely used as a method of chip stacking. The bonding process using the DAF can easily stack chips, but has a problem the voids frequently occur between the chips during stacking. In particular, the generated void is a major cause of chip crack due to thermal expansion due to device operation. Therefore, void inspection is becoming important during the semiconductor chip package process. Ultrasonic inspection is the most widely used method for void inspection, but ultrasound inspection can not be reused due to invasion problems during underwater inspection [2]. IR inspection is impossible due to the absorption rate of polymer materials in semiconductors [3]. X-ray inspection has high

Collection @ kmou

resolution, but low-density samples are almost impossible to detect. Further, there arises a problem that the semiconductor operation voltage is changed due to the ionization of the semiconductor material by the X energy [4]. Due to these problems, a new inspection technique capable of conducting full inspection without destroying semiconductors is required.

Terahertz (THz) wave technology is emerging as a new test tool in many areas [5-12]. In particular, non-contact, non-destructive and non-invasive testing is expected to be useful in areas where stringent and safe testing is required, such as semiconductors, food and pharmaceuticals. The low photon energy of the THz waves does not ionize the material. In addition, the wavelength is short and high spatial resolution can be obtained. Above all, THz waves are considered as an ideal source for semiconductor inspection due to their high transmittance to semiconductor materials such as silicon, polymers [13-16]. Also, the sensitive phase change of the THz wave at the boundary of the medium is very useful for finding various semiconductor defects such as cracks and voids. Despite this advantage, the focused beam is limited in finding small defects in the semiconductor due to the diffraction and dispersion of the THz wave. And, the output power is reduced as the THz source frequency increases [5]. Also, as the sensitivity of the detector is lowered, the signal-to-noise ratio (SNR) of the detection signal is remarkably reduced. Therefore, in order to apply THz technology to the field of semiconductor inspection, continuous (CW) THz wave in the low frequency region must be used in order to secure the output for semiconductor transmission, detection sensitivity of the detector and the detection speed required for the process inspection. It is essential to develop a high resolution THz probe capable of detecting voids using a low frequency CW THz source and a signal processing system that improves

Collection @ kmou

detection speed in a inspection system using a high resolution THz probe.

1.2 Outline

Recently, the resonant slit structure has been proposed as a probe that can be used in the THz region due to its high transmission efficiency, linear polarization and spatial resolution using a small slit structure. However, in order to obtain a high coupling efficiency in the slit structure of the THz region, a thin slit thickness must be maintained. A stepped or tapered matching structure is proposed to improve the slit thickness, but it is difficult to apply to the narrow waveguide of the THz region.

In this paper, a modified resonant slit type probe with a rounded matching structure at the inner edge of the slit is proposed to improve the conventional resonant slit probe. The proposed resonant probe has less return loss because of its thick slit thickness with an impedance-matching structure to detect signal. The return loss and the variation in the resonant frequency according to the change in the matching structure using commercial simulation tools was calculated. The proposed probe with a resonant frequency in THz region was fabricated by the electroforming method and return loss was measured using a vector network analyzer. In addition, a reflective THz imaging system with a fabricated THz probe was established. The performance of the THz probe was also verified by measuring the THz image of the sample with various defects. As an approach to industrial application of THz wave technology, the proposed probe was used to verify the void detection in the stacked semiconductor package.

Collection @ kmou

In Chapter 2, current inspection technology and their limitations in the semiconductor field are introduced, and the advantages and challenges of semiconductor inspection technology using THz wave are reported.

In Chapter 3, the design of resonant slit-type probe for use in the THz region and the characteristics of resonant slit-type probes are investigated. The fabrication process of the proposed resonator slit-type probe is described and the transmission characteristics of the THz wave using a vector network analyzer (VNA) are investigated for the fabricated probe.

In Chapter 4, a CW THz imaging system with a proposed probe is presented. The CW THz source, CW THz detector, and the FPGA based on fast lock-in amplifier for the imaging system are described. The components of the CW THz system for semiconductor inspection and the structure of the reflective CW THz imaging system based on the THz transceiver module is described.

In Chapter 5, the transmission characteristics of pulsed THz waves are investigated according to the type of semiconducting sample and the polarization direction of each sample. Also, for the optimization of the semiconductor inspection module using CW THz wave, the reflection signal for the standard sample is investigated for CW THz system based on directional coupler and CW THz system based on magic tee. Also, the performance of the inspection system according to the moving speed of the sample is verified. A lateral inspection method is proposed for laminated semiconductor package inspection and the propagation characteristics of the proposed structure is analyzed. The possibility of void inspection in semiconductor using lateral inspection method is verified and image improvement method by applying image filter is suggested. A conclusion is presented in Chapter 6.

Collection @ kmou

2. Background

2.1 Multi-chip package inspection technology and their limit

In recent semiconductor technology, a structure for stacking several chips according in accordance with the demand for miniaturization and high density is becoming common [1]. However, when the chips are stacked, voids are generated between the chip and the dia attach film (DAF) used as the adhesive material. Voids are expanded due to heat generated during operation of the device, so that cracks are generated in the chips. Therefore, in order to avoid such a problem, the void inspection inside the chip must be performed in advance.

2.1.1 Multi-chip package inspection using ultrasound

The ultrasonic wave is transmitted through the object to be inspected using the directivity of the ultrasonic wave and the ultrasonic holography is used

Collection @ kmou

to irradiate the transmitted pulse or the reflected pulse. In particular, ultrasonic waves can be transmitted through various media such as metals and liquids using transcription in media, and their use is very broad. Recently, development of small size, high sensitivity, and high sensitivity ultrasonic transducer has been able to detect objects of several tens of nanometers, and various inspection equipments using this are being developed. In particular, it is most widely used for inspection of defects in semiconductor chip because there are few restrictions on the medium [2]. However, as is well known, in the case of ultrasonic inspection, a medium for ultrasonic transmission in a semiconductor chip is required. Most of the water is used as an ultrasonic transmission medium and inspection is done in a water tank. However, most tested samples are quashed due to the use of water due to semiconductor chip flooding problems. Also, the defect size, the direction of the ultrasonic beam and the frequency of the ultrasonic source are important.

2.1.2 Multi-chip package inspection using infra-Red (IR)

Due to the development of high-sensitivity IR camera, IR application range has been expanded in various tests such as defect inspection and peeling test in composite materials. Harmless to the human body, CMOS-based detectors can be used in a variety of industries because they can measure large areas with very short measurement times. The IR inspection method is a method of converting the amount of change in infrared energy emitted from a defect or sample skin or an imperfect part of the interior into an electrical signal. It can measure a variety of physical properties such as degradation diagnostics, strength and stress as well as imperfections through imaging [3].

Collection @ kmou

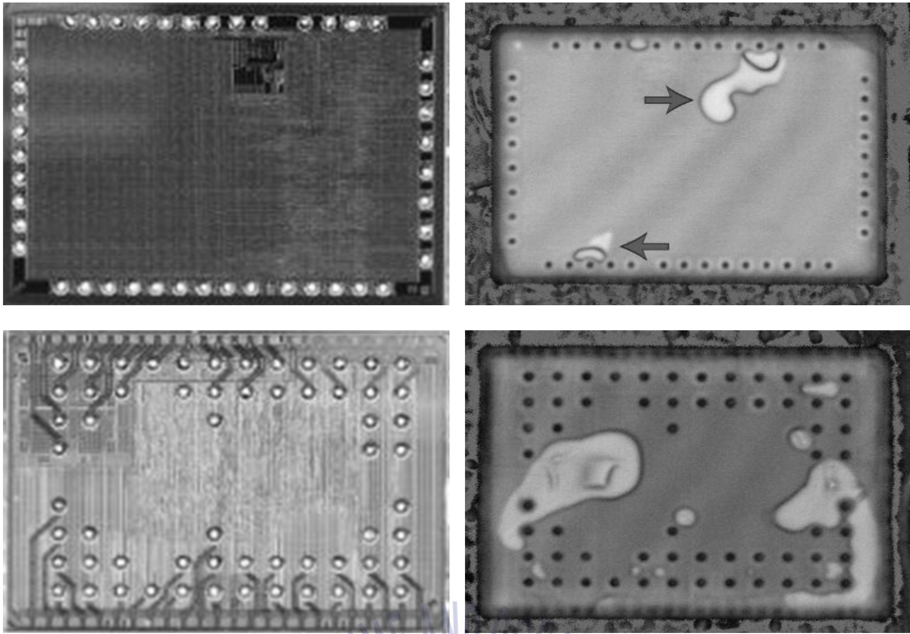

Figure 2-1 230 MHz acoustic image of an underfilled memory die (Upper) & the DSP die(Bottom)

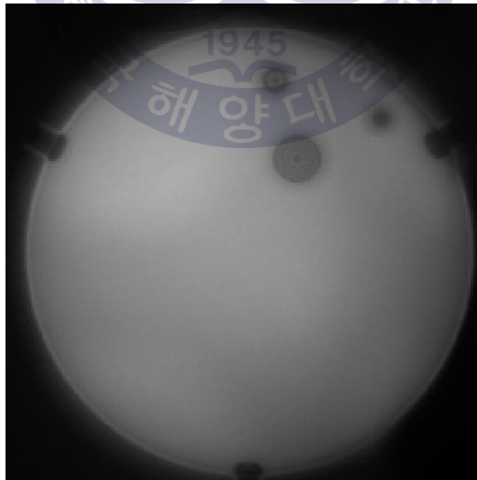

Figure 2-2 IR image of bonded wafer pair showing particle generated voids

Collection @ kmou

However, the background noise should be removed so that the emissivity changes according to the surface condition. And it is affected by absorption and scattering in the propagation pathway. Because of the high adsorption of plastics and polymers widely used in semiconductor package materials, package samples can not be measured and transmitted images are not suitable for defect inspection due to poor image quality.

2.1.3 Multi-chip package inspection using X-ray

X-ray inspection technology is widely used in a variety of fields such as food, security, machinery, electrical and electronics, and medical. In particular, X-rays have high transmittance and linearity, and the accuracy of the results is very high. X-ray inspection technology is a method to measure the intensity change of radiation according to the density gradient inside the sample, and it is expanding the application range by combining with the latest 3D tomography technology in existing 2D image. In semiconductor chip inspection, various inspections such as deviation, density and structural deformation are possible as well as short-circuit and disconnection inspection of internal wires in semiconductor chip [4]. In recent years, the importance of X-ray inspection technology has grown as semiconductor chip structures become smaller, smaller and more complex. In addition, by developing a 2D digital image sensor, various algorithms using it, and various measurement techniques, it is possible to realize resolution of nanometer size. However, it is difficult to distinguish between thin and low density defects such as voids, as well as changes in the energy level of the semiconductor material by X-ray energy.

Collection @ kmou

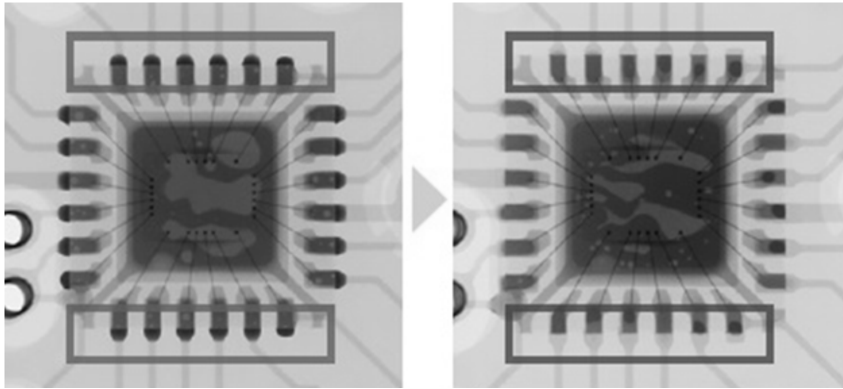

Figure 2-3. Failed QFN (quad-flat no-lead) joint connections due to lack of solder paste

KOREA MARITIME AND OCEAN UNIVERSITY 1945

2.2 THz inspection technology

2.2.1 Advantages of THz inspection technology

Terahertz (THz) technology has emerged as a new tool in various fields such as information and communications, biology and medical, security, quality control, etc [5-12]. Non-contact, non-destructive and non-invasive inspection using THz technology is suitable for stringent and safety inspections such as semiconductor, food and pharmaceuticals. In particular, the high sensitivity of THz to water molecules and the high transmittance of various materials are increasing the potential of THz waves in various fields [13-16]. The THz wave has high transmittance for opaque materials in visible light areas such as wood, paper, ceramics, plastics, silicon, and cloth. Among them, high transmittance to semiconductor materials such as silicon,

Collection @ kmou

polymers and the like is considered as the most ideal light source in semiconductor chip inspection. Both the polymer and silicon have refractive indexes in the THz region that are constant along the frequency and absorption coefficients of less than 5 [17-21].

In semiconductor chip inspection, the sensitive phase change of the THz wave at the intermediate boundary is very useful for finding various defects such as void, crack, and delamination [5],[22-25]. And, the low photon energy of the THz wave does not ionize the material, unlike x-rays. In addition, the size of the defects considered in semiconductor chip inspection is often in the range of tens of micrometers to several millimeters, similar to the wavelength of THz waves.

THz waves can achieve high spatial resolution, perspective imaging in the shortest wavelength band with material transparency on the electrical surface. Further, since the optical characteristics are similar to those of light, highly integrated THz image systems can be realized by using optical components

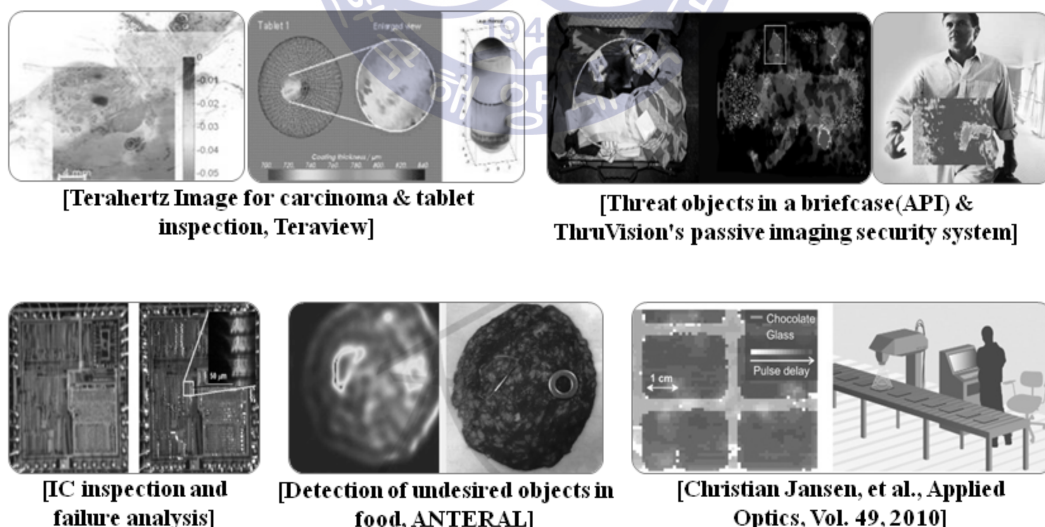

Figure 2-4 Applications of THz wave

Collection @ kmou

such as optical lenses and reflectors. Also, the magnitude and phase of the signal vary in various optical characteristics such as transmittance, absorptivity, refractive index, and dielectric constant depending on the type of the medium. The THz wave propagation has a sensitive phase shift at the boundary of the sample. In addition, the time resolution due to short pulses can be distinguished from the position of the sample as well as the defect size.

As THz sources, laser based pulsed THz sources and CW THz sources using QCLs, vacuum electronics and frequency multipliers are widely used. CW THz sources using vacuum electronics and frequency doublers are being adopted as sources for THz applications because of their small size and high power. In the case of THz detectors, there are Schottky diodes for CW

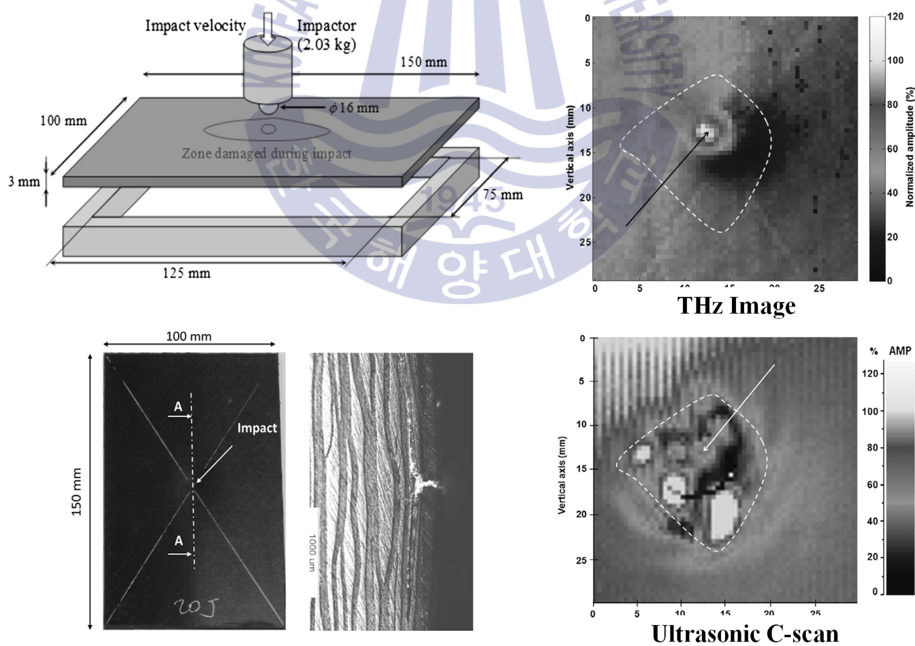

Figure 2-5. Falling weight impact testing system and sample(Left) THz reflection image and ultrasonic C-scan (Right) [26]

Collection @ kmou

detection, Pyroelectric and bolometers, and Photoconductive antenna (PCA) and electro-optic (EO) sampling for pulse THz wave detection are currently the most widely used. The THz detection method using PCA has a high singlet-to-noise ratio of over 10,000: 1. The Schottky diode detector has a dynamic range of several tens of dB or more, so small signals can be easily detected. In recent years, THz imaging technology has moved beyond 2D imaging to 3D tomography. It is possible to use X-ray tomography technology as it is, but it is possible to construct 3D structure by using 2D phase measurement using THz wave phase information.

2.2.2 Issues in the applications of THz inspection technology

Generally, THz waves are distinguished as pulsed THz waves and CW THz waves depending on the shape of the emitted THz wave. The output power of pulsed THz wave is small but has high peak power and high SNR. In addition, the broadband frequency spectrum is included various information such as spectral information and phase change, and spectral information can be used to detect spectral images and defects. Although many laser-based compact systems have been developed in recent years, there are many problems to be solved in industrial applications and their application is very limited. In particular, because of the low average output limit of pulsed THz waves, it is difficult to apply to samples with high absorption rate.

On the other hand, CW THz wave has recently been actively developed by various compact and high output THz sources. Recent development of semiconductor-based CW THz wave devices has made it possible to develop compact systems. In addition, the schottky diode detector is compact and

dCollection @ kmou

highly sensitive, making it easy to optimize in industrial process environments. However, as the frequency of the CW THz wave increases, the output of the device sharply decreases, so the utilization rate is very low. In addition, as spatial resolution is determined by the frequency of use in measurement, a high-power, high-frequency THz source is required to improve image quality. However, there is no high frequency THz source available for process inspection.

As shown in Figure 2-6, various types of compact high-power CW THz sources are under development [5]. But, most CW high-power sources operate in the low THz frequency range and the frequency variation of the source is less than 10 GHz. These sources with low operating frequencies are inherently low in spatial resolution because the spatial resolution is typically determined by the wavelength. Nonetheless, high-power sources

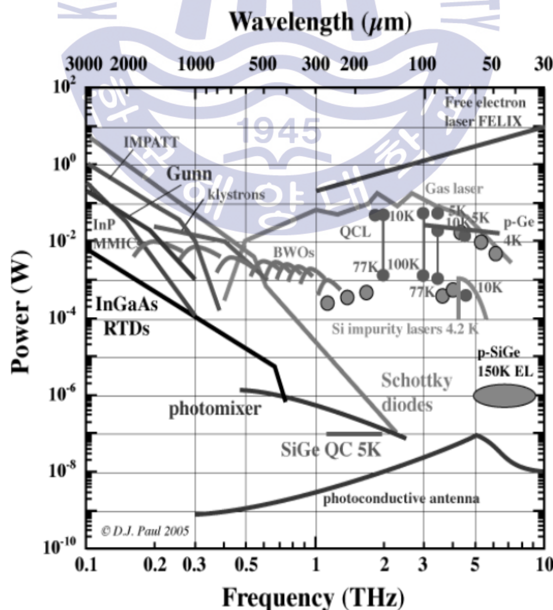

Figure 2-6 Comparison of available THz sources of high power

dCollection @ kmou

offer many benefits such as high transmittance for thick samples and large area scanning. Various methods to achieve high spatial resolution with a low frequency radiation source have been proposed.

Recently, a method for concentrating electromagnetic waves at a small tip end of a metal wire tip or using a small pin-hole has been proposed as a method for improving spatial resolution while using a low frequency. The probes with a small aperture or metal tips are widely used in many inspection applications because they use a simple structure to achieve high spatial resolution [27-28]. In particular, an extremely small aperture probes achieve spatial resolution on the nanometer scale [29-34]. However, an aperture probe experiences extreme power loss and a low signal-to-noise ratio (SNR). The metal wires has been proposed as a waveguide for the transmission of THz waves. A metal wire waveguide with a pointed end can focus the THz wave on the tip [29],[35-40]. However, due to the spherical THz radiation at the tip, the spatial resolution is drastically reduced as object moves away from the tip. In order to obtain high resolution in this structure, the object should be close to the aperture or tip. That is, these structures are not suitable for finding defects existing inside the semiconductor chip. As a recent alternative, a method using a waveguide directly used in the THz domain has been proposed, but the spatial resolution is determined by the waveguide size depending on the frequency.

In recent years, resonant slit-type probes have been proposed as suitable probes in the THz frequency range due to their simple structure, high coupling efficiency, and linear polarization. In particular, a slit height of less than λ/10 and a slit width of approximate λ/2 of the resonant slit-type probe can easily achieve high spatial resolution [41-43]. However, in order to obtain a high coupling efficiency at the slit of the THz region, the slit

Collection @ kmou

thickness must be maintained within only several tens of micrometers. A matched waveguide having a stepped or tapered structure has recently been proposed to couple the two waveguide having different dimensions to increase slit thickness and coupling efficiency. However, the waveguides with this matching structure are not suitable for resonant slit-shaped probes in the THz range. This is because the short wavelength of the THz wave increases the frequency shift and the return loss even if the waveguide changes its structure. It is also difficult to fabricate an accurate matching structure

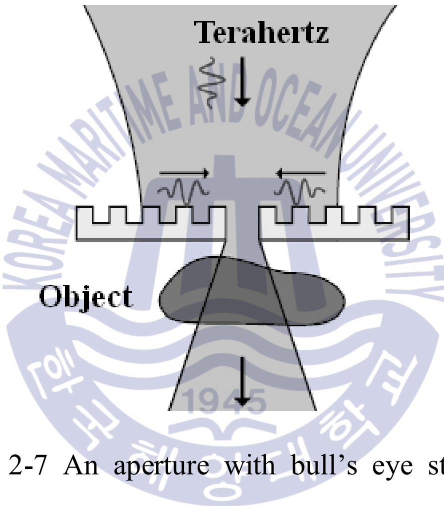

Figure 2-7 An aperture with bull's eye structure

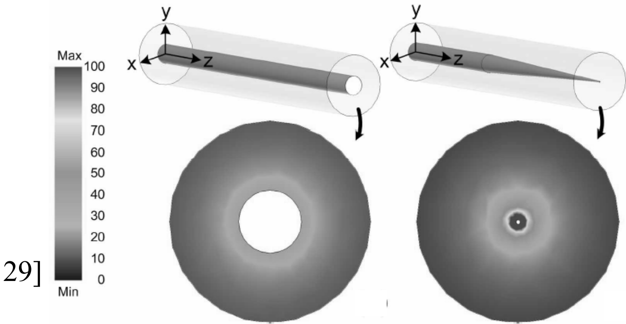

Figure 2-8 A needle probe with a metal wire waveguide [39]

dCollection @ kmou

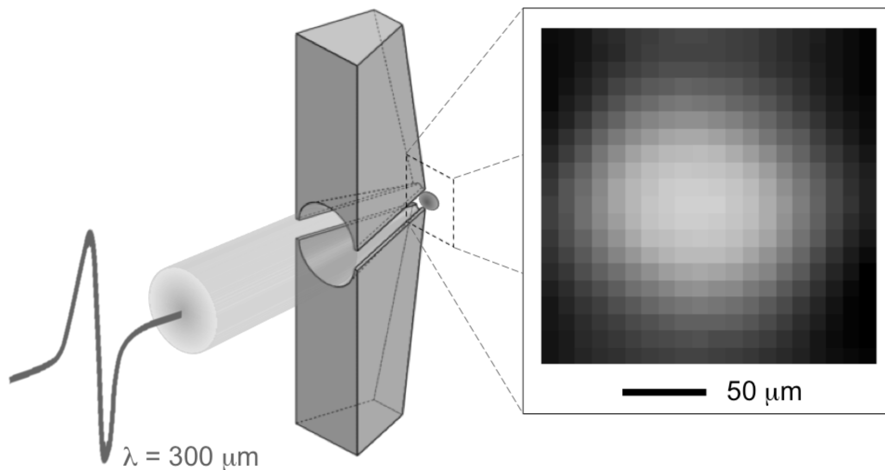

Figure 2-9 Schematic diagram of the split conical waveguide [40].

waveguide. In addition, if a sudden change in impedance occurs at the coupling portion of the waveguide, high coupling efficiency can not be expected due to reflection loss.

2.2.3 THz technology for multi-chip package inspection

A study on high-resolution images using a single resonant slit has been reported. When a resonant slit is installed at the end of a waveguide, most of the radio waves are transmitted through a thin slit, which is much smaller than the waveguide, and high-resolution images can be obtained. Further, the linear electric field of the resonant type slit can maintain a high transmittance for a sample having a polarization property.

The resonant slit-type probe is proposed for use in the THz frequency domain. It is proposed because of its simple structure, good coupling

Collection @ kmou

efficiency, and linear polarization. The slit probe has a metal slit aperture that has a height much less than the operating wavelength λ, and a silt width of about 0.5 wavelength. In particular, the resonant slit can theoretically bring the height of the slit close to 0 at a certain frequency and the output loss can be almost zero. However, in order to satisfy such a condition, it is necessary to keep the slit thickness in a thin film form. Even if a slit structure in the form of a thin film can be made, it is susceptible to high temperature, vibration and impact in an industrial environment.

In order to increase the efficiency of the coupling in the THz region, the thickness of the slit should be made as a thin film of several micrometers. Therefore, a stable structure for using the THz application must be accompanied. In recent years, a tapered matching waveguide or step matching structure has been proposed to improve coupling efficiency when coupling waveguides of different sizes. However, this structure requires a complex structure and a certain length to translate waves. If the impedance in the complex structure is not matched, it causes a sudden reflection loss inside. Also, As the length of the section increases, the ohmic loss on the metal surface increases.

In this paper, a resonant slit structure using a simple structure and an impedance matching structure with a short transition length is proposed. The characteristics of resonant slit probes are analyzed by simulation and the possibility of detecting voids in multi-chip packages using resonant slit probes is verified.

Collection @ kmou

Collection @ kmou

3. Resonant slit-type probe

3.1 Design of a resonant slit-type probe

3.1.1 Advantages of resonant slit-type probe

The long wavelength of the THz wave is a problem in semiconductor chip inspection to find small defects. Although many research groups have used pin-hole and wire coupled waveguide to obtain high resolution images in recent years, they can not be applied to thick samples with low signal-to-noise ratios (SNR) due to loss of output instead of high resolution. It also has a low detection capability for depth-wise fault detection. On the other hand, in semiconductor applications, it is important to satisfy high resolution and high transmission capability at the same time in order to maintain a high reception sensitivity for a defect existing within a certain thickness.

Collection @ kmou

Slotted antenna used with waveguide is a popular antenna in navigation, radar and other high-frequency systems. It is simple to fabricate, have low-loss (high efficiency) and radiate linear polarization with low cross-polarization. This antenna is often used in aircraft applications because they can be made to conform to the surface on which they are mounted. For slit dimensions, the thickness can generally be kept thinner than 0.1 of the wavelength (theoretically, with almost no limitations) and the slit width has about 0.5 of the center wavelength. In addition, it has a high linear polarization in the slit, allowing high transmittance for samples sensitive to polarization directions, such as semiconductor and carbon composites.

Figure 3-1 Photograph of flash memory chip

3.1.2 Theory of resonant slit-type probe

Figure 3-2 shows the equivalent circuit of the iris in a waveguide. The iris of the waveguide is largely regarded as three types of electrical circuits

Collection @ kmou

depending on the structure [42],[44]. Among them, one slit-shaped iris horizontally installed in the waveguide is an LC parallel equivalent circuit. The LC parallel circuit has resonance frequencies of L and C values. It is used as a high gain slit antenna by matching the impedance according to the load change of the device connected to the waveguide or by improving the transmission characteristics by using the narrow bandwidth according to the resonance characteristics.

Slit antennas are widely used (similar to linear wire antennas) because the polarization is linear and the radiation has an approximately omnidirectional radiation pattern. It also provides various design variables to adjust the performance, such as slit size, shape, and so on. The slit antenna is simple, robust and easy to fabricate. A thin slit in an infinite ground plane is the complement to a dipole in free space. Consider an infinite conducting sheet with a rectangular slit cut into dimensions a and b as shown in Figure 3-3. If the appropriate field of the slit can be excited, it can be a slit antenna.

Babinet's principle associates the radiation field and impedance of an aperture or slit antenna with the impedance of a dual antenna field. The dual structure of the slit antenna is when the conductive material and air are interchanged, that is, the slit antenna becomes a metal slab in space. An example of a dual antenna is shown in Figure 3-4.

Babinet's principle is related to these two antennas. The first result indicates that the impedance of the slit antenna (Z_s) is related to the impedance of the dual antenna (Z_c) by the following relationship:

$$Z_c Z_s = \frac{\eta^2}{4} \ , \ Z_s = Z_0 \frac{\pi b}{2a} \frac{1}{\sqrt{1-\left(\frac{\lambda_0}{2a}\right)^2}} \quad \text{---- (1)}$$

Collection @ kmou

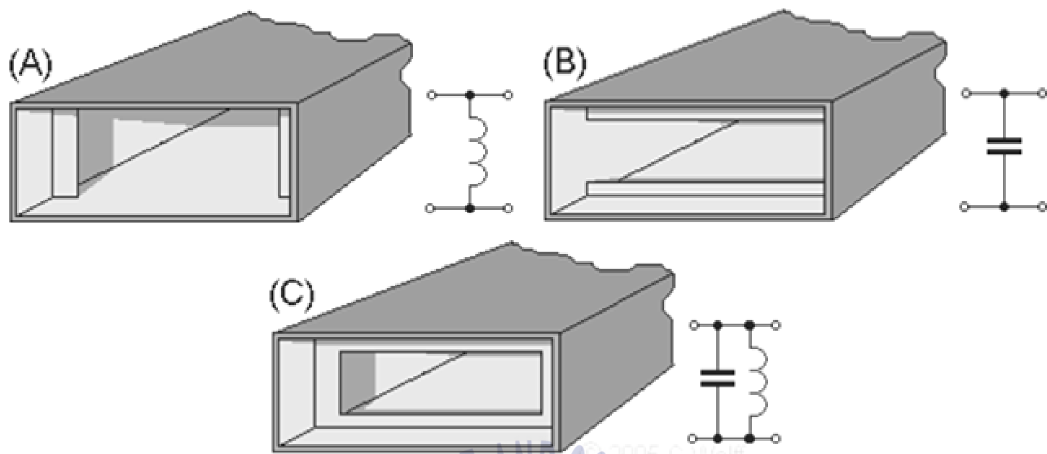

Figure 3-2 Equivalent circuit according to iris structure in waveguide

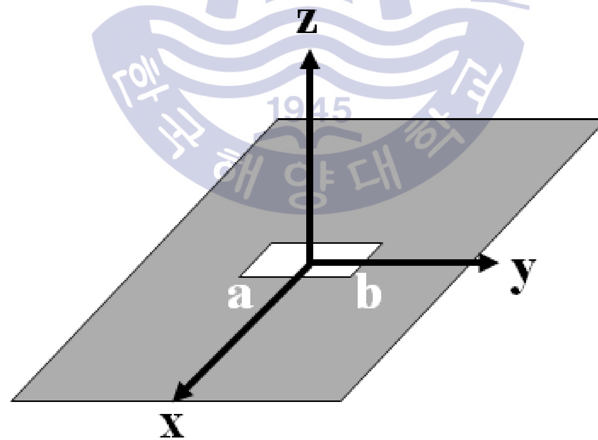

Figure 3-3 Rectangular slit antenna with dimensions a and b.

Collection @ kmou

where, η is intrinsic impedance $(\eta = E/H = \sqrt{\mu_0\mu_r/\epsilon_0\epsilon_r})$ and λ_0 is free space wavelength. Assuming that a narrow slit is installed at the end of the waveguide as shown in Figure 3-5, the maximum transmission is when the impedance of the waveguide matches the slit.

From the above equation (1)

$$Z_0 \frac{\pi b}{2a} \frac{1}{\sqrt{1-\left(\frac{\lambda_0}{2a}\right)^2}} = Z_0 \frac{\pi b'}{2a'} \frac{1}{\sqrt{1-\left(\frac{\lambda_0}{2a'}\right)^2}} \quad \text{------ (2)}$$

and

$$\frac{a}{b}\sqrt{1-\left(\frac{\lambda_0}{2a}\right)^2} = \frac{a'}{b'}\sqrt{1-\left(\frac{\lambda_0}{2a'}\right)^2} \quad \text{--------(3)}$$

That is, in the above condition, the slit becomes transparent. For $b' \rightarrow 0$ equation (3) yields $\lambda = 2a' - (b'/b)^2(a^2/a' - a')$. This means that even a very narrow slit is transparent at a certain wavelength [42].

3.1.3 Resonant slit-type probe for THz wave

The above condition is satisfied in a slit having a thickness of 0 (= 0). In other words, the slit thickness is not considered. If the wavelength of the operating frequency is much smaller than the slit thickness, the influence of the slit thickness can be ignored. However, since the wavelength is short in the THz region, the influence of the slit thickness can not be ignored.

Collection @ kmou

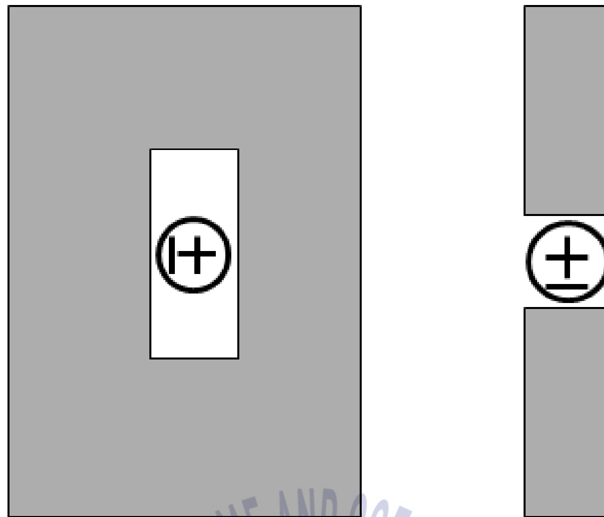

Figure 3-4 Dual antennas - (left) the slit antenna, (right) the dipole antenna.

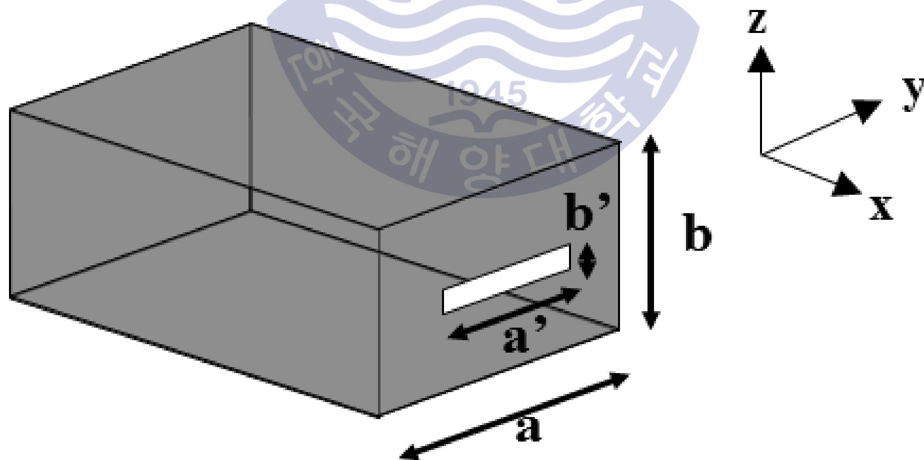

Figure 3-5 Slit antenna attached rectangular waveguide

dCollection @ kmou

In a conventional resonant slit type probe, resonance changes with slit thickness variations were calculated. Several parameters for numerical analysis were fixed. First, an input waveguide defined a rectangular structure, and the slit height was fixed at 1/10 of the wavelength of the resonant frequency. The simulation was performed using the commercial software CST Microwave Studio (MWS), which was used with a waveguide excitation port, 40 mesh lines per wavelength and an accuracy of -40 dB. It is assumed that the resonance slit type probe has a rectangular structure operating at a center frequency of 200 GHz. The input waveguide used was a standard WR-5 [1.3 mm (w) × 0.65 mm (h)] rectangular structure with a bandwidth from 140 to 220 GHz. The width and height of the slit were fixed at 150 (= λ/10) and 740 μm (=λ/2), respectively. In the resonant slit-type probe, the slit height, slit width, and slit thickness can represent the equivalent circuit of the LC coupling. If the slit height is fixed, there is a slit thickness corresponding to the slit width in order to obtain the optimal transmission efficiency [45].

Figure 3-7 shows the frequency as a function of slit thickness when the radio waves are radiated to the outside through the slit. The calculated minimum return loss of the designed resonance probe is -68 dB at the frequency of 199.1 GHz, and then the slit thickness is 90 μm. As a result, the resonance frequency shifts and the reflection loss increases at the same time even when the slit thickness is slightly changed. This change in resonance frequency shift and return loss is caused by a change in induction susceptance value corresponding to the slit thickness [45]. Therefore, to maintain high coupling efficiency at the probe tip, a slit thickness that is appropriate for height and width should be considered.

Collection @ kmou

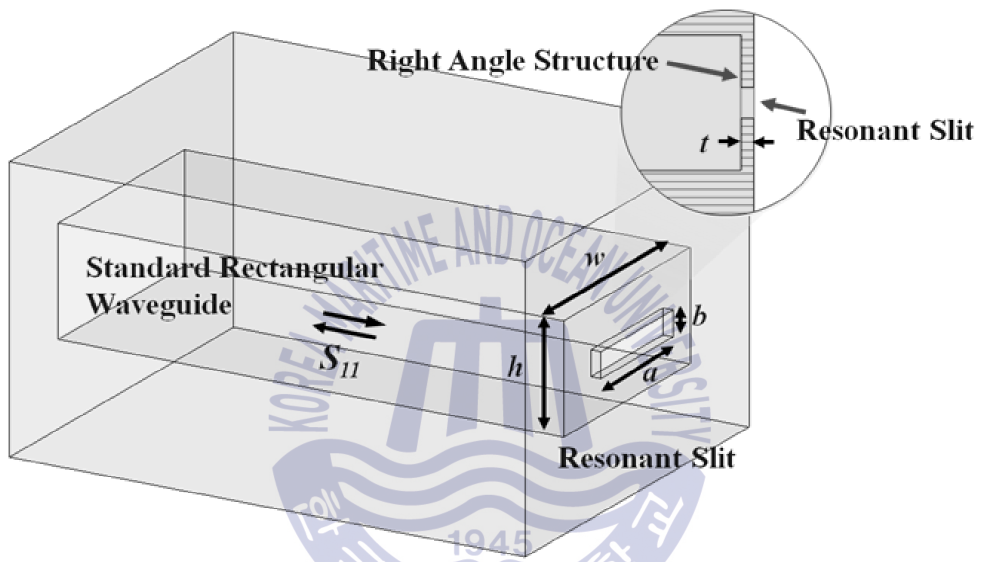

Figure 3-6 Schematic of the resonant slit-type probe with right angle structure. The inset shows the cross-sectional view at the slit.

Collection @ kmou

3.1.4 Matching structure of resonant sit-type probe

A slit waveguide with a tapered or stepped matching structure has been recently proposed to increase the coupling efficiency by combining waveguides with different dimensions [46-48]. Tapered Resonant Slide Waveguide is a method to increase transmission efficiency by minimizing reflection loss due to sudden impedance change by using taper part of a certain length. Meanwhile, the stepped resonator slit waveguide uses a multi-stage impedance matching structure to reduce the internal reflectance. However, a tapered or stepped matching structure probe results in a sudden return loss if the impedance matching in the coupling section is not met. Therefore, in order to use the slit probe in the THz region, a coupling structure is required which has a high coupling efficiency and minimizes the shift of the resonance frequency.

3.2 Resonant Slit-type Probe with Rounded Matching Structure

3.2.1 Resonant Slit-type Probe with Rounded Matching Structure

Figure 3-9 is a schematic diagram of a new resonant slit-type probe structure with a round matching structure proposed in this paper. The proposed resonant probe consists of a round transformer at the inner edge to enable impedance matching between the waveguide and the resonant slit. The matching structure is designed in the form of a quarter cylinder of radius r, which is simple in structure and can be easily fabricated with a

Collection @ kmou

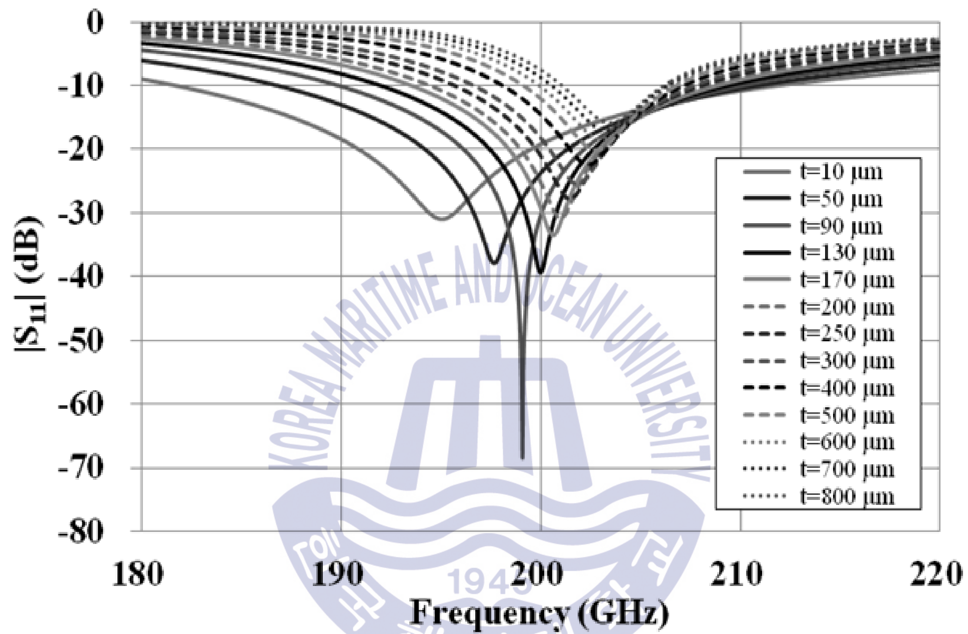

Figure 3-7 Return loss according to the slit thickness for the resonant slit-type probe with right angle structure when a = 150 μm and b = 740 μm.

Collection @ kmou

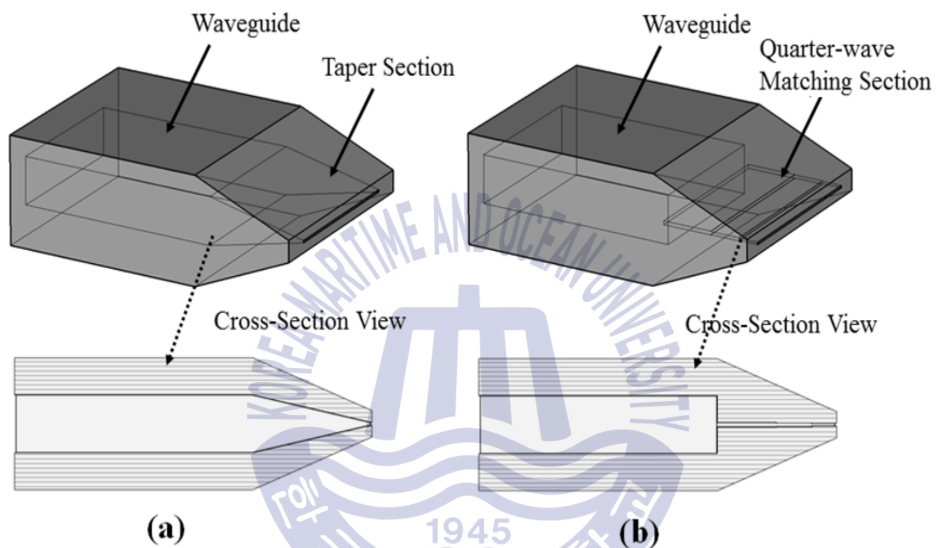

Figure 3-8 Schematic diagram of tapered Resonant slit waveguide(left) and Stepped Resonant slit waveguide(right)

Collection @ kmou

spherical tip. The characteristics of the proposed resonant slit type probe were analyzed using CST simulation tool. Considering the CW THz source, a resonant slit type probe with a resonant frequency of 200GHz is designed.

Figure 3-10 shows the resonant frequency shift according to the slit thickness of the resonant slit type probe. The height and width of the slit are fixed at 150 μm and 740 μm, respectively. The optimal slit thickness of the conventional resonant slit-type probe with right angle structure was 90 μm. On the other hand, the slit thickness of the resonant slit-type probe with the proposed matching structure was increased to 290 μm at r = 100 μm and 730 μm at r = 200 μm. As a result, the slit thickness of the proposed resonant slit-type probe is 3.2 and 8.1 times thicker than that of a right angle structure for r = 100 and r = 200, respectively. The advantage of the proposed resonant probe is that it has low return loss due to thick slit thickness and gradual matching impedance due to the round matching structure. Particularly, the shift of the resonance frequency with the change of the slit thickness is remarkably reduced. The resonance frequency of about 640MHz was shifted in the conventional slit-type resonant probe if the thickness error of 20 μm occurred in the slit of the same structure. But, by applying the proposed matching structure, the shit of the resonant frequency is reduced to 280 MHz at r = 100 μm and 80 MHz at r = 200 μm, respectively. By applying the proposed structure, it is confirmed that the resonance frequency shift can be minimized even though there is little return loss. Also, as the radius of the matching structure increases, the shift of the resonance frequency with respect to the thickness error is reduced.

Figure 3-11 shows the reflection signal according to the scanning position in the right angle slit and the round matching slit when detecting metal foreign object using resonant slit type probe. The diameter of the metal ball

dCollection @ kmou

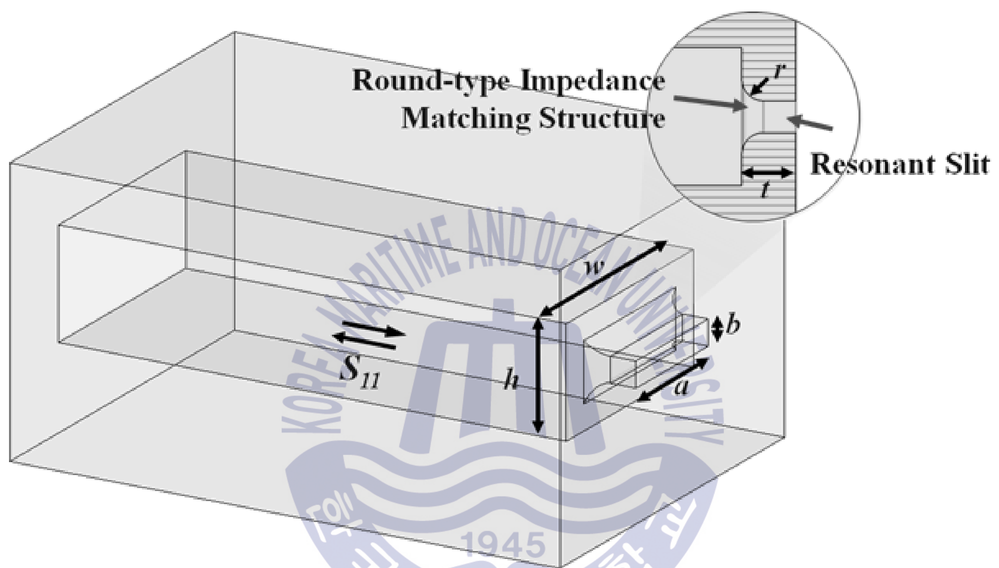

Figure 3-9 Schematic of a resonant slit probe with a rounded matching structure. The inset shows the cross-sectional view at the slit.

Collection @ kmou

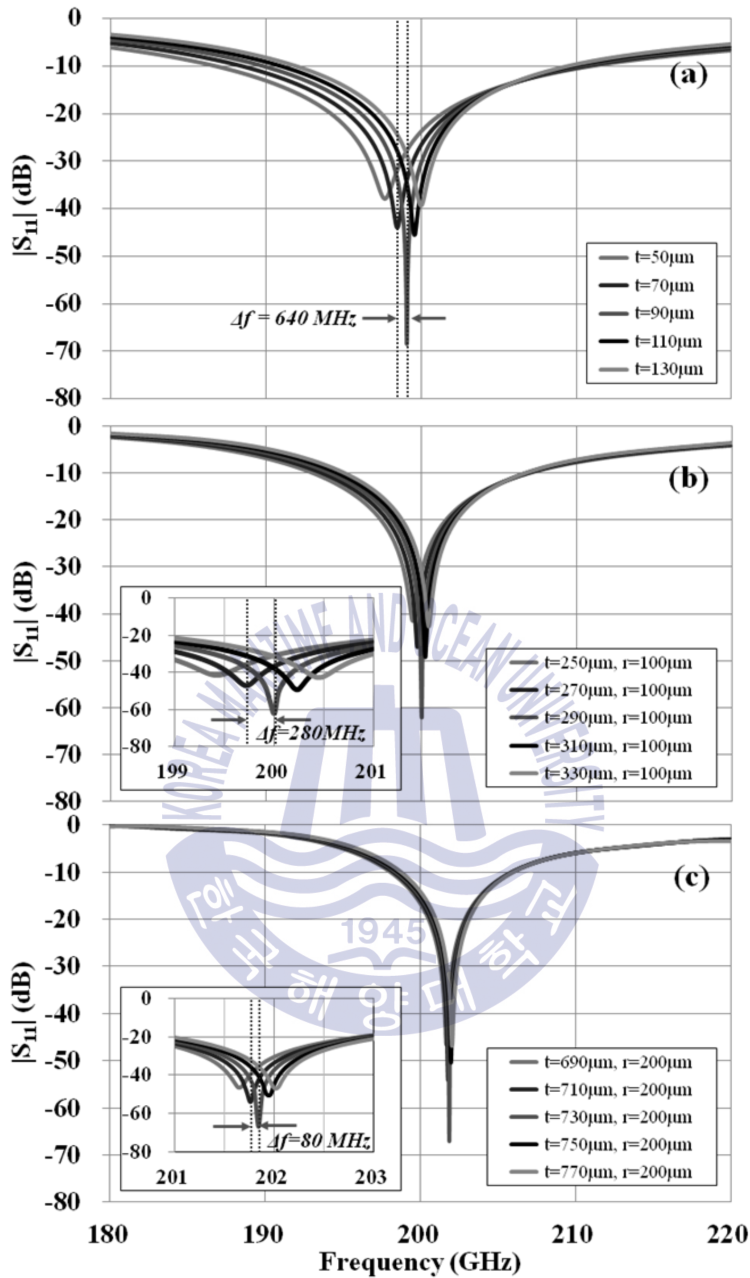

Figure 3-10 Shift of the resonant frequency according to slit thickness for a resonant slit-type probe (a) with right angle structure (b) with rounded matching structure of 100 μm and (c) 200 μm. The height , and width of the slit were fixed at 150 μm and 740 μm, respectively. The insets show the expanded resonant frequency.

Collection @ kmou

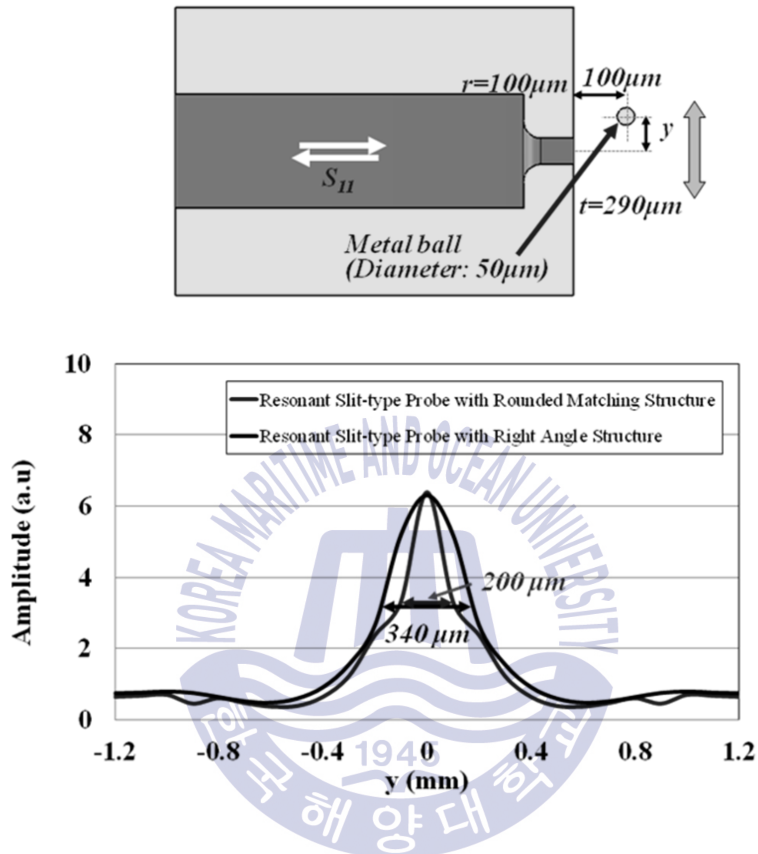

Figure 3-11 A reflection signal according to a scanning position when a metal foreign objects is detected using a resonant slit-type probe with right angle structure slit of a = 740 μm, b = 150 μm and t=90 μm and a resonant slit-type probe with rounded matching structure of a = 740 μm, b = 150 μm, t= 290 μm, and r = 100 μm.

Collection @ kmou

was fixed to 50 μm and the distance from the probe to 100 μm . The resonant frequency is changed by an object in front of the slit. Particularly, when the object is located in the middle of the slit, the reflectance increases due to the movement of the resonant frequency by the object. In other words, when the resonant probe moves in the y direction, the amplitude of the sensed signal is at zero, which represents the metal ball located at the center of the slit gap. The proposed resonant probe can improve the resolution because the thick slit carries only the reflected wave from the object at a narrow angle to the waveguide. As a result, the full width at half maximum (FWHM) detected by the rounded matching structure slit is 140 μm smaller than the FWHM by the right angle structure slit. The simulation results show that the proposed probe can detect signals more sensitively than resonant slit-type probes with right-angled slits.

3.2.2 Fabrication of Slit-type Probe with Rounded Matching Structure

To verify the characteristics of the proposed resonant probe, a resonant probe with = 740 μm, = 150 μm, = 290 μm, and = 100 μm closest to the resonant frequency of 200 GHz was designed. The resonant probe was fabricated using the electroforming technology to build a rounded matching structure inside the waveguide. The electroforming method uses soluble aluminum to make the mandrel corresponding to the internal structure, then electroplating to form the metal on the outside, and then to process the external structure. And finally, the internal structure can be precisely molded by removing the internal structure. Figure 3-13 shows the design and photograph of the fabricated resonant slit type probe. The fabricated probe is made of high conductivity copper and gold coated to minimize ohmic losses.

Collection @ kmou

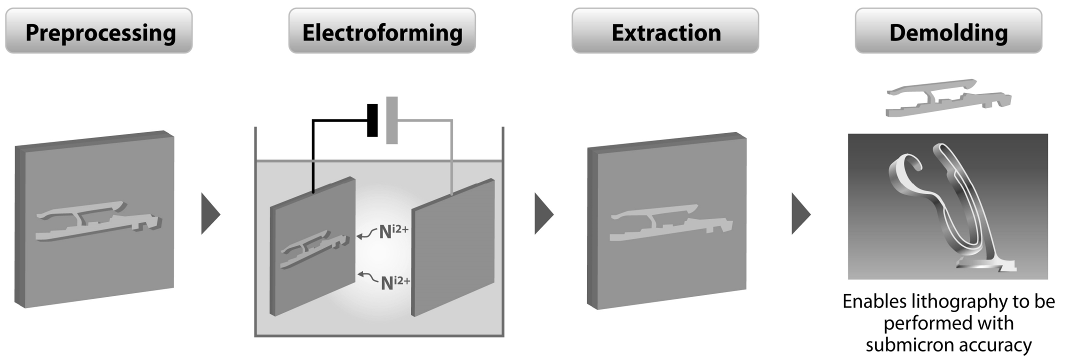

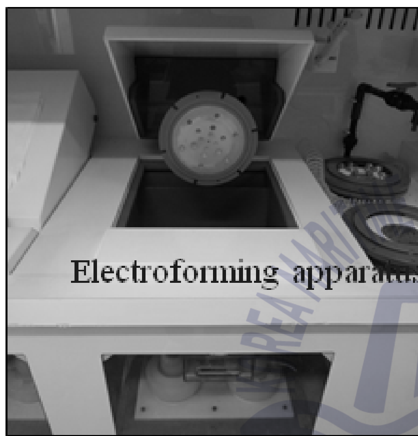

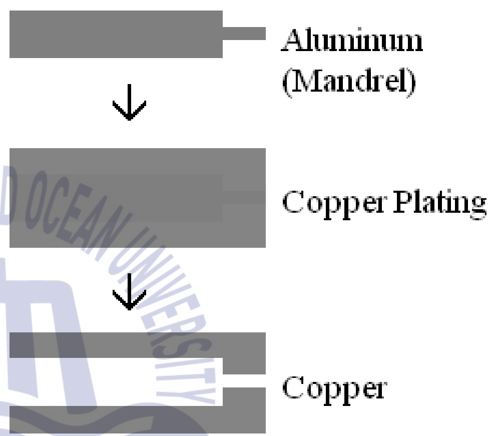

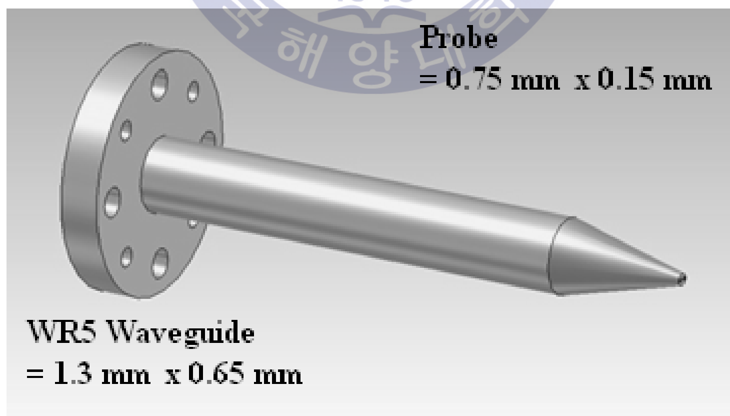

Figure 3-12 Electroforming process sequence (upper) and fabrication of resonant slit structure (bottom)

Collection @ kmou

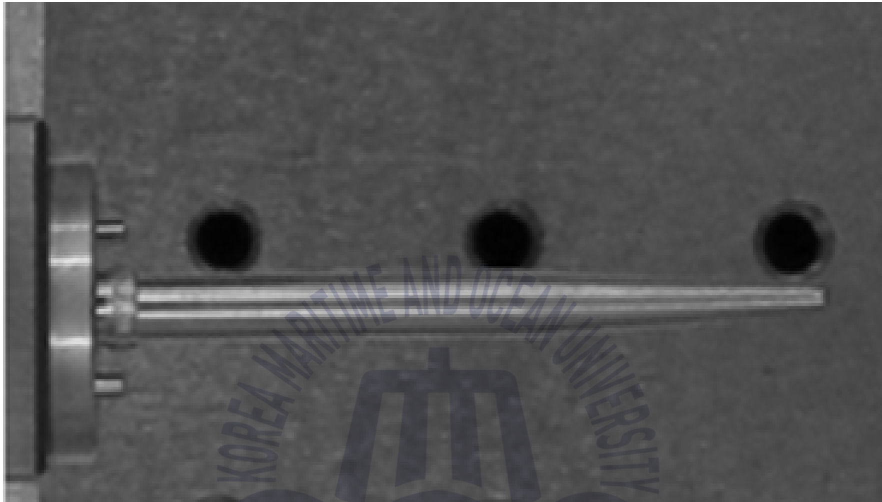

Figure 3-13 A resonant slit probe with a rounded matching structure manufactured by electroforming process

Collection @ kmou

3.2.3 Measurement of Slit-type Probe with Rounded Matching Structure

The slit width and height of the fabricated probe were 720 μm and 140 μm, which were as small as 20 μm and 10 μm, respectively, as shown in Figure 3-14(a). The resonance characteristics of the probe fabricated using VNA were measured. Figure 3-14(b) shows the results of the CST simulation of the designed resonant probe and VNA measurement results of the fabricated resonant probe. The resonant frequency of the probe was designed to be 200 GHz. However, the resonant frequency was measured at 205.3 GHz by the VNA. The shift in the resonant frequency is due to the reduced slit width and height in the fabrication.

The resonant frequency was recalculated using the dimension of the fabricated probe. The recalculated resonant frequency was 205.2 GHz which was almost identical to that of the measurement. Also, the return loss at 205.2 GHz increased from -62 dB to -41.3 dB as shown in Figure 3-14 (b). The measured return loss was -35.4 dB, which increased only 5.9 dB compared with the simulation. If the probe is a right angle structure slit, the optimal return loss is -31.9 dB at 205 GHz when a = 720 μm, b = 140 μm, and t= 130 μm. This result indicate that the proposed rounded matching structure slit has less return loss than the right angle structure slit.

Collection @ kmou

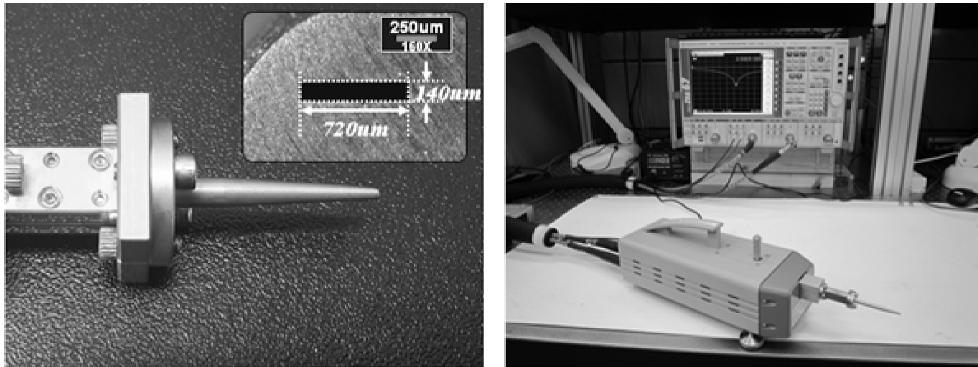

(a)

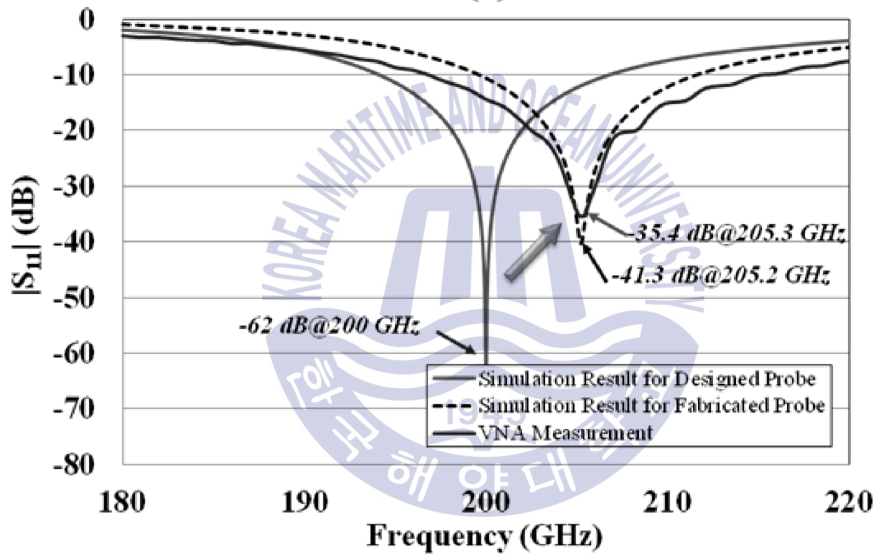

(b)

Figure 3-14 (a) Fabricated resonant probe with a rounded matching structure slit and experimental setup to measure return loss using the VNA. (b) Comparison of the VNA measurement values of and CST MWS simulation results of the designed and fabricated a resonant slit-type probe with rounded matching structure.

Collection @ kmou

4. Experimental Setup

Most semiconductor chips consist of solder balls, PCBs, chips, underfills for chip and chip connections, and Dia Attach Film (DAF). PCBs are mostly made of metal thin films, making it difficult to transmit electromagnetic waves. Therefore, for the semiconductor chip inspection, the module is basically constructed considering reflection type measurement.

Reflective measurement systems based on magic tees and directional couplers are well known as typical reflective structures using CW THz sources. The reflection measurement method using the magic tee has high detection performance by removing the reflection from the semiconductor chip surface and the inside of the probe, but it requires a little tuning. On the other hand, the reflection measuring method using a directional coupler has an advantage that the system configuration is simple, but there is a high signal offset due to the reflection on the semiconductor chip surface and the probe.

Collection @ kmou

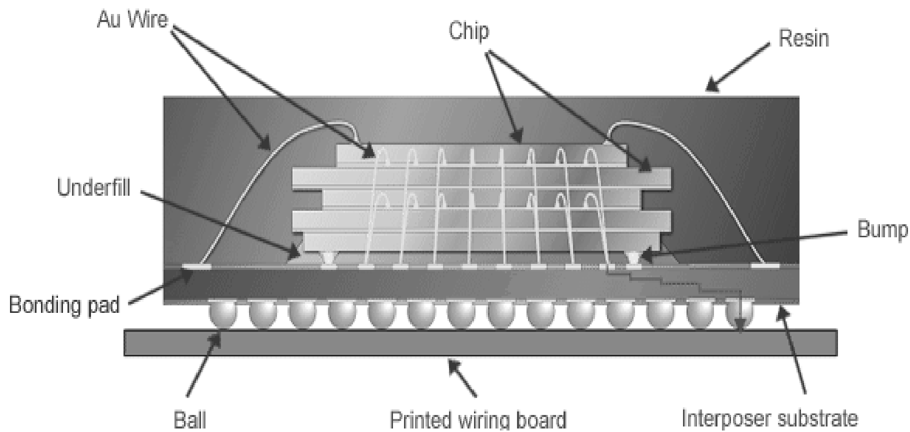

Figure 4-1 Schematic diagram of multi-chip package structure

4.1 Components for CW THz imaging system

4.1.1 CW THz source

There are various CW THz sources, THz source based on multiplier is used in this system. The THz source used has a center frequency of 200 GHz, an output of 70 W, and a frequency bandwidth of ± 4 GHz. In addition to TTL modulation as well as output control using voltage regulation, signal levels can be improved by lowering the SNR using lock-in amplifier-based signal acquisition. Also, high-speed modulation of THz wave is possible by using high-speed PIN switch. In this study, a high-speed lock-in amplifier based on field programmable gate array (FPGA) is constructed to enable high-speed measurement.

Collection @ kmou

4.1.2 CW THz detector

Recently, various kinds of CW detectors such as schottky diode, pyroelectric, bolometer, CMOS based detector have been developed. In this configuration, a schottky diode was used as the detector for detection sensitivity. Zero bias Schottky diode detectors have low noise equivalent power (NEP) of 2.0 or less and high detection sensitivity. The Zero bias detector used is a detector (WR5.1ZBD, VDI) with a low noise equivalent power (NEP) of 2.0 $pW/\sqrt{Hz}$ or less and a high sensitivity of 2000V/W.

Figure 4-3 shows the frequency response of the WR5.1ZBD detector and shows a response of more than 1500V / W at 140 GHz ~ 220 GHz.

In addition, the Schottky diode has high-frequency response characteristics even at high-speed modulation up to the GHz band, so it can be used for high-speed measurement.

Figure 4-4 shows that when the TTL modulation frequency is 10 kHz and 125 kHz, the measured signal has almost no phase delay even when the frequency increases. It is confirmed that the response characteristic is the same as the response characteristic used for signal amplification or TTL modulation frequency.

4.1.3 FPGA based on fast lock-in amplifier (LIA)

The lock-in amplifier is used to detect and measure very small signals. Accurate measurements can be made even if the small signal is covered by thousands of times the noise source. A lock-in amplifier uses a technique

Collection @ kmou

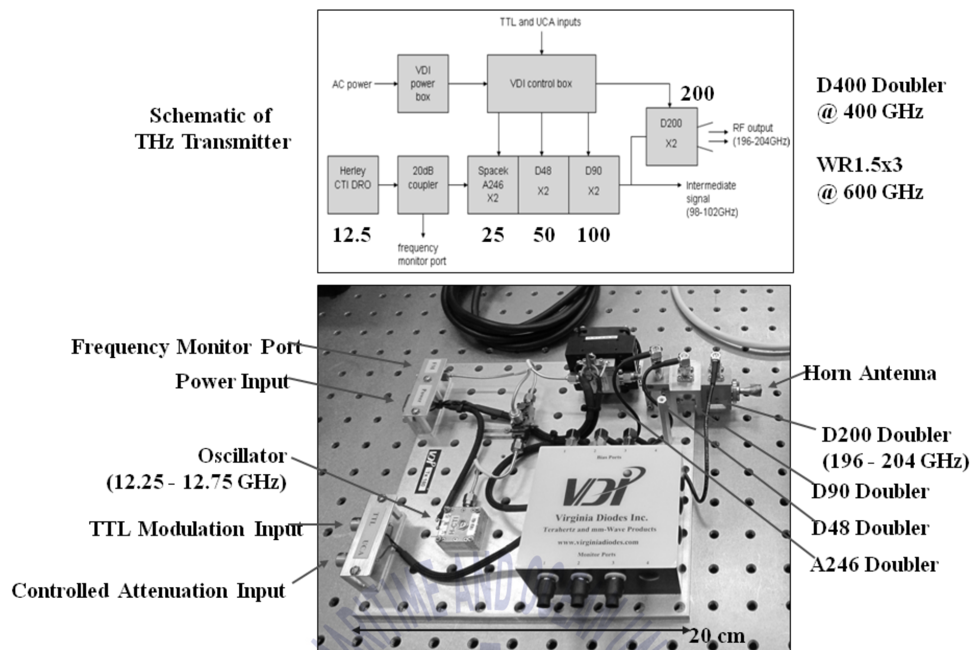

Figure 4-2 THz source module configured for high-speed & high-power operation

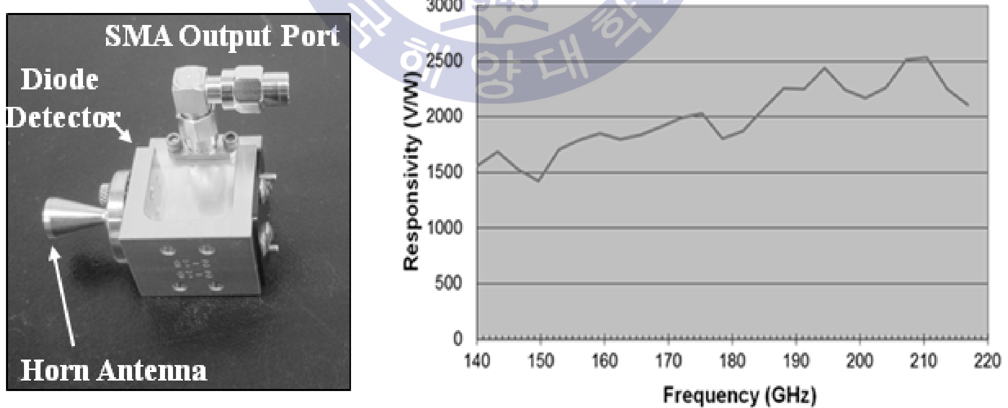

Figure 4-3 WR5.1ZBD Detector (VDI) and frequency-dependant responsivity

Collection @ kmou

known as phase-sensitive detection to extract the components of a signal at a specific reference frequency and phase. Noise signals at frequencies other than the reference frequency are rejected and do not affect the measurement.

If the sine output of the function generator is used as a reference signal to stimulate the experiment, the response can be a signal waveform as shown in figure 4-5. The signal is $V_{signal}\sin(w_r t+\theta_{signal})$ where V_{signal} is the signal amplitude, w_r is the signal frequency, and θ_{signal} is the signal's phase. Lock-in amplifiers generate their own internal reference signal usually by a phase-locked-loop locked to the external reference signal. The internal reference signal is $V_L\sin(w_L t+\theta_{ref})$. The lock-in amplifies the signal and then multiplies it by the lock-in reference signal using a phase-sensitive detector or multiplier. The output of the phase-sensitive detector (PSD) is simply the product of two sine waves.

$$V_{PSD} = V_{signal}V_L\sin(w_r t+\theta_{signal})\sin(w_L t+\theta_{ref})$$

$$= 1/2\, V_{signal}V_L\cos((w_r-w_L)t+\theta_{signal}-\theta_{ref})$$

$$-1/2\, V_{signal}V_L\cos((w_r+w_L)t+\theta_{signal}+\theta_{ref})$$

The PSD output is two AC signals, one at the difference frequency w_r-w_L and the other at the sum frequency w_r+w_L. If the PSD output is passed through a low pass filter, the AC signals are removed. And, if w_r equals w_L, the difference frequency component will be a DC signal. In this case, the filtered PSD output will be:

Collection @ kmou

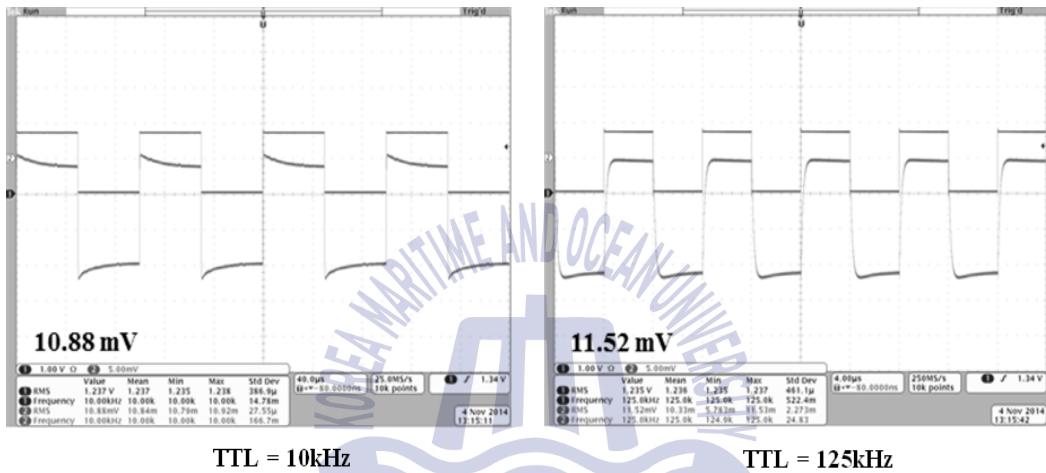

Figure 4-4 Detector response according to TTL frequency (a) TTL Frequency = 10 kHz, (b) TTL Frequency = 125 kHz

Collection @ kmou

$$V_{PSD} = 1/2\, V_{signal} V_L \cos(\theta_{signal} - \theta_{ref})$$

It is a DC signal proportional to the signal amplitude.

Typical commercial lock amplifiers have high dynamic range, but maintain high dynamic range, making them difficult to use in high-speed mode. Recently, a commercial lock-in amplifier that can be used in the high-speed mode has been developed, but it is not only costly, but also difficult to expand multi-channel. Recently, many commercial boards based on Field Programmable Gate Array (FPGA) have been developed. The FPGA board uses ns-level internal clock to enable high-speed sampling while synchronizing multi-channel measurement signals. In other words, you can simultaneously measure multiple signals from one module while simultaneously processing the signals. Figure 4-6 shows a schematic of an FPGA-based lock-in amplifier and sample measurement system. For high-speed signal measurements, the NI 5733R digitizer used 16-bit, 120 MS/s and 12 dB gain, and the lock amplifier was configured using the 7962 FPGA module.

To verify the performance of the FPGA-based lock-in amplifier, compare the signals with commercial lock-in amplifier (AMETEK 7265). AMETEK 7265 lock-in amplifier has an analog input range of 250 kHz. A 125 kHz sine wave is used as a reference signal for measurement. The performance was verified by reconstructing a 5 kHz analog modulated (AM) signal. The signal source is function / Arbitrary waveform generator (Agilent 33522A). To compare the performance of the lock-in amplifier, the X output auxiliary port was used for high-speed measurement and the response characteristic was measured according to the time constant.

Collection @ kmou

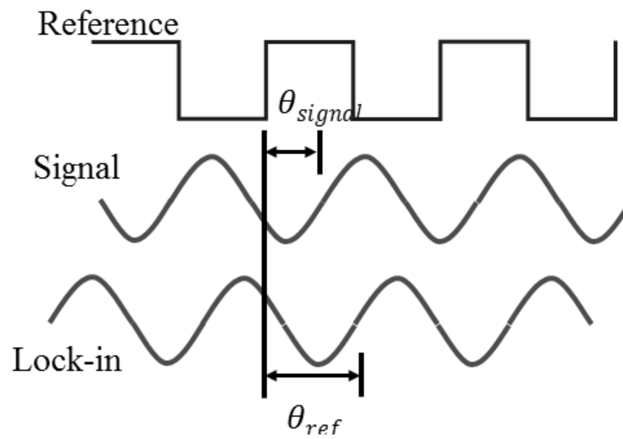

Figure 4-5 Phase measurement in lock-in amplifier

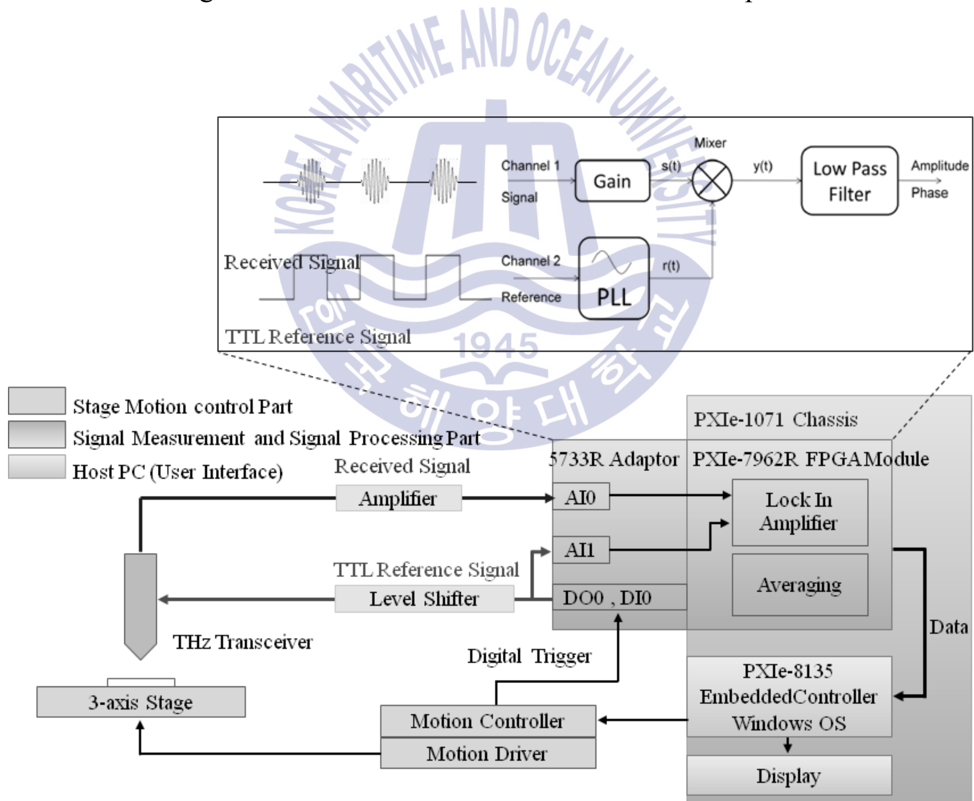

Figure 4-6 Schematic diagram of CW THz System with FPGA-Based Lock-in Amplifier

Collection @ kmou

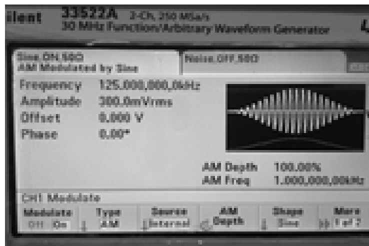

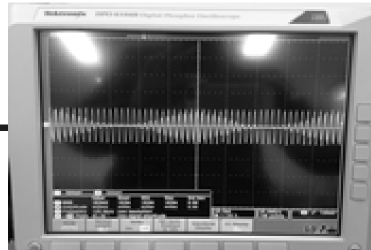

Figure 4-7 Comparison of FPGA-based lock-in amplifier and AMETEK 7256 lock-in amplifier

Collection @ kmou

As a result of measurement using AMETEK 7265 lock-in amplifier, when the time constant (TC) is 320us, only the root mean square (RMS) value of the DC component of the signal is measured, but the modulation signal is restored as TC becomes smaller. However, when the TC is lower than 10us, the reference signal is also detected.

Figure 4-9 shows a signal measured using an FPGA-based lock amplifier. For performance verification, the modulation signal varied from 25 Hz to 5 kHz and the TC was fixed at 1 ms and 10 ㎲, respectively. When TC = 1 ms, the response characteristic is displayed up to about 1 kHz, but the value of the measured signal decreases sharply because TC is long. On the other hand, when TC = 10 ㎲, the modulated signal of 5 kHz is also restored stably.

4.1.4 Fabrication of Standard Sample

Spectroscopic properties of silicon, plastics and polymers widely used as semiconductor materials in the THz region have already been reported. Figure 4-10 and Figure 4-11 show the spectral characteristics of the THz region for semiconductor materials [20],[49]. For silicon, the refractive index is 3.42, which has a near constant refractive index in the THz range and a low absorption coefficient of less than 5. In addition, for polymers widely used in semiconductor chip packages or junctions, the refractive index is 1.51, which is similar to silicon and has a substantially constant refractive index in the THz region. Plastics used in semiconductor chip package materials have a nearly constant refractive index in the THz range, but the absorption rate increases with frequency. However, since the thickness of the sample is thin, the absorption rate can be used with little consideration.

Collection @ kmou

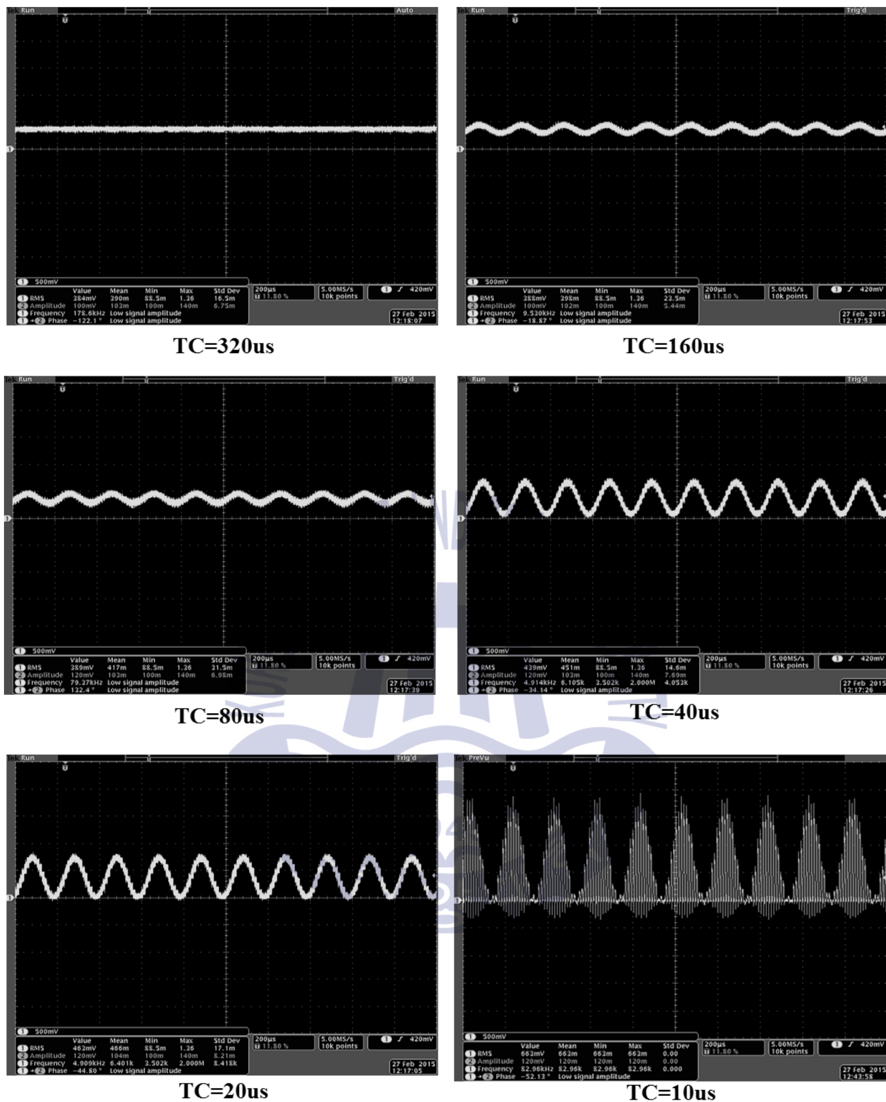

Figure 4-8 Signal response of AMETEK 7256 lock-in amplifier according to time constant

Collection @ kmou

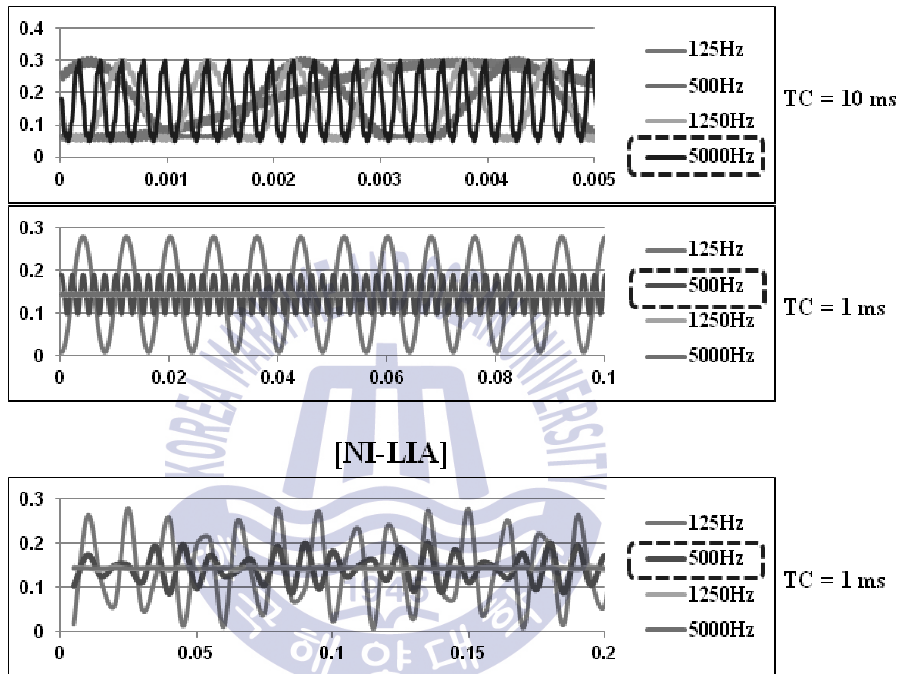

Figure 4-9 Comparison of detection signal of FPGA-based lock-in amplifier according to time constant (a) TC = 10 us (b) TC = 1 ms (c) None FPGA

Collection @ kmou

Therefore, in the semiconductor chip inspection, the influence of THz by the material can be almost neglected. On the other hand, complicated wiring is included in the semiconductor chip. Such wiring is formed like a metal thin film, thereby preventing.

In order to evaluate the THz wave transmittance of metal thin films and the ability to detect voids behind metal thin films, standard samples with conductive metal thin film coatings on silicon surfaces were prepared. A standard sample was prepared and used for the measurement system and the performance of the manufactured probe.

As the coating material of the standard sample, three materials such as silicon, TiO_2 and ITO were used in consideration of the reflectance depending on the structure and material of the semiconductor. On one side, the silicon itself was used without coating for comparison. In the middle of the sample, the conductivity was similar to that of silicon but coated with TiO_2 with a refractive index twice. On the other side, the ITO coating with a conductivity of 1000 [/Ωcm] or more was taken into consideration, considering the conductivity of the wiring inside the semiconductor chip. Defects of 2 mm, 1 mm and 0.5 mm in diameter were prepared for each area to evaluate the performance of the inspection system. The thickness of the wafer is 200 μm, which is similar to the thickness used for stacked semiconductor chip, and the defect depth is 50 μm by laser processing.

4.2 CW THz Transceiver module for multi-chip package inspection

4.2.1 Design of THz transceiver module

Collection @ kmou

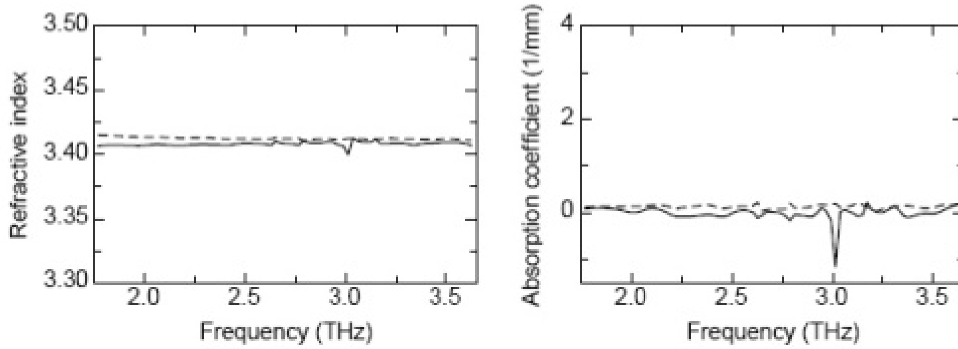

Figure 4-10 The optical properties of silicon in the THz region [49]

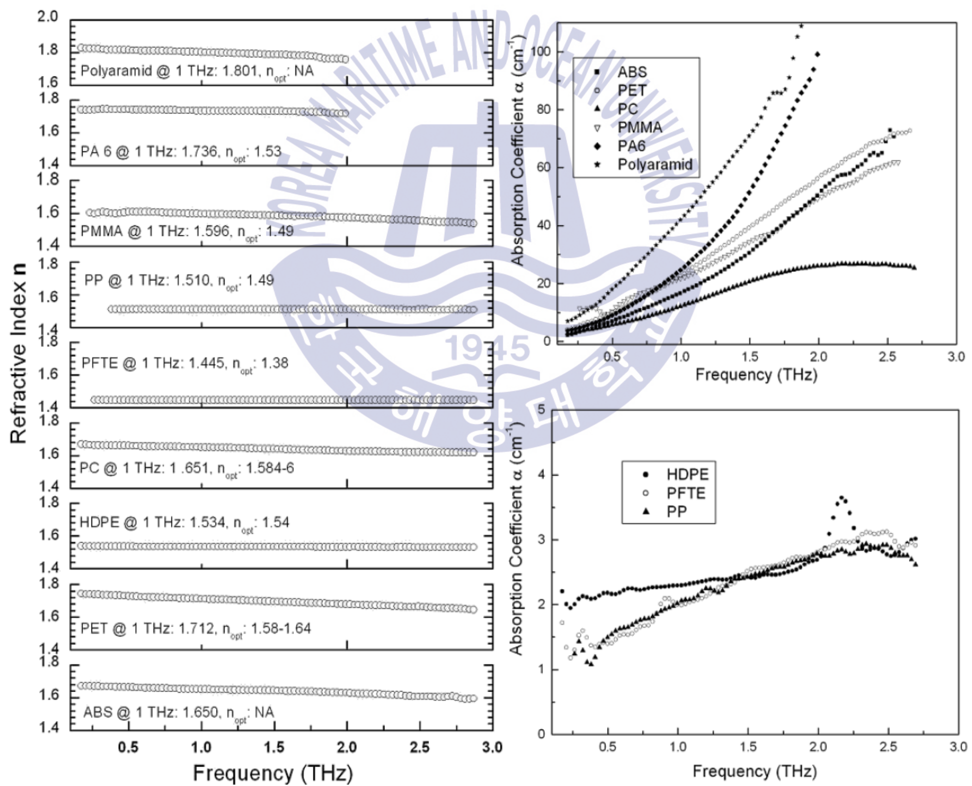

Figure 4-11 The optical properties of polymers in the THz region [20]

electromagnetic waves from penetrating the semiconductor chip.

Collection @ kmou

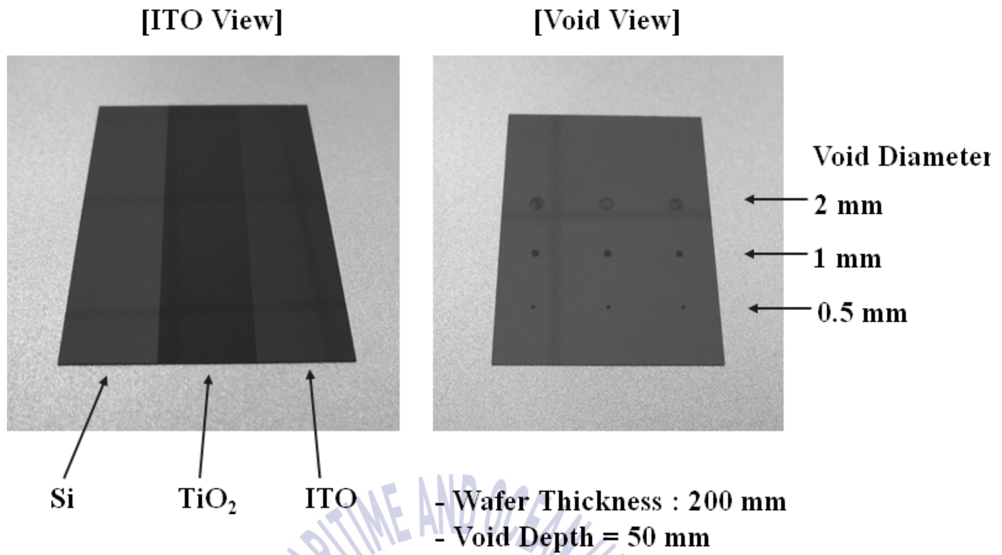

Figure 4-12 Manufactured standard sample

Table 4-1. Optical properties of coating material in standard sample

Material	Coating Thickness	Refractive Index	Conductivity [/Ωcm]
SiO2	-	3.42	~ 0.1
TiO2	300nm	8	<1
ITO	100nm	85	>1000

Collection @ kmou

As a method of detecting defects in a multi-layer using a focused THz wave, there is a method of introducing a sample at a certain angle to a THz wave or detecting a defect by making a THz wave incident perpendicularly to the sample. The structure that makes incident with a certain angle is not only easy to align the beam but also can refocus the reflected THz wave to secure a SNR. However, the beam size in the measurement region differs depending on the incident angle. Also, the beam path and beam path length was changed according to the refractive index of the sample. In this study, the normal incidence method of the sample was used. The vertical incidence method can accurately discriminate the spatial resolution and the defect position as the emission path of the beam and the detection path are the same. This makes it easy to determine the position of the defect in the multi-chip package.

The THz system employs a THz transceiver configuration that uses a near field measurement method. The near field measurement method uses one hole, so the position of the THz source coincides with the position of the sample. Also, since the aperture size is directly connected to the spatial resolution, no special optimization is needed to improve spatial resolution.

The CW THz system configuration was designed for two types of signal detection method using a directional coupler (DC) and a signal detection method using a magic tee (MT) in order to compare the detection sensitivity according to the measurement method.

Figure 4-14 is a schematic diagram of a reflective THz transceiver module. The detection method using directional coupler is very simple structure by separating the input signal and the reflected signal and transmitting the reflected signal from the sample to the detector. On the other hand, if the surface reflectance of the sample and the reflectance of

Collection @ kmou

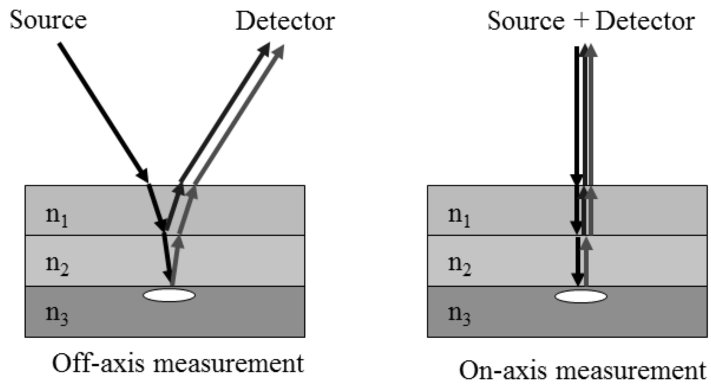

Figure 4-13 Comparison of THz paths in Off-axis and On-axis measurement

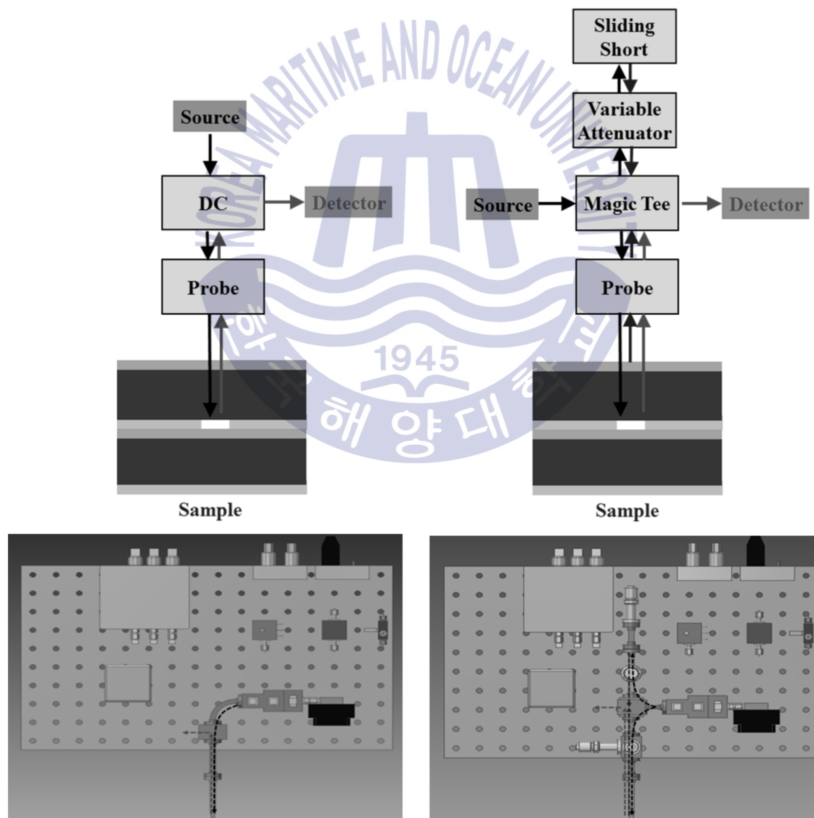

Figure 4-14 Schematic Diagram of Reflective THz Transceiver Module

Collection @ kmou

the probe end are high, it is difficult to relatively detect the defect of the sample. The detection method using magic tee can detect only the defect detection by removing the surface reflection of the sample and the signal reflected from the probe tip. However, there should be improvement for low SNR due to the small signal.

4.2.2 Magic-tee based THz Transceiver

Figure 4-15 is a schematic and major component of the THz transceiver using magic tee. The THz wave generated from the THz source is divided into 50:50 magic tees. One THz wave is radiated as a sample through the probe, and the other THz waves propagate to the variable attenuator and the sliding short. The THz wave reflected from the sample side is equal to the output of the THz wave reflected by the variable attenuator and the sliding short, but when the phase is opposite, the signal detected by the detector is zero. If there is a defect in the sample, the magnitude and phase of the signal change directly at the detector.

4.2.3 Directional coupler base THz Transceiver

Figure 4-16 shows a schematic of a THz transceiver using a directional coupler. The THz wave generated from the source passes through the directional coupler and is incident on the sample. When the THz waves reflected from the sample are incident on the directional coupler through the probe, the THz wave incident on the directional coupler is transmitted to the detector by the coupling factor of the directional coupler. The THz wave

Collection @ kmou

transmitted to the detector includes both the reflection in the probe and the reflection on the sample surface as well as the reflection in the defects.

Collection @ kmou

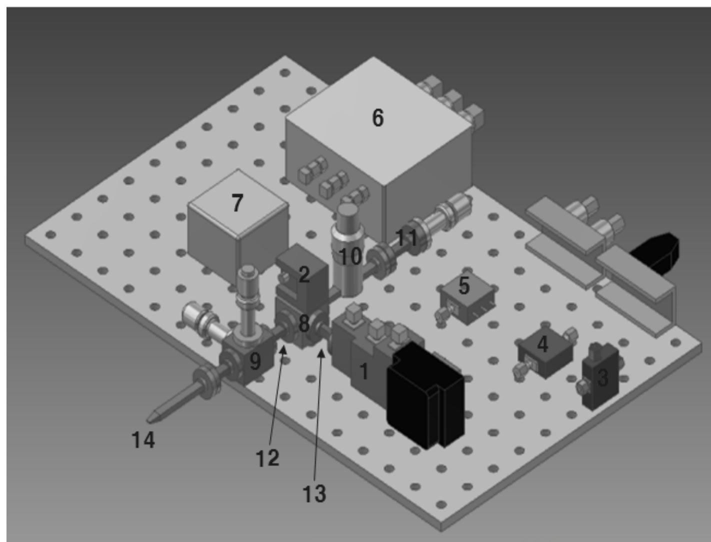

No	Component
1	Doubler Module
2	Detector
3	Oscillator
4	Coupler
5	PIN Switch
6	Power Supply Module
7	LNA
8	Magic Tee
9	EH tuner
10	Variable Attenuator
11	Sliding Short
12	Waveguide Straight
13	Waveguide Twist
14	THz Probe

Figure 4-15 THz Transceiver module based on Magic-Tee

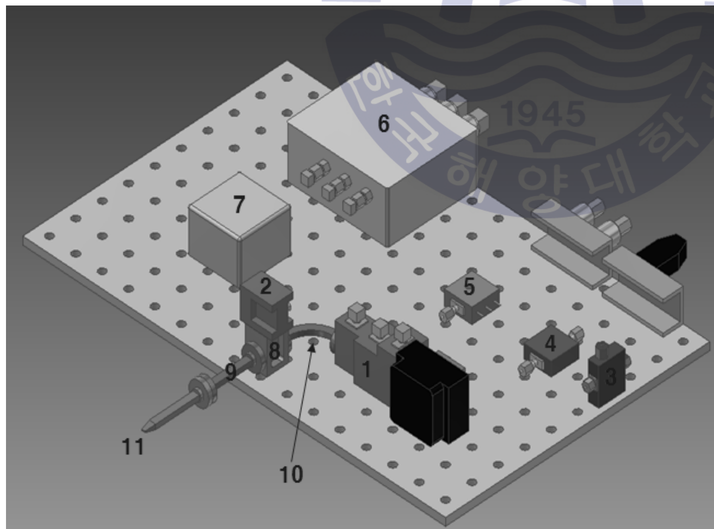

No	Component
1	Doubler Module
2	Detector
3	Oscillator
4	Coupler
5	PIN Switch
6	Power Supply Module
7	LNA
8	Directional Coupler
9	Waveguide Straight
10	Waveguide Bend
11	THz Probe

Figure 4-16 THz Transceiver module based on Directional Coupler

Collection @ kmou

5. Measurements and results

5.1 Verification of performance of THz imaging system

5.1.1 Measurement of spatial resolution of resonant slit-type probe with rounded matching structure

To verify the spatial resolution of our fabricated THz probe, a reflective THz imaging system based on a waveguide matched hybrid-tee was installed. The imaging system can shift the operating point of the detector by adjusting the attenuator and sliding short. In order to increase the detection sensitivity, a detection method using a lock-in amplifier was used. Meanwhile, a standard sample with defects of various sizes and shapes, such as circles, squares, bars, and “KERI” logo on the wafer was fabricated. The minimum defect size of the sample is a circular defect with a diameter of 100 μm and the depth of the defect is 30 μm. A laser processing method was used to prepare the sample. The scan area size was 40 mm × 18 mm. To reduce measurement time, a board-based data acquisition system was

Collection @ kmou

configured. Also, signal were acquired at 25-μm intervals during the linear movement of the sample in the in the X-axis direction. The step size in the Y-axis direction was 50 μm. The distance between the sample and the probe was fixed approximate 100 μm. The total measurement time was approximately 2 min.

A reflective THz image of the sample using our imaging system was obtained. Figures 5-2 (a) and (b) show the amplitude and phase images of the sample, respectively. Figures 5-2 (c) shows the profile of the amplitude and phase signals represented by the dashed line. The phase signal noticeably changes at the edge of the defect. This phase change can be used as a marker to evaluate the defect size such as in voids and cracks. The amplitude signal sharply decreases due to the reduction of the interaction area in small defects. Nevertheless, as shown in the signal profile, the proposed rounded matching structure slit was able to detect metal defect with a diameter of 100 μm as shown in Figure 5-1. This result is similar to that of a previous study at similar slit height although the operating frequencies are different [43]. A 20-μm-thick aluminum foil was used to obtain a small slit thickness in the previous study. However, in the proposed probe, the same results can be obtained with a thick slit of 290 μm.

5.1.2 High-speed signal processing and image acquisition

To verify the performance of an FPGA-based high-speed lock-in amplifier, THz images were compared with the moving speed of the sample. Figure 5-4 is a photograph of the sample used for the measurement. The sample surface has grooves with a line width of 350 ㎛ and the sample material is

Collection @ kmou

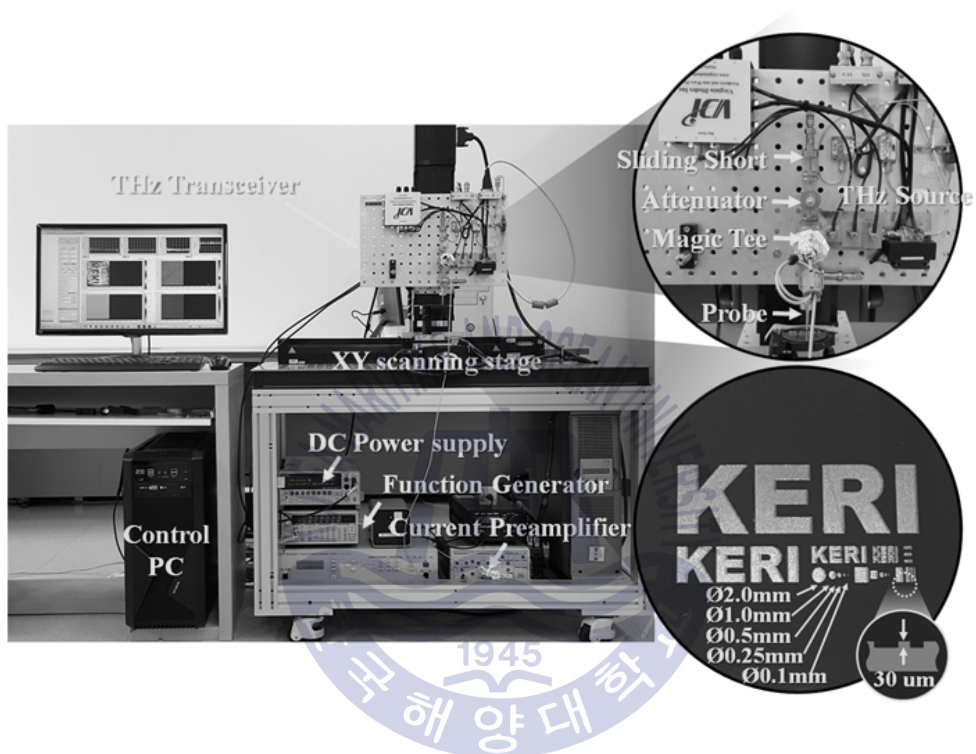

Figure 5-1 Reflective THz imaging system based on (left) a waveguide matched hybrid-tee. (Right) Photograph of the standard sample.

Collection @ kmou

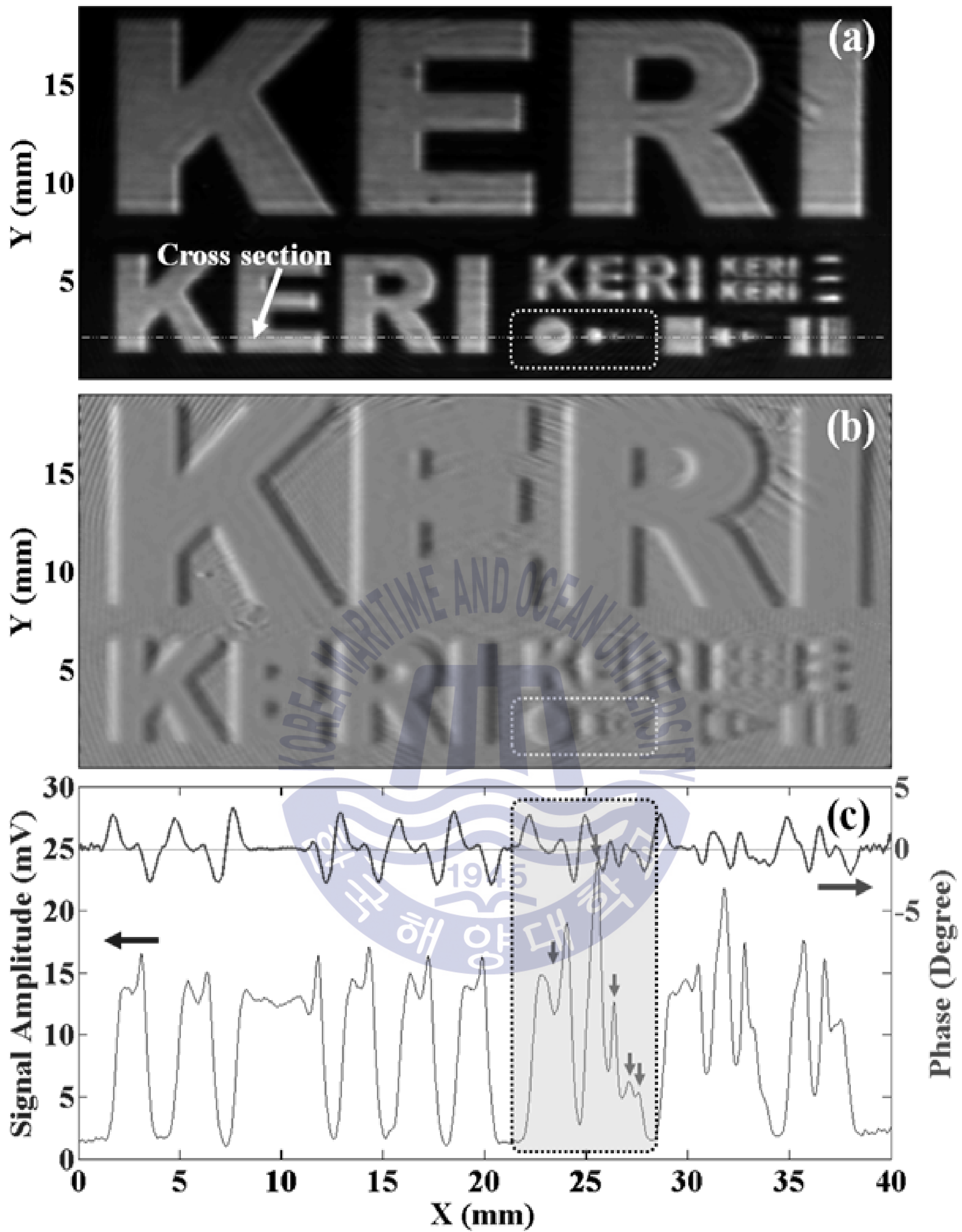

Figure 5-2 (a) Amplitude THz image. (b) Phase image of the standard sample. (c) (Bottom) Profile of the amplitude and (top) phase signals represented by the dashed line.

Collection @ kmou

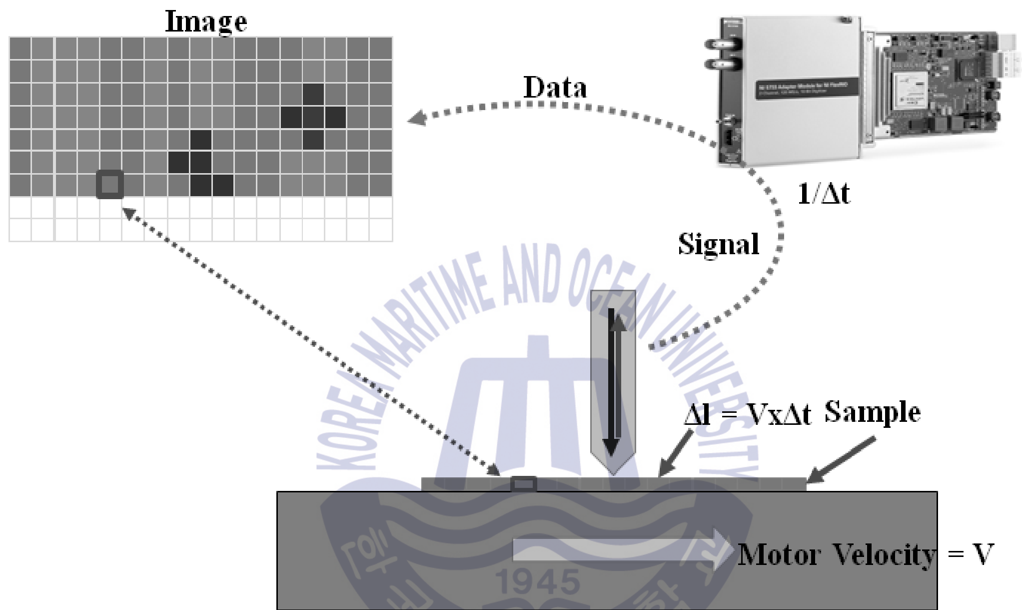

Figure 5-3 Signal measurement synchronized with motor speed.

Collection @ kmou

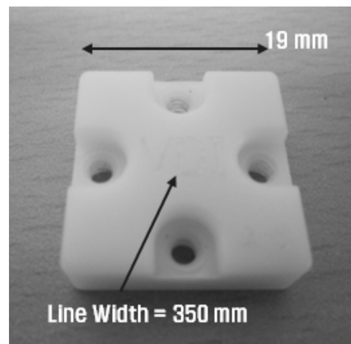

Figure 5-4 Sample with 350 ㎛ line width

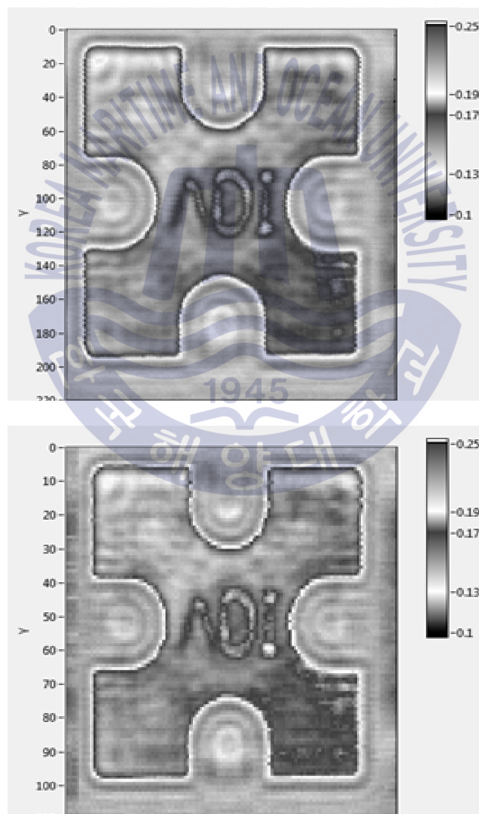

Figure 5-5 Image comparison according to sample moving speed (upper) 10 mm/s (bottom) 1000 mm/s

Collection @ kmou

a polymer. The distance between the sample and the probe was maintained at 300 ㎛. Figure 5-5 shows the THz image according to the speed. THz images were obtained at motor speeds of 10 mm/s and 1000 mm/s, respectively. As a result, although slight blurring occurred according to the detection signal processing speed at the edge due to the increase in the speed, almost the same image was obtained. That is, the processing speed of the developed FPGA-based lock-in amplifier can be used at higher speeds.

5.2 Semiconductor chip inspection using pulsed THz wave

5.2.1 Inspection system using pulsed THz wave

PCA antenna based generation and detection methods for semiconductor chip inspection were used for semiconductor chip inspection. In order to increase the transmission efficiency of THz waves, a transmission type THz wave system based on a 4-parabolic mirror was constructed. The sample was scanned in two dimensions using a motorized stage after installation at installed in the beam waist section to improve spatial resolution. The 1mm pin hole output was reduced by 50%, but the center frequency increased to the THz beam focusing position. A pin-hole with a diameter of 1 mm was about 0.6 THz. To minimize the effects of humidity, a dry air generator was used to keep the relative humidity below 2 %. Adhesive tape was used to hold the sample, and the tape exhibited an absorption rate of about 10 %.

dCollection @ kmou

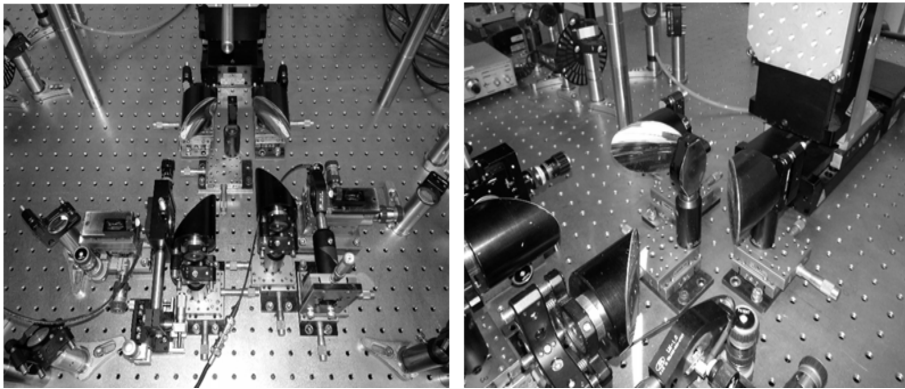

Figure 5-6 Transmission-type THz wave system based on 4-parabolic mirrors

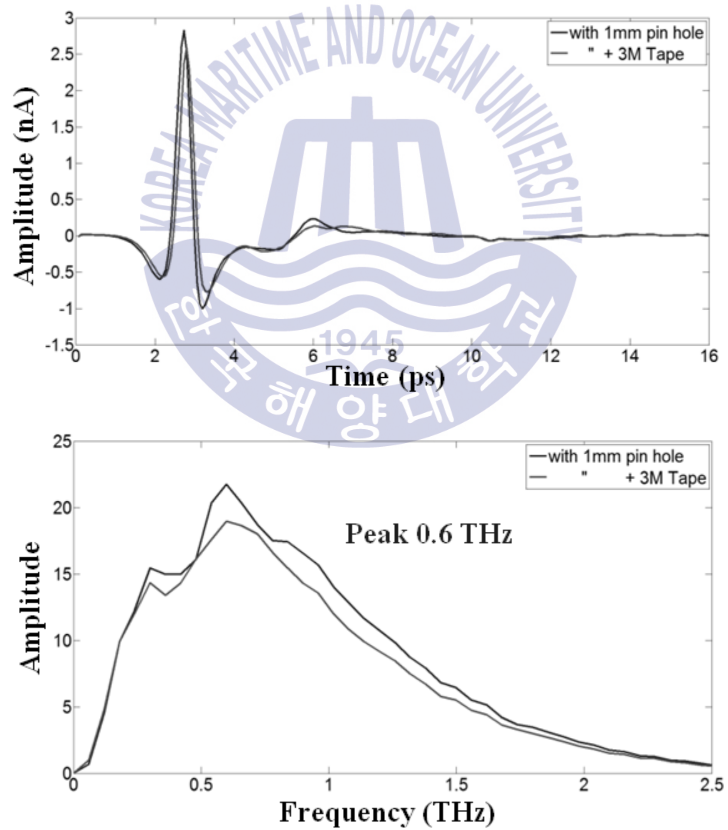

Figure 5-7 THz transmission characteristics according to pin-hole and adhesive tape

dCollection @ kmou

5.2.2 Semiconductor chip inspection using Pulsed THz Wave

To verify the THz transmission characteristics, a flash memory with a void of 1 mm and 2 mm in diameter and a DRAM with a void of 1 mm in diameter were measured. Sample measurements were taken at 500 μm intervals

Figure 5-9 (a) shows the measured pulse and spectra of the flash memory with a 1 mm diameter void, and Figure 5-9 (b) is picture of the sample. Figure 5-9 (c) shows a reconstructed image of 4 ps in the time domain and 0.55 THz in the spectral domain, respectively. As a result, it can be seen that the THz wave passes well through the flash memory chip. Also, it can be seen that the void detection image is clearly distinguished from the THz image in the time domain. This is because all THz signals measured at each measurement location are used for spectrum calculations. Most of voids were detected, but voids were not detected in some areas. This is because the density of the metal wire inside the semiconductor chip is high and the THz wave is not transmitted.

Figure 5-10 (a) shows the measured pulse and spectrum for a flash memory sample with 2 mm diameter voids, and Figure 5-10 (b) shows the sample photograph. Figure 5-10 (c) shows the reconstructed image at 4 ps in the time domain and 0.55 THz in the spectral domain, respectively. As a result, it was almost the same as the result of 1 mm void measurement.

Figure 5-11 (a) shows the measured pulse and spectrum for a DRAM sample with 1 mm diameter voids, and Figure 5-11 (b) shows the sample photograph. Figure 5-11 (c) shows the reconstructed image at 4 ps in the time domain and 0.65 THz in the spectral domain, respectively. As shown

Collection @ kmou

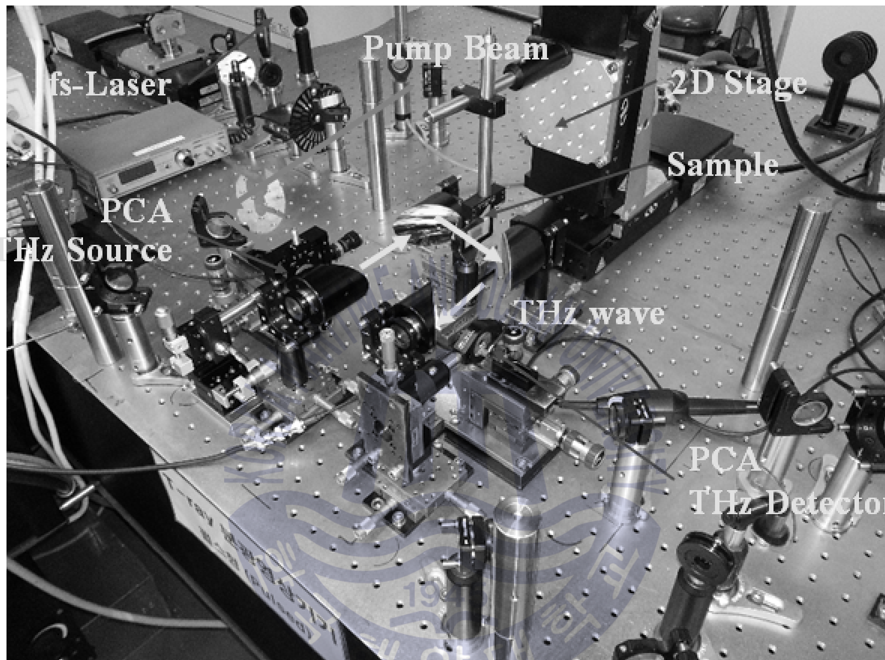

Figure 5-8 Experimental setup for semiconductor chip inspection using pulsed THz wave

Collection @ kmou

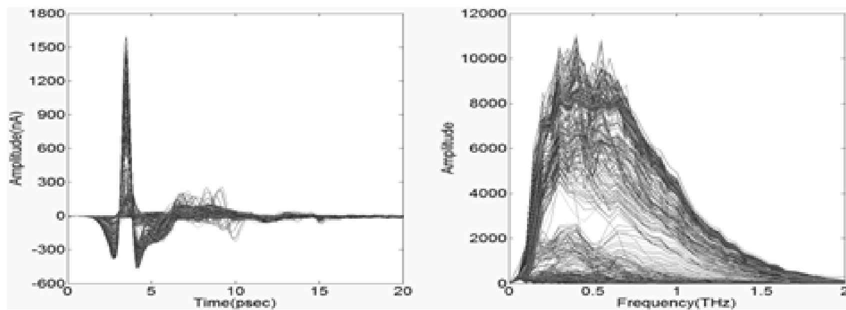

(a)

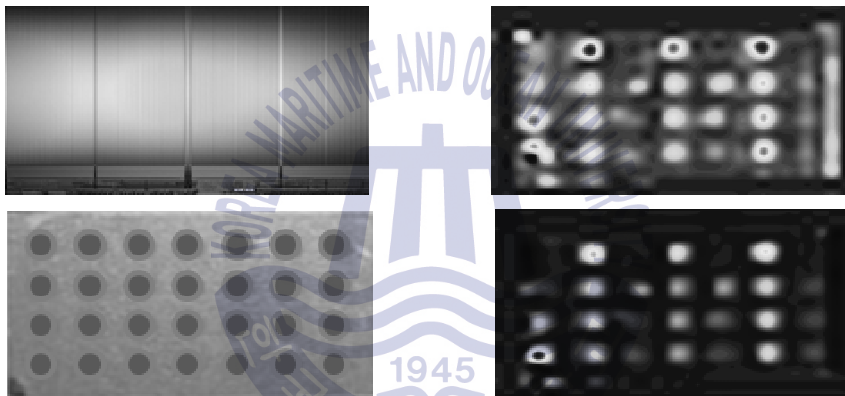

(b) (c)

Figure 5-9 (a) Measured THz pulse and spectra for a flash memory with 1 mm diameter voids. (b) Photograph of sample (c) Reconstructed THz image at 4 ps and 0.55 THz, respectively.

Collection @ kmou

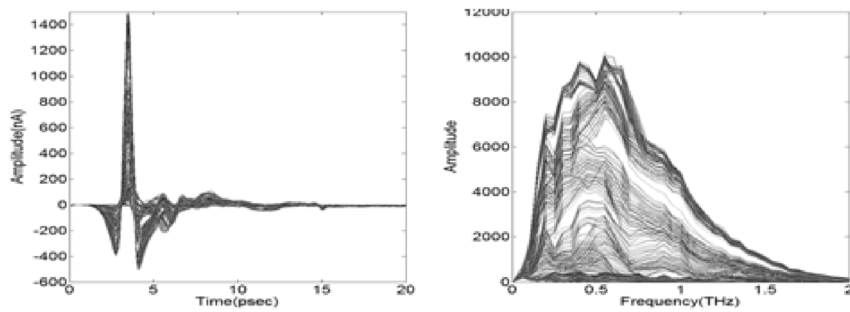

(a)

(b) (c)

Figure 5-10 (a) Measured pulse and spectra for a flash memory with 1 mm diameter voids. (b) Photograph of sample (c) Reconstructed image at 5.2 ps and 0.65 THz, respectively.

Collection @ kmou

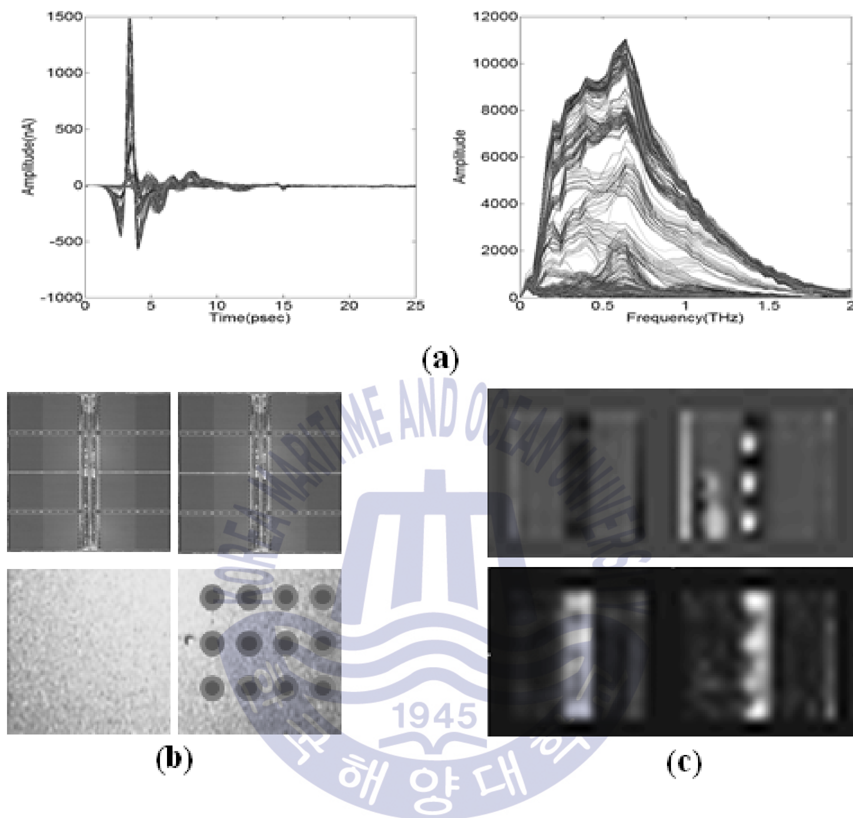

Figure 5-11 (a) Measured pulse and spectra for a DRAM with 1 mm diameter voids. (b) Photograph of sample (c) Reconstructed image at 4 ps and 0.65 THz, respectively.

Collection @ kmou

in the THz image, the internal wiring of the DRAM is denser than the flash, and is rarely detected except for some voids. That is, it is impossible to detect defects in the DRAM by the transmission type THz wave transmission method.

5.2.3 Transmission characteristics according to the polarization

The inside of the semiconductor device is composed of complicated wiring for power supply. In order to increase the density, most of the wirings are formed in a constant direction or a vertical crossing type thereof. This structure has the same effect as the wire grid filter, so the transmittance can be changed according to the polarization of incident THz wave. Assuming these characteristics, the transmission characteristics according to the incident polarization of THz wave are compared. In order to shorten the total measurement time, the optical delay line was fixed at the position where the THz wave signal was maximum, and then the sample was measured while moving the sample.

Figure 5-12 shows the THz image according to the polarization direction for a flash memory with a void of 1 mm in diameter. The polarization direction was defined based on the long side of the sample and the polarization direction of the THz wave. As a result of the measurement, the characteristics of the void detection are clearly distinguished according to the polarization direction. Most of the voids were detected in the horizontal direction, but some voids were also detected in the vertical direction. The magnitude of the signal measured in the void region was detected to be more than 2 times larger in the horizontal direction. Above all, voids that were not detected in the horizontal direction were detected in the vertical

Collection @ kmou

direction. The magnitude of the signal measured in the void region was detected to be more than 2 times larger in the horizontal direction.

Figure 5-13 shows the THz image according to the polarization direction for a flash memory with a void of 2 mm in diameter. Figure 5-14 shows the THz image according to the polarization direction with respect to the DRAM with 1 mm diameter voids. Remarkably, voids not detected in the horizontal direction were detected in the horizontal direction. From the results, it is most appropriate to use THz wave polarized vertically and horizontally for semiconductor chip inspection. However, detection was still impossible in a region where some wiring was dense. From the result, it is preferable to use the THz polarized in the horizontal direction as much as possible for the semiconductor chip inspection. If possible, it has been confirmed that it is more appropriate to use a circularly polarized THz source.

Figure 5-14 shows the THz image according to the polarization direction with respect to the DRAM with 1 mm diameter voids. Remarkably, voids not detected in the horizontal direction were detected in the horizontal direction. From the results, it is most appropriate to use THz wave polarized vertically and horizontally for semiconductor chip inspection. However, detection was still impossible in a region where some wiring was dense. From the result, it is preferable to use the THz polarized in the horizontal direction as much as possible for the semiconductor chip inspection. If possible, it has been confirmed that it is more appropriate to use a circularly polarized THz source.

5.3 Semiconductor chip inspection using CW THz wave

Collection @ kmou

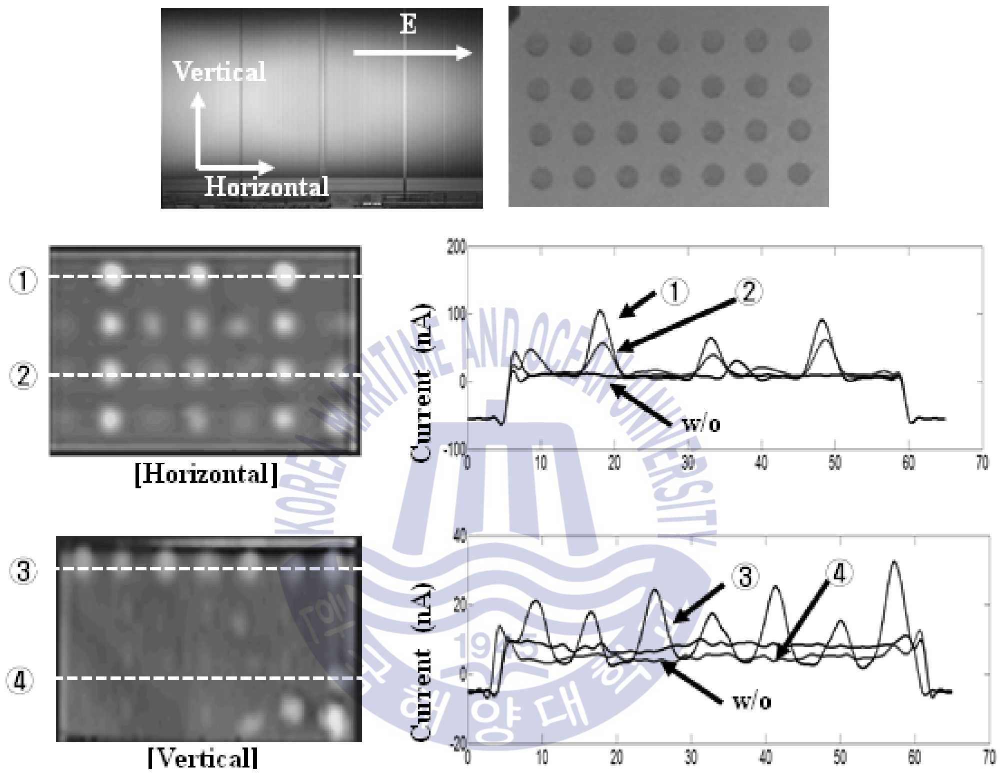

Figure 5-12 THz image according to polarization direction for a flash memory with 1 mm diameter voids.

Collection @ kmou

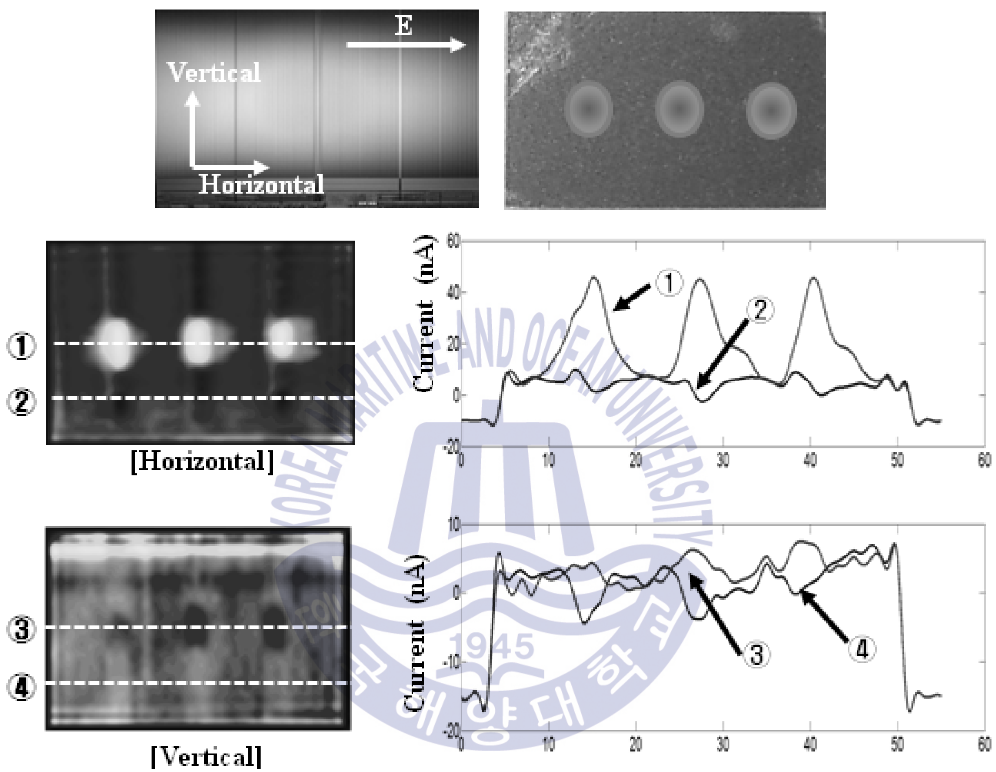

Figure 5-13 THz image according to polarization direction for a flash memory with 2 mm diameter voids.

Collection @ kmou

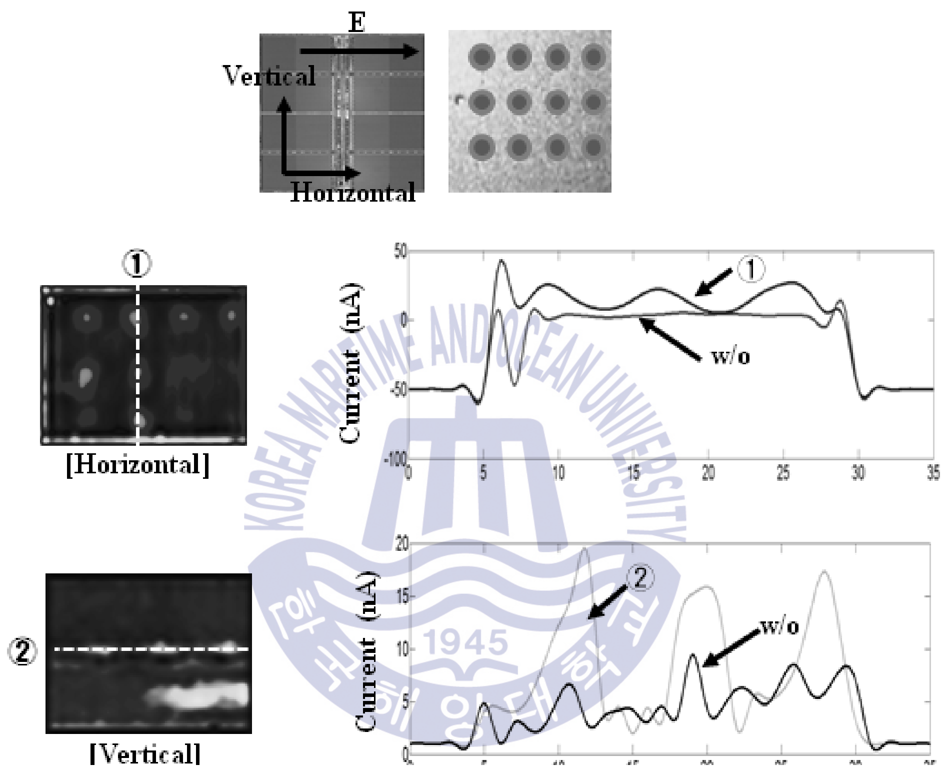

Figure 5-14 THz image according to polarization direction for a DRAM with 1 mm diameter voids.

Collection @ kmou

As mentioned earlier, pulsed THz waves have high peak power and high transmittance. However, the pulsed THz wave system uses a femto-second laser, and the system size is large. Also, the measurement speed is slow because the optical delay line is used for signal measurement. Recent piezo methods have improved speed, but detection speeds of less than 1 kpS / s are not yet available in industries requiring high-speed detection. On the other hand, since CW THz sources using semiconductor devices can modulate high-speed signals, high-speed scanning can be performed using high-speed signal processing. System size is small and system configuration is simple.

5.3.1 Semiconductor chip inspection using CW THz system based on directional coupler

Figure 5-15 is a CW THz source module based on a directional coupler. The directional coupler uses VDI WR5.1DC with a directivity of about 20 dB and a coupling coefficient of −7 dB. A 90 degree bending waveguide was attached to the front of 200 GHz doubler to make it compatible with directional coupler and magic tee.

Figure 5-16 is a photograph of the experimental set-up. The output from the resonant slit type probe was 23 mW. The distance between the probe and the sample was maintained at 200 ㎛ and the distance was measured using a microscope. Samples were mounted on gold coated Si-wafer.

Figure 5-17 shows the amplitude and phase signals of the THz signal measured on the ITO coated surface. Since the reflected THz wave is directly input to the detector, it can be seen that the measured value is offset. These offsets cause disadvantages not only in measurement but also

Collection @ kmou

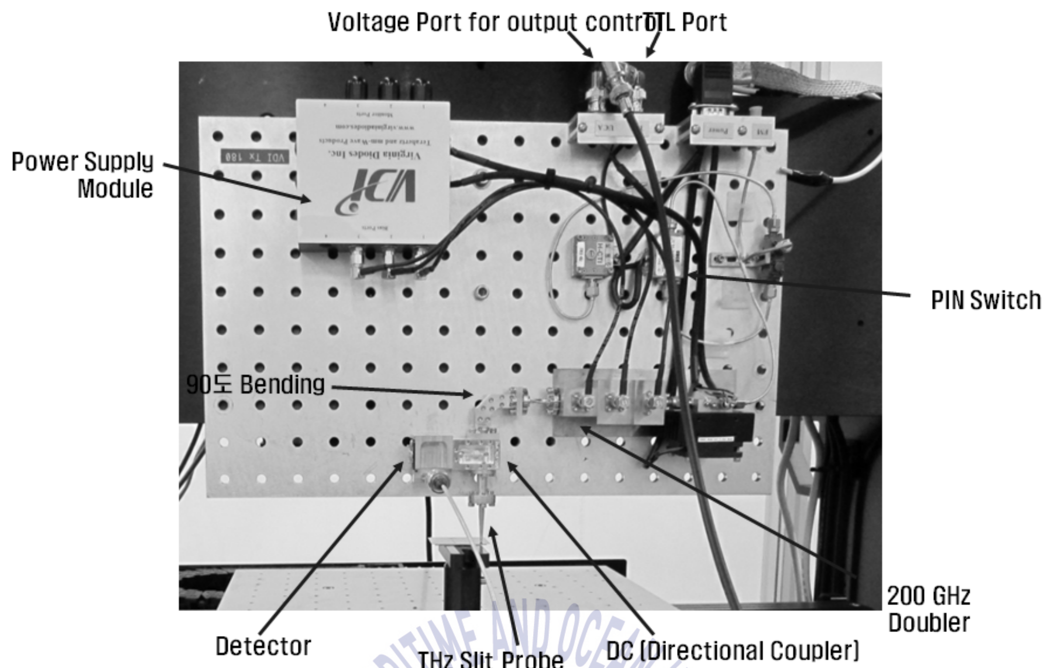

Figure 5-15 Continuous THz Source module based on Directional Coupler

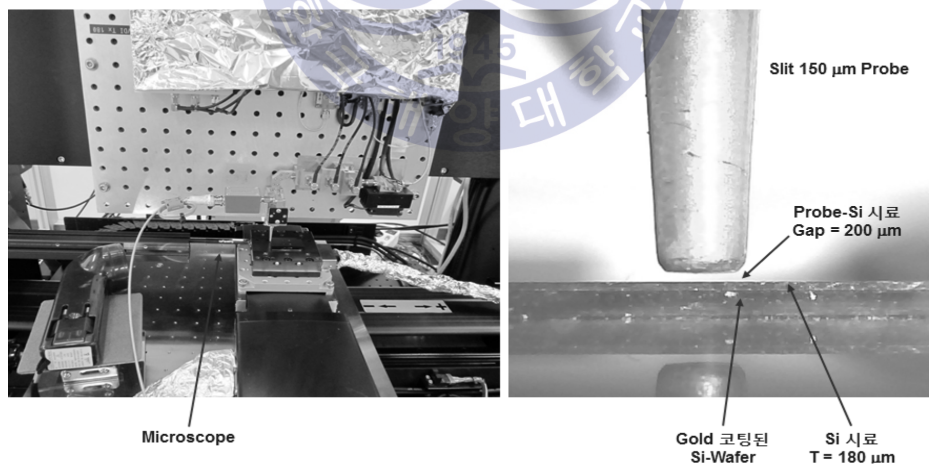

Figure 5-16 Experimental Setup for measuring standard samples

Collection @ kmou

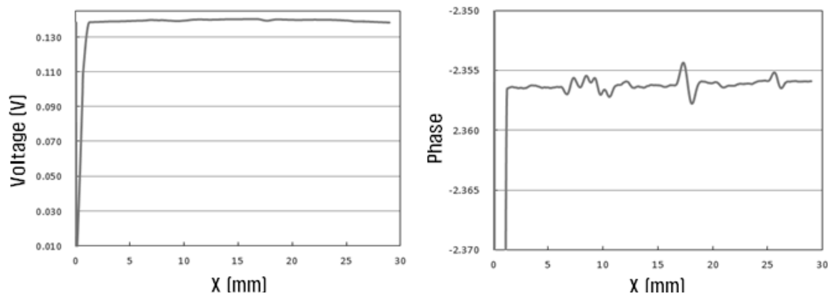

Figure 5-17 The amplitude and phase signals measured on the ITO coated surface using a DC-based THz Transceiver module

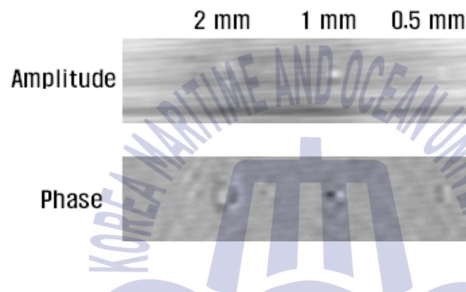

Figure 5-18 THz image obtained from ITO coated surface using DC-based THz transceiver module

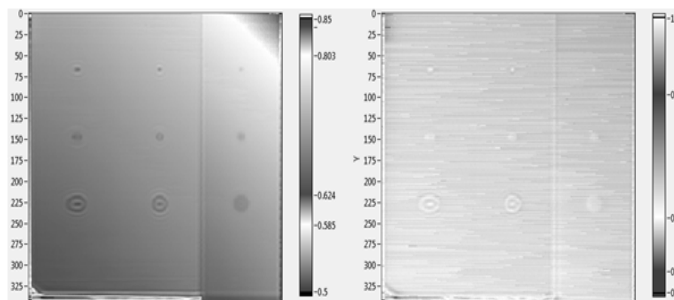

Figure 5-19 THz image for standard sample using DC-based THz transceiver module (left) Coated surface (right) Void surface

Collection @ kmou

in image evaluation. If more than a certain level of power is input to the detector, the detector will be damaged. Therefore, input power can not be kept high. It is also difficult to distinguish defects in image evaluation when the offset signal is very large in the signal reflected from the defect. Also, as the offset signal is large, the phase change due to the defect is detected to be small. Figure 5-18 is a THz image obtained from an ITO coatedsurface using a DC-based THz transceiver module.

5.3.2 Semiconductor chip inspection using CW THz system based on magic-tee

Figure 5-20 shows a semiconductor chip inspection system using a magic tee-based CW THz transceiver module. The sliding short and variable attenuator can control the phase at the detector position. The sliding shot and the variable attenuator can be adjusted to cancel out the reflected signal from inside the waveguide and from the surface of the sample. As a result, only the change in the defect can be detected. Figure 5-21 shows the experimental setup and signal detection configuration. The signal detected by the Schottky diode detector was amplified using a low-noise voltage preamplifier and then either monitored using an oscilloscope or measured an FPGA-based lock amplifier. Figure 5-22 shows the magnitude and phase ousing f the THz signal measured on the ITO coated surface. It showed sufficient detection sensitivity in amplitude signal as well as phase signal.

Figure 5-23 is a THz image obtained from an ITO coated surface using a DC-based THz transceiver module. As a result, it has been found that the method of measuring the magic-tee method is more suitable for void detection than the directional coupler method. As a result, the detection

Collection @ kmou

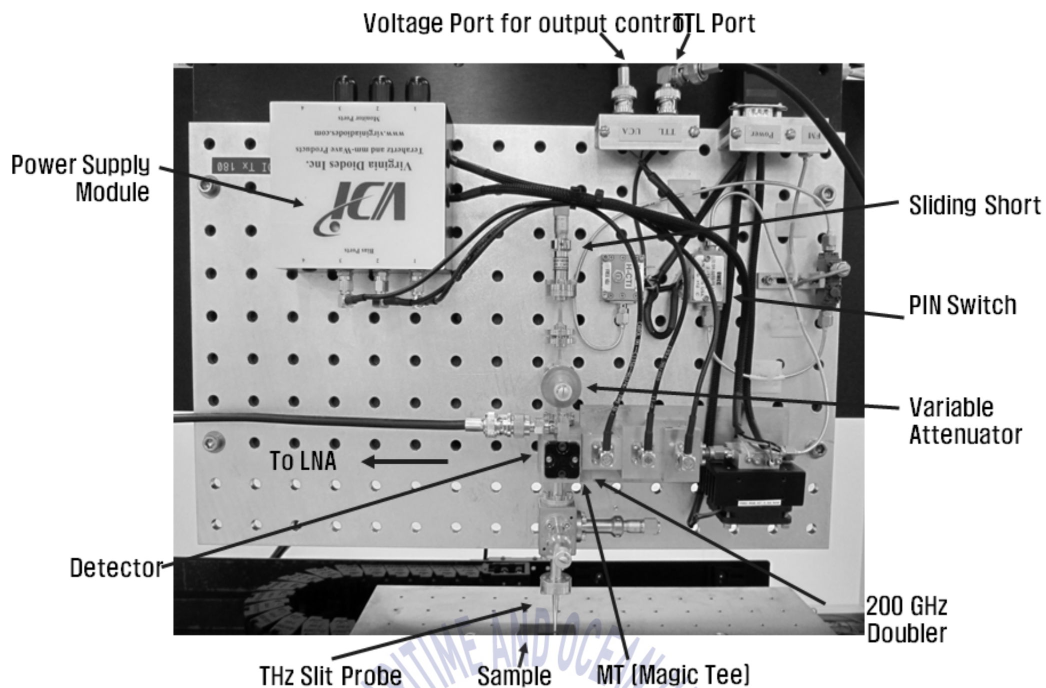

Figure 5-20 Continuous THz Source module based on Magic Tee

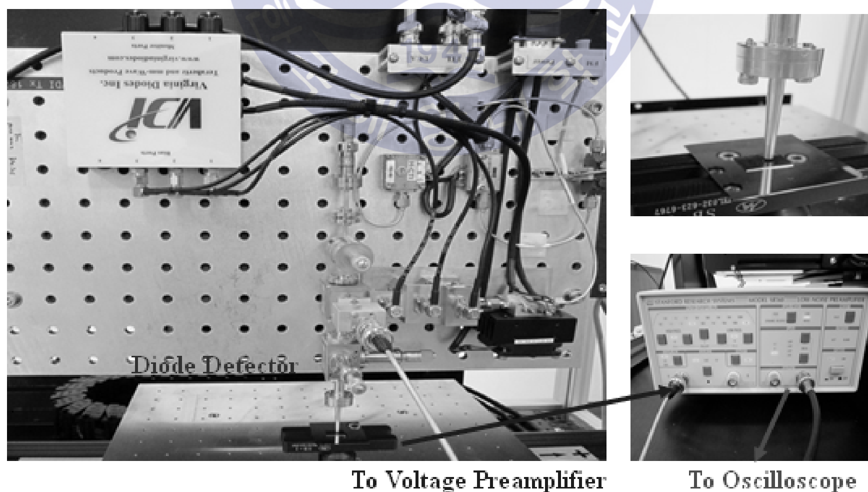

Figure 5-21 Experiment setup and signal detection configuration

Collection @ kmou

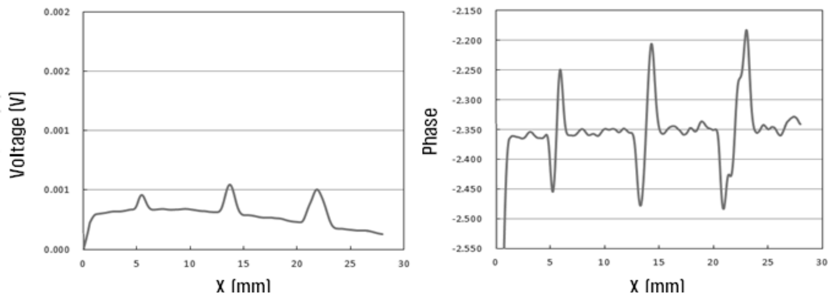

Figure 5-22 The amplitude and phase signals measured on the ITO coated surface using a magic-tee based THz Transceiver module

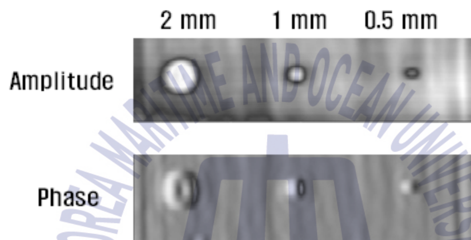

Figure 5-23 THz image obtained from ITO coated surface using magic-tee based THz transceiver module

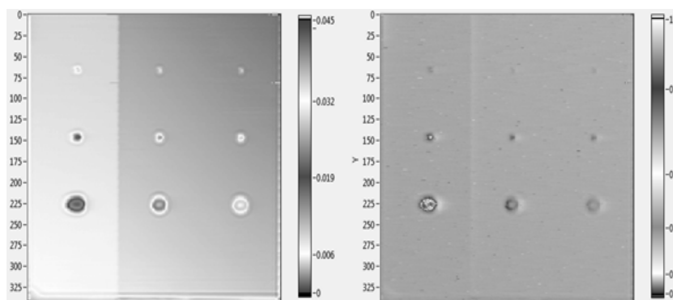

Figure 5-24 THz image for standard sample using magic-tee based THz transceiver module (left) Coated surface (left) Coated surface (right) Void surface

Collection @ kmou

method using magic tee is more suitable for void detection than the detection method using directional coupler. Figure 5-24 shows THz images measured on the coated side and void side using a magic-tee-based THz transceiver module.

5.3.3 Semiconductor chip inspection using CW THz wave

Figure 5-25 is an experimental setup for void detection in semiconductor chip using a reflective measurement system. A flash memory with a void of 2 mm in diameter was used as a sample. A sample was mounted on a gold coated Si-wafer assuming a stacked structure. Figure 5-26 shows the measured THz image. As shown in the figure, some line patterns on the surface were detected but voids were not detected. This is because, when the THz wave travels back and forth over the surface of the sample, most of the THz waves are lost due to the reflection on the metal line on the surface of the sample. That is, in the transmission type method, the void test of the semiconductor chip was almost impossible. As an alternative, the measurement method was changed by a method of transmitting the THz wave at the side instead of the method of transmitting the THz wave at the front side.

5.4 Multi-chip package inspection using CW THz wave

5.4.1 THz propagation in voids of multi-chip package in lateral inspection

The dia attach film used in the semiconductor lamination mostly uses a polymer such as pp, so THz waves can easily pass between the films. Also,

Collection @ kmou

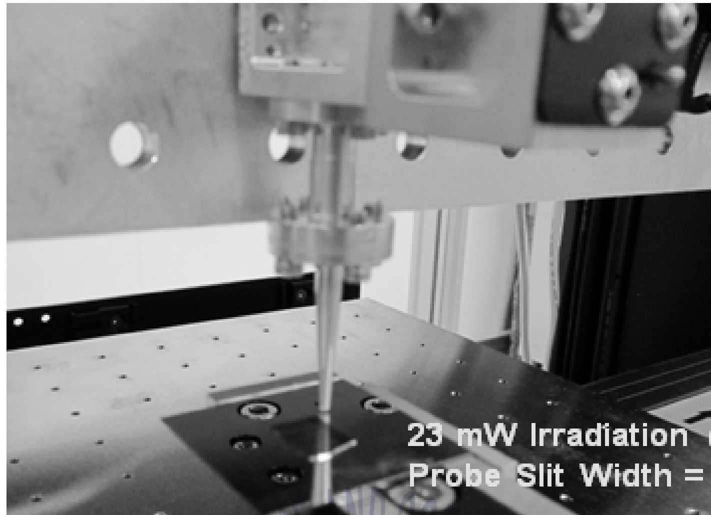

Figure 5-25 Semiconductor chip inspection using CW THz wave

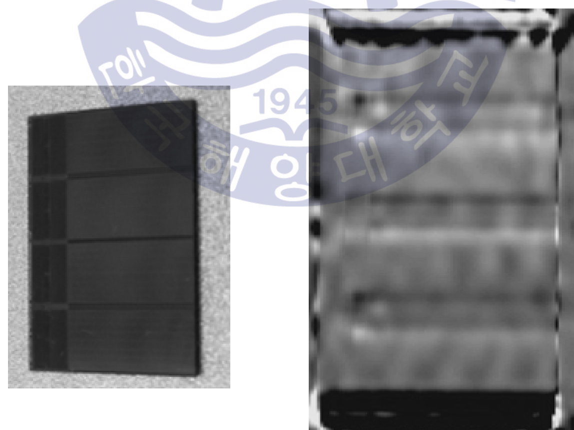

Figure 5-26 THz image measured by reflection method

Collection @ kmou

because the dia attach film thickness is almost similar to the height of the slit probe, it can have spatial resolution to find defects in the dia attach film. Figure 5-27 is simulation modeling to verify the propagation characteristics of THz waves by voids in the multi-chip package. A thin sheet of metal thin film with conductivity was added to the top of the silicon. The THz wave was incident through the waveguide on the side.

Figure 5-28 shows simulation results for THz propagation characteristics with or without voids and void sizes in a multi-chip package. In the absence of voids, the THz waves propagate uniformly, whereas in the presence of voids, the signal measured on the void axis decreases as the THz waves are separated by the voids. In the absence of voids, the THz wave propagates uniformly, whereas in the presence of voids, the THz wave propagates separately around the void. Figure 5-29 shows the THz power distribution measured on the line in Figure 5-28. If there is no void, the power distribution is almost gaussian shape, but if the void is present, the output is reduced in the path where the THz wave passes through the void. This is because THz wave is refracted or diffracted due to void.

5.4.2 Multi-chip package inspection using lateral inspection method

Figure 5-30 shows the THz experiment setup for multi-chip package inspection using the lateral inspection method. The probe was connected directly to the 200 GHz output to ensure sufficient power for sample transmission. The samples were stacked with several single chips and placed between two metal bars. In order to distinguish the THz wave passing through the neighboring film, a slit probe was attached to the front of the detector. Figure 5-31 is THz a image obtained using the lateral inspection

Collection @ kmou

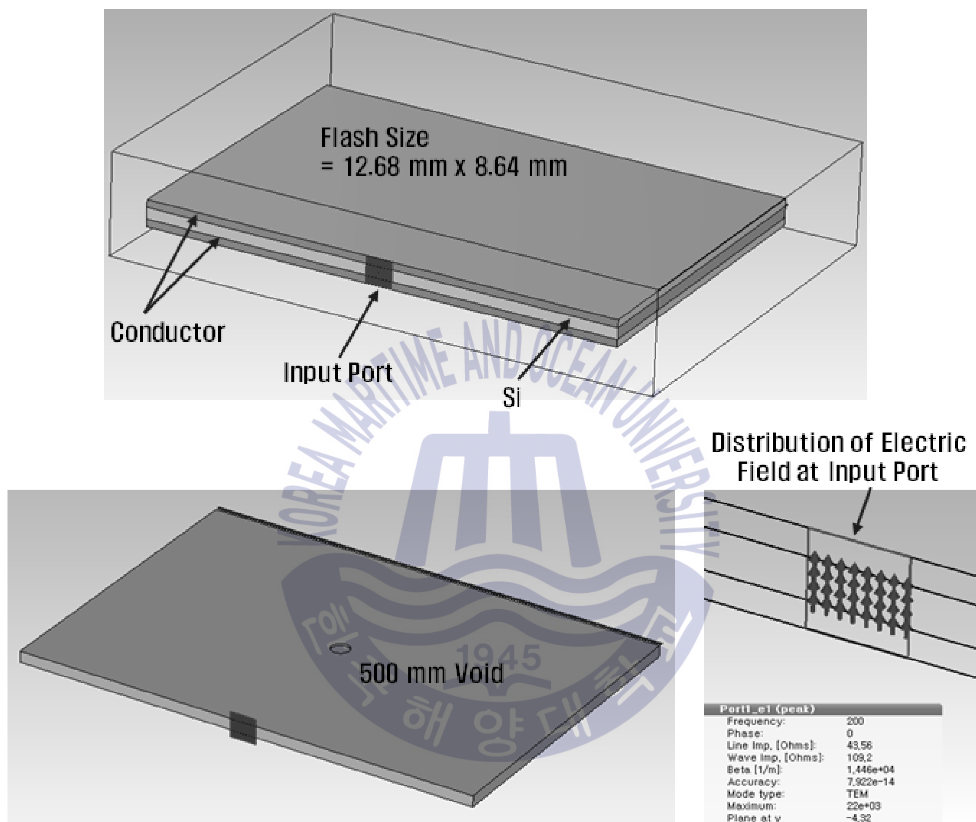

Figure 5-27 Simulation modeling to verify the propagation characteristics of THz waves in the multi-chip package by lateral inspection.

Collection @ kmou

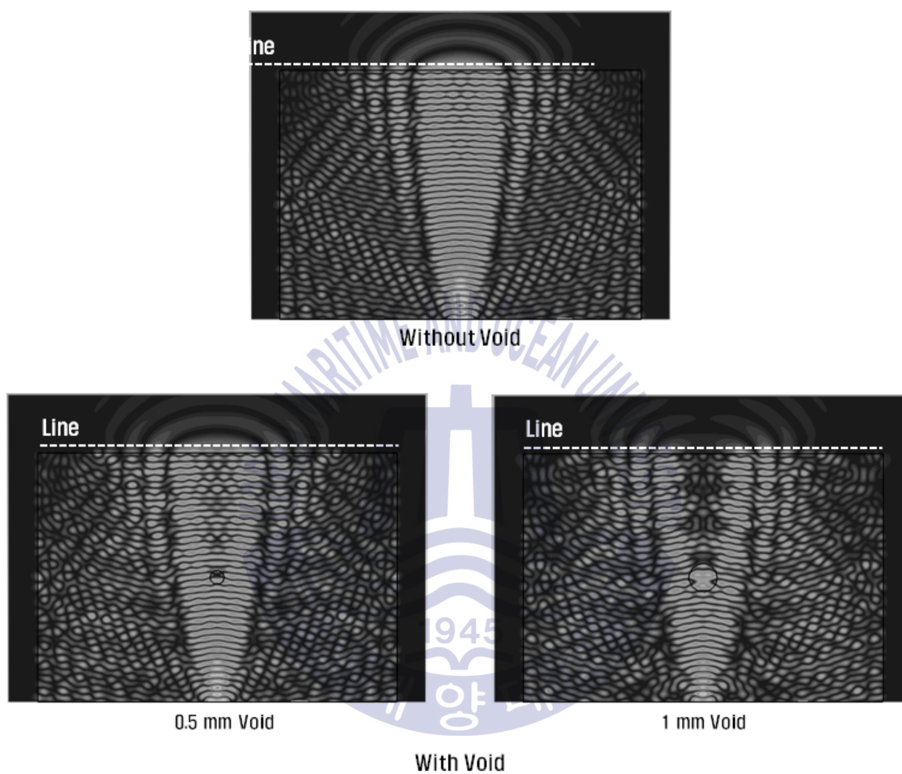

Figure 5-28 Simulation results for THz propagation characteristics with or without voids and void sizes in a multi-chip package

Collection @ kmou

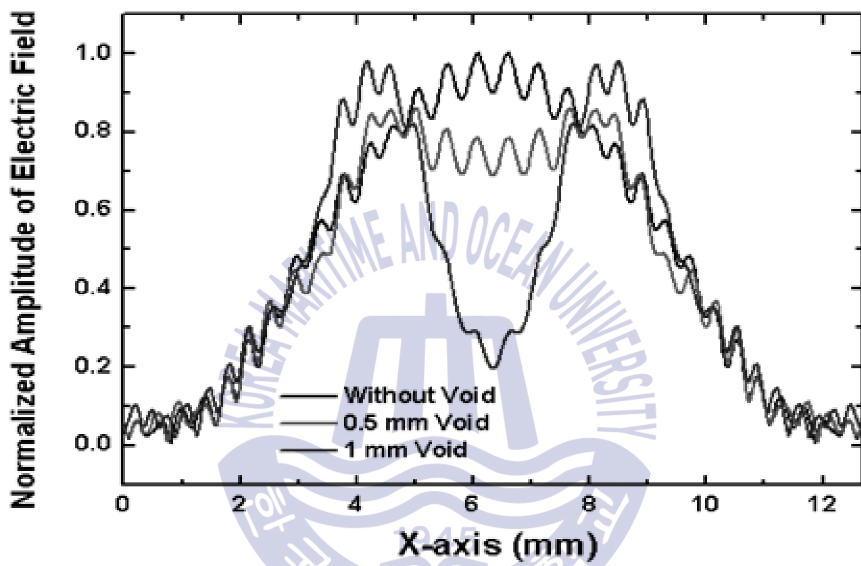

Figure 5-29 THz power distribution measured on the line in Figure 5-28

dCollection @ kmou

method for two voids in a multi-chip package.

As a result, voids within a thickness of about 8.6 mm were well detected in phase image as well as amplitude image. When the void is small, it can be seen that the void is easily detected in the phase image rather than the amplitude image. This is because the maximum and minimum values of the image signal due to the silicon wafer and the film are constant, while the smaller the void size, the smaller the change in the signal due to the defect. In order to detect only the change due to the defect in the measured image, the signal in each line was differentiated. As a result, the THz image changed by the void was obtained.

5.4.3 Improvement of void image using image processing technique

Figure 5-32 shows the amplitude and phase signals measured when a THz wave passes through a layer with a diameter of 1 mm in Figure 5-30. The change in the signal at the center of the void was measured to be more than about 100 mV, and in the case of the phase, the phase was reversed to the center of the void. As shown in the measured signal, the THz wave is detected over an area wider than the void size due to the width of the slit. Therefore, it is difficult to determine the exact void size.

Contrast stretching is a simple image enhancement technique that attempts to improve the contrast in an image by `stretching' the range of intensity values it contains to span a desired range of values [50]. The function is of the form

$$s = T(r) = \frac{1}{1+(m/r)^E} \quad \text{--- (3)}$$

Collection @ kmou

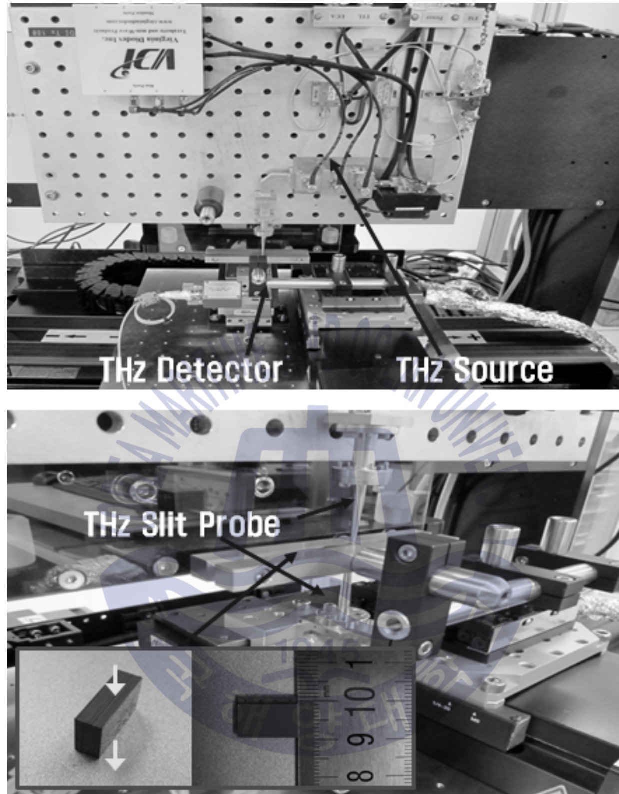

Figure 5-30 THz experiment setup for multi-chip package inspection using the lateral inspection method.

Collection @ kmou

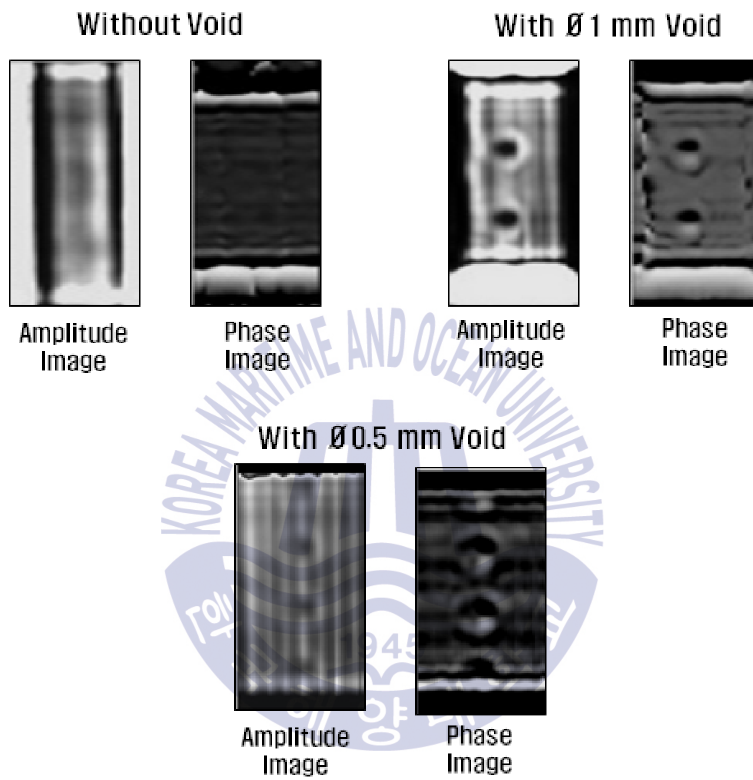

Figure 5-31 THz a image obtained using the lateral inspection method for two voids in a multi-chip package.

Collection @ kmou

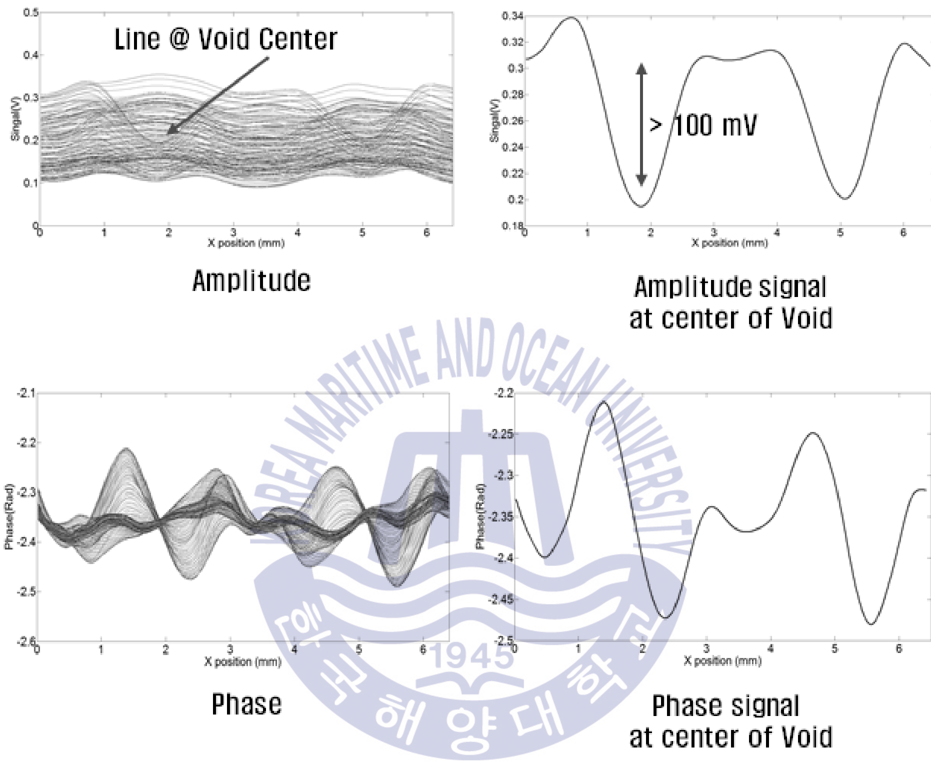

Figure 5-32 The amplitude and phase signals measured when a THz wave passes through a layer with a diameter of 1 mm

Collection @ kmou

where r represents the intensities of the input image, s the corresponding intensity values in the output image, and E controls the slope of the function. It can be implemented as eps is used to prevent overflow if f has any 0 values. Since the limiting value of s is 1, output values are scaled to the range (0,1) in this transformation. Compress input levels lower than m to a narrower range of dark levels, and compress the values above m to the light level of the output image at a narrower level [51]. The result is a higher contrast image.

Figure 5-34 shows the THz image for amplitude and phase versus input power for a sample with a 1 mm void in the multi-chip package. Input power was measured at 2.5 mW and 8.2 mW, respectively. As a result of the comparison, it is hard to distinguish the image difference according to the input power.

Figure 5-35 shows the THz image obtained by applying the contrast stretching transformation function to the amplitude image of Figure 5-31. It is shown that the detection sensitivity is significantly changed according to the input power using image processing.

5.4.4 Another application using slit-type probe (Food inspection)

To determine the potential of the proposed probe in THz applications, the possibility for the detection of foreign objects in food was studied the possibility for the detection of foreign objects in food. The THz images were compared with the flour thickness and the probe-to-flour distance for the foreign objects located at the bottom of the flour. The foreign objects were used metals, plastic, and sand, most frequently detected foreign objects in food. Figure 5-36 is an optical photo of the flour containing the foreign

Collection @ kmou

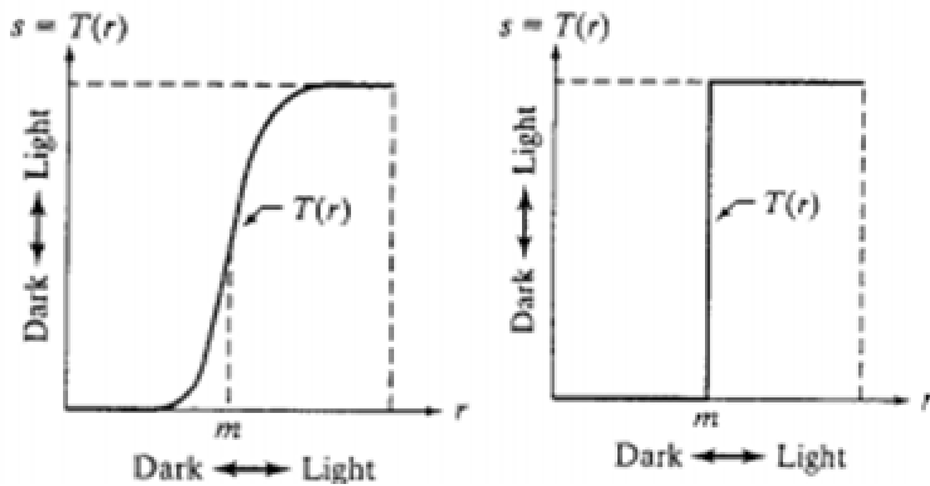

Figure 5-33 Contrast stretching transformation [51]

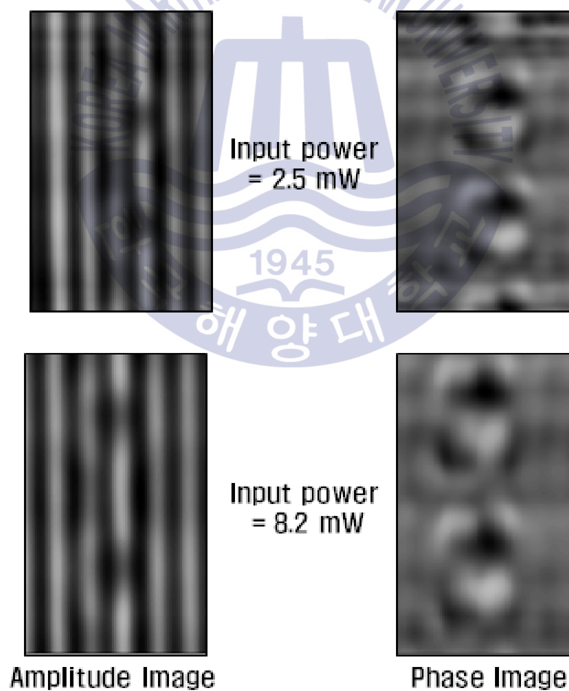

Figure 5-34 THz image for amplitude and phase versus input power for a sample with a 1 mm void in the multi-chip package

Collection @ kmou

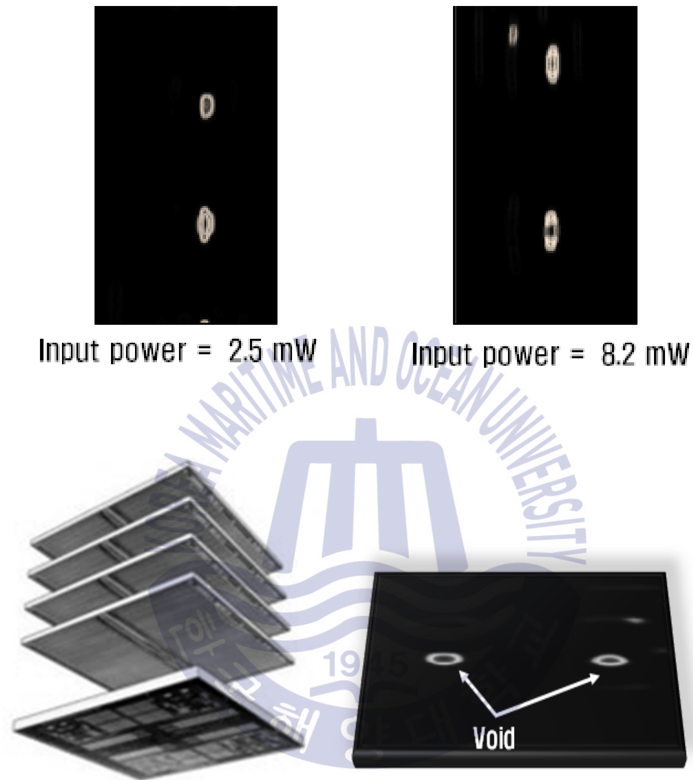

Figure 5-35 THz image obtained by applying the contrast stretching transformation function to the amplitude image of Figure 5-31

Collection @ kmou

objects. The inset is the top view of foreign objects before filling with the flour. The approximate diameter of plastic and sand is about 500 μm, and the diameter of metal wire is 70 μm.

Figure 5-37 is the THz image according to flour thickness *t* and flour-to-probe distance *d*. Figure 5-37 (a)-(c) show the THz images for sample of t =1.5mm, t=1.0mm, and t =0.5mm when the flour-to-probe distance *d* is 0.5mm, and Figure 5-37 (d)-(f) show the THz images with *d* = 1 mm. The Figure 5-37 (**c**) has the best resolution imaging because the *t* and *d* are the shortest distance among the measured conditions. As shown in the figure, the sensitivity of the detection and spatial resolution decrease as the flour thickness and the flour-to-probe distance increase. Although the sensitivity was decreased, metal wires with diameter of 70 μm was still detected at t =1.5 mm and d = 1 mm as shown in Figure 5-37 (d). The reversal of the brightness of the image according to the flour-to-probe distance is due to the phase of the reflected THz wave at the detector position. From these results, it is confirmed that the proposed resonant slit-type probe with rounded matching structure could be used enough to detect foreign objects in the size of hair in food or pharmaceutical field.

Collection @ kmou

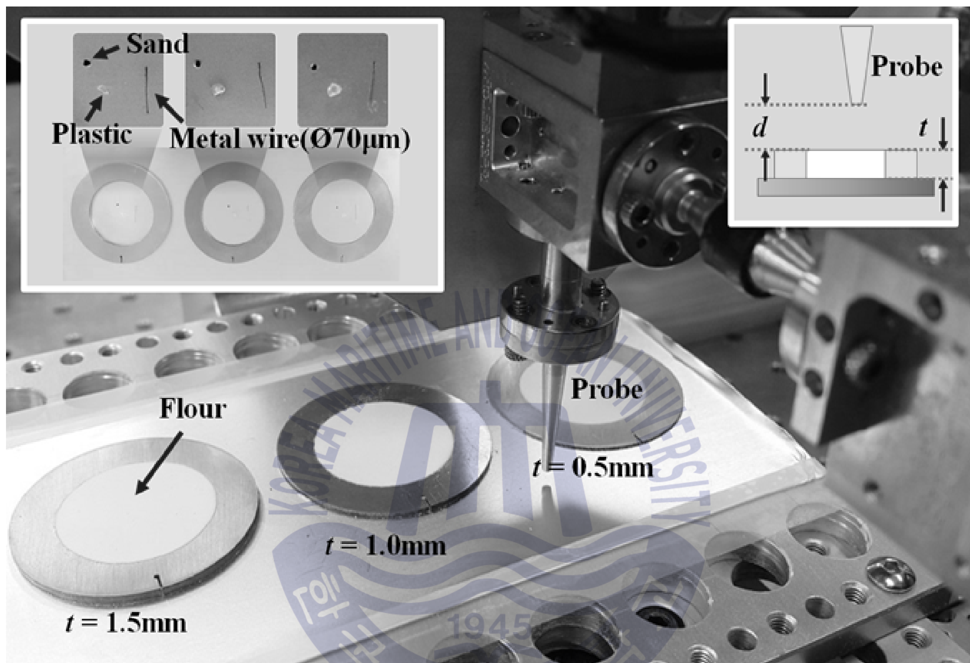

Figure 5-36 The optical photo of the flour containing the foreign object. The inset is the top view of foreign objects before filling with the flour.

Collection @ kmou

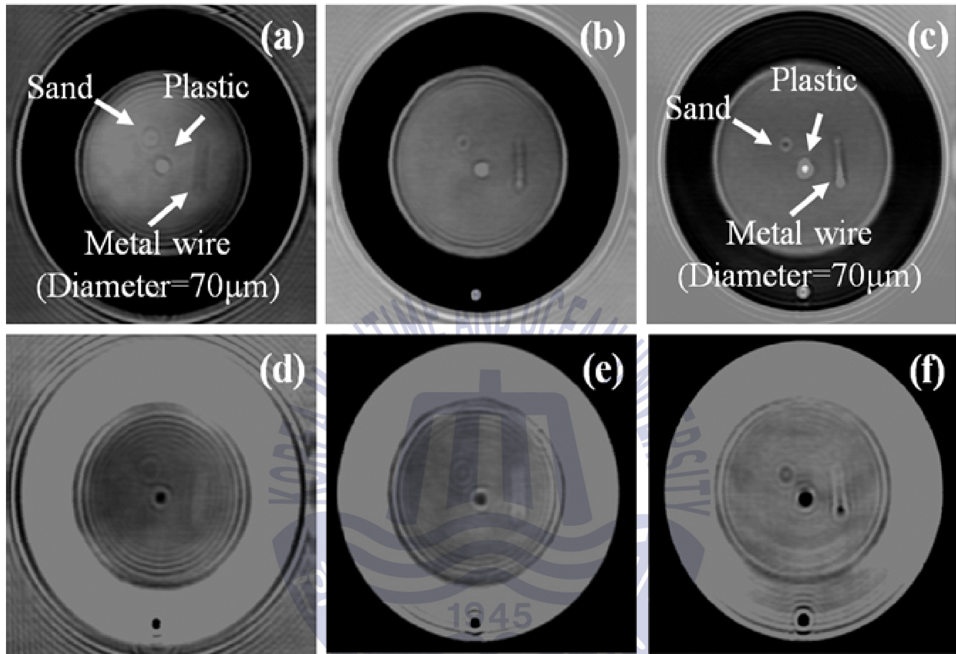

Figure 5-37 The THz image according to flour thickness t and flour-to-probe distance d. (a) t =1.5 mm, d =0.5 mm (b) t =1 mm, d =0.5 mm (c) t =0.5 mm, d =0.5 mm (d) t =1.5 mm, d =1 mm (e) t =1 mm, d =1 mm (f) t =0.5 mm, d =1 mm.

Collection @ kmou

6. Conclusion

In this paper, a resonant probe with a round-type matching structure slit for multi-chip package inspection using THz wave was proposed. The current multi-chip package inspection methods and limitations are investigated and the possibility of THz inspection is suggested. A resonant slit-type probe is proposed to obtain high resolution while using low frequency source for THz inspection. Particularly, in order to solve the structural problem of the conventional resonant slit-type probe, a rounded matching structure is applied to improve the slit thickness problem for use in the THz region and to increase the coupling efficiency. The proposed probe can maintain a high coupling efficiency despite the increase in the slit thickness and can provide a high spatial resolution using a narrow slit height. A prototype probe with a resonant frequency of 205GHz was fabricated and the VNA measurement results and CST MWS simulation results were compared. From these results, it was confirm that the proposed probe can be used as a new THz scanning probe owing to its simple structure and high coupling efficiency. The THz source, detector and FPGA-base fast lock-in

Collection @ kmou

amplifier ware constructed and a standard sample was fabricated and used for the performance of the measurement system and the manufactured probe. A THz image of a sample with various defects and achieved a spatial resolution of 100 μm was obtained. Pulsed THz waves were used to compare the polarization characteristics of the semiconductor chip with the transmission characteristics. It was confirmed that the transmission characteristics of the THz wave vary depending on the position and polarization direction. Considering future application in the industrial field, THz inspection system using CW THz wave is proposed. A THz transceiver module based on a directional coupler and a THz transceiver module based on a magic-tee were constructed, and the magnitude and phase of the detection signal were compared with standard samples. As a result, magic-tee-based THz transceiver modules have been verified to be more suitable for defect detection, which can be applied to offset reflected signals from and within the waveguide. It is difficult to detect the change of THz wave caused by void in the inspection using the semiconductor chip, and the lateral method is proposed instead of the transmission method. Since dia-attached films used in semiconductor laminating mostly use polymers such as PP sheets, THz waves can easily pass through between films. Also, the thickness of the dia-attached film is almost the same as the height of the slit probe, it can have spatial resolution to detect defects in the dia-attached film.

The CST simulation was performed to analyze the THz propagation characteristics with or without voids in the multi-chip package in a lateral measurement. The THz system for lateral measurement was constructed, and as a result, a void size of 500 μm in the multi-chip package was detected. Also, an image filter for detecting voids in a multi-chip package by

Collection @ kmou

applying a simple contrast stretching transformation was proposed. As a result, defects can be easily detected by improving the image of the stacked structure.

In addition, THz images of foreign objects in flour were obtained to confirm the industrial applicability of the proposed probe. The THz images were compared according to the thickness of the flour and the distance between the probe and the flour for foreign objects in the flour. The proposed resonant slit-type probe with rounded matching structure has less return loss and high coupling efficiency because of its thick slit thickness.

Consequently, the THz wave inspection technique is capable of nondestructive inspection and nondestructive inspection, the THz wave proved to be an appropriate tool in the absence of a multi-chip package inspection method suitable for the void test. In addition, the structure developed through this study can be applied to various fields such as medicine, medical care, and quality control in the future.

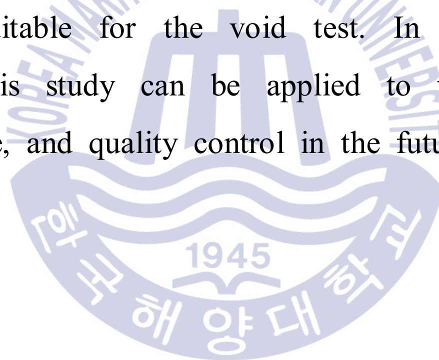

Collection @ kmou

Collection @ kmou

Reference

[1] S. N. Song, H. H Tan, P. L. Ong, “Die Attach Film Application in Multi Die Stack Package,” Electronics Packaging Technology Conference, 848 (2005).

[2] K. Kitami, K. Sakai, T. Tomita, K. Kurosawa, “Ultrasonic Imaging of Microscopic Defects to Help Improve Reliability of Semiconductors and Electronic Devices,” Hitachi Review 65, 272 (2016).

[3] N. Podjuea, W. Kerra, and K.T. Turnerb, “Inspection of Bonded Interfaces using Scanning Infrared Interferometry,” ECS Trans. 33, 537 (2010).

[4] D. Bernard1 and R. C. Blish, “Considerations for minimizing radiation doses to components during X-ray inspection,” Electronics Packaging Technology Conference, 697 (2005).

[5] M. Tonouchi, "Cutting-edge terahertz technology," Nat. photonics 1, 97 (2007).

[6] E-B. Moon, T.-I. Jeon, and D. Grischkowsky, “Long-path THz-TDS atmospheric measurements between buildings,” IEEE Trans. THz Sci. Technol. 5, 742 (2015).

Collection @ kmou

[7] J.-H. Son, "Terahertz electromagnetic interactions with biological matter and their applications," J. Appl. Phys. 105, 102033 (2009).

[8] E. Pickwell, and V. P. Wallace, "Biomedical applications of terahertz technology," J. Phys. D. Appl. Phys. 39, 301 (2006).

[9] A. J. Fitzgerald, V. P. Wallace, M. Jimenez-Linan, L. Bobrow, R. J. Pye, A. D. Purushotham, and D. D. Arnone, "Terahertz pulsed imaging of human breast tumors," Radiology 239, 533 (2006).

[10] S. J. Oh, J. Kang, I. Maeng, J.-S. Suh, Y.-M. Huh, S. Haam, and J.-H. Son, "Nanoparticle-enabled terahertz imaging for cancer diagnosis," Opt. Express 17, 3469 (2009).

[11] J. F Federici, B. Schulkin, F. Huang, D. Gary, R. Barat, F. Oliveira and D. Zimdars, "THz imaging and sensing for security applications—explosives, weapons and drugs," Semicond. Sci. Technol. 20, S266 (2005).

[12] C. B. Reid, G. Reese, A. P. Gibson, and V. P. Wallace, "Terahertz Time-Domain Spectroscopy of Human Blood," IEEE J Biomed. Health Inform. 17, 774 (2013).

[13] M. Yamashita, C. Otani, K. Kawase, K. Nikawa, and M. Tonouchi, "Noncontact inspection technique for electrical failures in semiconductor devices using a laser terahertz emission microscope," Appl. Phys. Lett. 93, 104 (2008).

[14] G. J. Kim, J. I. Kim, S. G. Jeon, J. Kim, K. K. Park, and C.H. Oh, "Enhanced continuous-wave terahertz imaging with a horn antenna for food inspection," J. Infrared, Millim. Terahertz Waves 33, 657 (2012).

[15] R. K. May, M. J. Evans, S. Zhong, I. Warr, L. F. Gladden, Y. Shen, and J.

Collection @ kmou

A. Zeitler, “Terahertz In-line sensor for direct coating thickness measurement of individual tablets during film coating in real-time,” J. Pharm. Sci. 100, 1535 (2011).

[16] A. Y. Pawar, D. D. Sonawane, K. B. Erande, D. V. Derle, “Terahertz technology and its applications,” Drug Invention Today 5, 157, (2013).

[17] M. van Exter and D. Grischkowsky, "Optical and Electronic Properties of Doped Silicon from 0.1 to 2 THz", Appl. Phy. Lett. 56, 1694 (1990).

[18] M. van Exter and D. Grischkowsky, "Carrier Dynamics of Electrons and Holes in Moderately-doped Silicon", Phys. Rev. B15, 41, 12140-9 (1990).

[19] T.-I Jeon and D. Grischkowsky, "Nature of Conduction in Doped Silicon," Phys. Rev. Lett. 78, 1106 (1997).

[20] Y. S. Jin, G. J, Kim and S. G. Jeon, “Terahertz Dielectric Properties of Polymers,” J. Korean Phys. Soc. 49, 513517 (2006).

[21] S. Wietzke, C. Jansen , M. Reuter, T. Jung, D. Kraft, S. Chatterjee, B.M. Fischer, M. Koch, “Terahertz spectroscopy on polymers: A review of morphological studies,” J. Molecular Structure 1006, 41 (2011).

[22] Z.-gang Di, Jian-quan Yao, Chun-rong Jia, De-gang Xu, Pi-bin Bing, Peng-fei Yang, Yi-bo Zheng, “Terahertz imaging technique and application in large scale integrated circuit failure inspection,” Proce. of SPIE 5, 7854 (2010).

[23] M. Yamashita, K. Kawase and C. Otani, Toshihiko Kiwa, Masayoshi Tonouchi, “Imaging of large-scale integrated circuits using laser terahertz emission microscopy,” Opt. Express 13, 115 (2005).

Collection @ kmou

[24] M. Yamashita, C. Otani, K. Kawase, T. Matsumoto, K. Nikawa, S. Kim, H. Murakami, and M. Tonouchi, "Backside observation of large-scale integrated circuits with multilayered interconnections using laser terahertz emission microscope," Appli. Phys. Lett. 94, 191104 (2009).

[25] M. Yamashita, C. Otani, K. Kawase, K. Nikawa, and M. Tonouchi, "Noncontact inspection technique for electrical failures in semiconductor devices using a laser terahertz emission microscope," Appli. Phys. Lett. 93, 041117 (2008).

[26] F. Destic and C. Bouvet, "Impact damages detection on composite materials by THz imaging," Case Studies in Nondestructive Testing and Evaluation 6, 53 (2016).

[27] N. V. Chernomyrdin, A. O. Schadko, S. P. Lebedev, V. L. Tolstoguzov, V. N. Kurlov, I. V. Reshetov, I. E. Spektor, M. Skorobogatiy, S. O. Yurchenko, and K. I. Zaytsev, "Solid immersion terahertz imaging with sub-wavelength resolution," Appl. Phys. Lett. 110, 221109 (2017).

[28] J. Zhao, W. Chu, L. Guo1, Z. Wang, J. Yang, W. Liu, Y. Cheng and Z. Xu, "Terahertz imaging with sub-wavelength resolution by femtosecond laser filament in air," Scientific Reports 4, 1 (2014).

[29] A. Joseph Louis Adam, "Review of Near-Field Terahertz Measurement Methods and Their Applications: How to Achieve Sub-Wavelength Resolution at THz Frequencies," J. Infrared, Millim., Terahertz Waves 32, 976 (2011).

[30] J. V. Rudd, and D. M. Mittleman, "Influence of substrate-lens design in terahertz time-domain spectroscopy,"J. Opt. Soc. Am. B 19, 319 (2002).

[31] M. Golosovsky and D. Davidov, "Novel millimeter-wave near field resistivity

Collection @ kmou

microscope," Appl. Phys. Lett. 68, 1579 (1996).

[32] A. J. Macfaden, J.L. Reno, I. Brener, and O. Mitrofanov, "3 μm aperture probes for near-field terahertz transmission microscopy," Appl. Phys. Lett. 104, 011110 (2014).

[33] A. J. L. Adam, J. M. Brok, M. A. Seo, K. J. Ahn, D. S. Kim, J. H. Kang, Q. H. Park, M. Nage, P. C. M. Planken, "Advanced terahertz electric near-field measurements at sub-wavelength diameter metallic apertures," Opt. Express 16, 7407 (2008).

[34] H.-T. Chen and R. Kerstinga, G. C. Cho, "Terahertz imaging with nanometer resolution," Appli. Phys. Lett. 83, 3009 (2003).

[35] T.-I. Jeon, J. Zhang, and D. Grischkowsky, "THz Sommerfeld wave propagation on a single metal wire", Appl. Phys. Lett. 86, 161904 (2005).

[36] K. Wang, and D. M. Mittleman, "Metal wires for terahertz wave guiding," Nature 432, 376 (2004).

[37] S. A. Maier, S. R. Andrews, L. Martín-Moreno, and F. J. García-Vidal, "Terahertz surface plasmon-polariton propagation and focusing on periodically corrugated metal wires," Phys. Rev. Lett. 97, 176805 (2006).

[38] Y. B. Ji, E. S. Lee, J. S. Jang, S-H. Kim, and T.-I. Jeon, "Coupling properties of a conical tungsten-wire waveguide in the terahertz frequency range," J. Korean Phy. Soc. 53, 584 (2008).

[39] Y. B. Ji, E. S. Lee, J. S. Jang, and T.-I Jeon, "Enhancement of the detection of THz Sommerfeld wave using a conical wire waveguide", Opt. Express 16, 271 (2008).

Collection @ kmou

[40] S. Liu, O. Mitrofanov and A. Nahata, “Near-field terahertz imaging using subwavelength apertures without cutoff,” Opt. Express 24, 2728 (2016).

[41] N. Qaddoumi, H. Abiri, S. Ganchev, and R. Zoughi, “Near-field analysis of right angle structure probe used for imaging,” Review of Progress in Quantitative Nondestructive Evaluation 15, 727 (1996).

[42] T. Nozokido, T. Ohbayashi, J. Bae, and K. Mizuno, “A Resonant slit-type probe for millimeter-wave scanning near-field microscopy,” IEICE Trans. Electron. E87-C, 2158 (2004).

[43] T. Nozokido, J. Bae, and K. Mizuno, “Scanning near-field millimeter-wave microscopy using a metal slit as a scanning probe,” IEEE Trans. Microw. Theory Tech. 49, 491 (2001).

[44] Samuel Silver, Microwave Antenna Theory and Design, Peter Pergrinus Ltd, London, 1997.

[45] N. Marcuvitz, Waveguide Handbook, New York, NY, USA: Dover, 1965.

[46] G. Ronald Hadley, “Design of Tapered Waveguides for Improved Output Coupling,” IEEE Photonics Technol. Lett. 5, 1068 (1993).

[47] S. Dwari, A. Chakraborty, and S. Sanyal, “Analysis of Linear Tapered Waveguide by Two Approaches,” Progress In Electromagnetics Research, PIER 64, 219 (2006).

[48] S-H. Kim, E. S. Lee, Y. B. Ji, and T.-I. Jeon, "Improvement of THz coupling using a tapered parallel-plate waveguide", Opt. Express 18, 1289 (2010).

[49] F. D. J. Brunner, A. Schneider, and P. Günter , “A terahertz time-domain

Collection @ kmou

spectrometer for simultaneous transmission and reflection measurements at normal incidence," Opt. Express 17, 20684 (2009).

[50] N. Radha, M. Tech, "Comparison of Contrast Stretching methodes of Image Enhancement Techniques for Acut Leukemai Images," Int. J. Eng. Res. Technol. 1, 1 (2012).

[51] R. C, Gonzalez, R. E. Woods, S. L. Eddins, Digital Image Processing using Matlab, Prentice-Hall, Inc., NJ, USA, 2004.

Collection @ kmou